POLITECNICO DI MILANO

Facoltà di Ingegneria Industriale e dell'Informazione

Corso di Laurea in Magistrale in Ingegneria Biomedica

Assessment of frequency response of respiratory system in newborns during High Frequency Oscillatory Ventilation

Relatore: Prof. Raffaele Dellacà

Correlatore: Ing. Emanuela Zannin

Tesi di Laurea di:

Lara MARCONI Matr. 800505

Martina PEREGO Matr. 798722

ANNO ACCADEMICO 2013-2014

INDEX:

FIGURE INDEX:

TABLE INDEX:

Abstract

Every year 15 million babies are born pre-term[1] and their morbidity and mortality are in most cases consequence of respiratory diseases. In fact infants, at birth, have to face the crucial transition from uterine to air life and being born with an immature respiratory system increases the probability of failing this transition and of developing respiratory diseases.

High-frequency oscillatory ventilation (HFOV) is used in clinical practice to treat severe neonatal lung disease. HFOV is a protective non-conventional ventilation that employs supra-physiological breathing rates and small tidal volumes (frequently less than dead space). HFOV has the potential to reduce ventilator-induced lung injury but, in order to have a successful ventilation, a correct setting is essential.

While for the identification of the optimal values of some ventilatory parameters (Continuous Distending Pressure (CDP), Peak-to-peak pressure (P/P pressure), Fraction of inspired oxygen (FiO_2) and Inspiratory/Expiratory time ratio (TI/TE)) there are standard procedures[2], no demonstrated rules are established for the setting of oscillatory frequency.

However, up to now no tools are available for the assessment of the optimal frequency at bedside. Therefore, in clinical practice the frequency of oscillatory ventilation is normally chosen on baby's body weight: if the body weight is less than 1.5 Kg, the frequency is set to 15 Hz, otherwise is set to 10 Hz.

The aim of the study is to investigate the frequency response of the respiratory system in newborns during HFOV and to understand the thoraco-abdominal mechanical features, in particular characterizing the regional heterogeneities of chest wall displacements at different oscillatory frequencies. The evaluation of global and compartmental mechanical properties is performed through the computation of input impedance (Z_{in}) from the pressure and flow signals measured at the airways opening and transfer impedance (Z_{tr}) from the pressure measured at the airways opening and flow obtained by OptoElectronic Plethysmography (OEP) measurements. This technique allows evaluating total and compartmental volume changes from chest wall marker oscillations.
While Z_{in} describes the whole respiratory system, Z_{tr} considers the regional and local mechanical response once applied the pressure wave at airway opening.
In fact, the frequency response of the respiratory system is influenced by the response of the different tissues through which the oscillatory pressure propagates: *i.e.* rib cage and abdomen frequency response are significantly different.

In this study we developed an experimental set-up for the analysis of the global and regional respiratory system mechanics in infants receiving HFOV. Specific algorithms have been defined and developed for the data analysis: in particular for input impedance computation from pressure and flow signals, for the compensation for the low-pass filtering effect of the measurement system, and for the flow dependence of the endotracheal tube disclosed by the high amplitude ventilation waveform. . Moreover other algorithms have been designed to analyze single marker movements for the reconstruction of regional changes after the application of oscillatory pressure waves at specific frequencies.
In order to validate the clinical setup and the application of these computational methods an in-vitro study was performed. Moreover the frequency behaviour of the entire setup and of all its components was tested, and the respiratory system response of different types of

patients was examined using several test lungs that simulate different resistance and compliance properties.

This set-up has been validated in vitro against standard frequency response computation (when small amplitude oscillatory waves are applied) and proved to be accurate over a wide range of mechanical characteristics.

In the clinical study five different oscillatory frequencies (5 Hz, 8 Hz, 10 Hz, 12 Hz, 15 Hz) were tested in random order on twelve patients (gestational age=29±4 wks; postnatal age=5±8 days; body weight=1.35±0.8 Kg).

Input impedance has been described as real part (system resistance) and imaginary part (system reactance). While the first one remains almost constant with frequency, the reactance tends to increase with increasing frequencies and crosses the zero line at the resonant frequency, f_0.

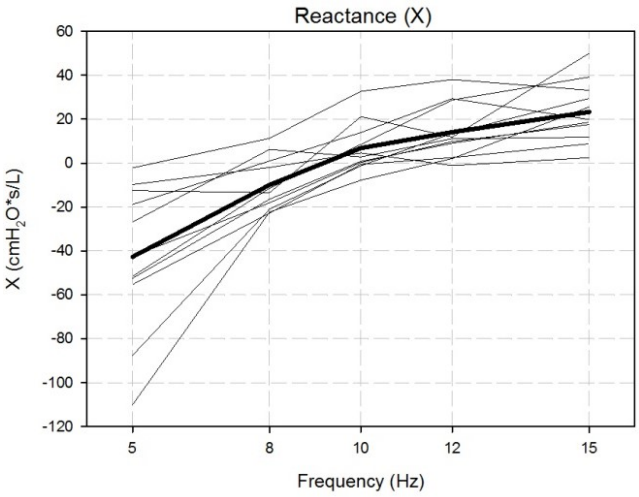

Figure 1 Imaginary part of input impedance.

f_0 is defined as the frequency at which the pressure cost of achieving flow is minimal.[3]

Resonant frequencies, computed with a fitting curve, could be considered the optimal frequency of ventilation insofar less energy could generate the greatest efficiency. The f_0 found are in a range from 7 Hz to 12 Hz, values settable on the HFOV ventilator.

The analysis of individual markers oscillations shows that, while the rib cage oscillates almost uniformly, in the abdomen the phase lag between midline markers increases in the cranio-caudal direction up the maximum near the waistline. At 15 Hz, the phase lag in the

most caudal regions approaches 180°, indicating opposite movements in the different regions.

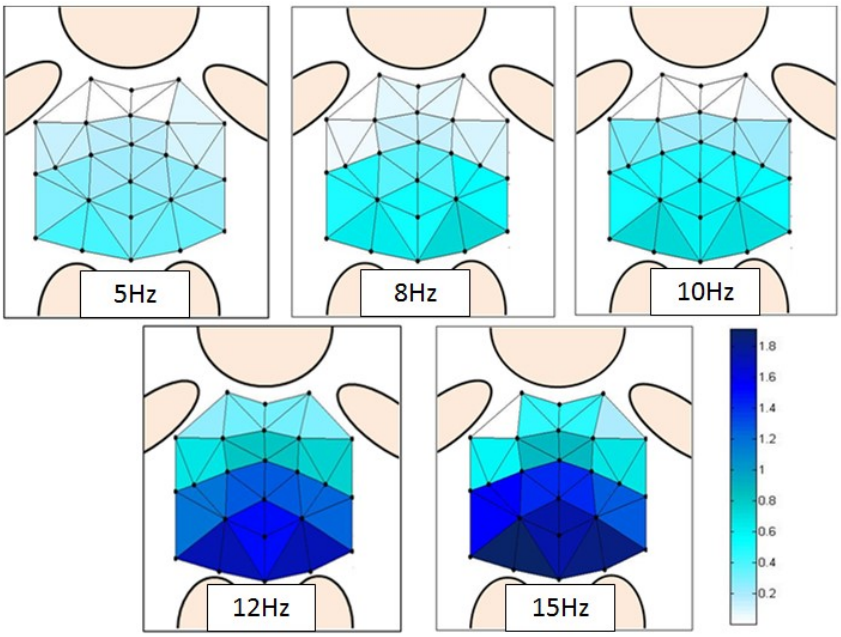

Figure 2 Phase shift [rad] on the thoraco-abdominal surface.

In infants receiving HFOV, the chest wall oscillates asynchronously and non-uniformly. This behavior is more evident with increasing oscillatory frequencies, with the abdominal compartment being, in average, more sensitive to changes in frequency.

Since the infant respiratory system cannot be considered as a single compartment, the total transfer impedance alone is not able to entirely characterize the mechanical response of the respiratory system at high frequencies. The solution is to consider rib cage volume and abdomen volume separately with the same oscillating pressure signal imposed at the mouth.

Nine regions of the chest wall have been considered and the transfer functions between the local flow and pressure were estimated to describe the spatial distribution of respiratory system transfer impedance. The additional information is represented by a spatial position of the regional transfer impedance values on the thoraco abdominal surface of the newborns.

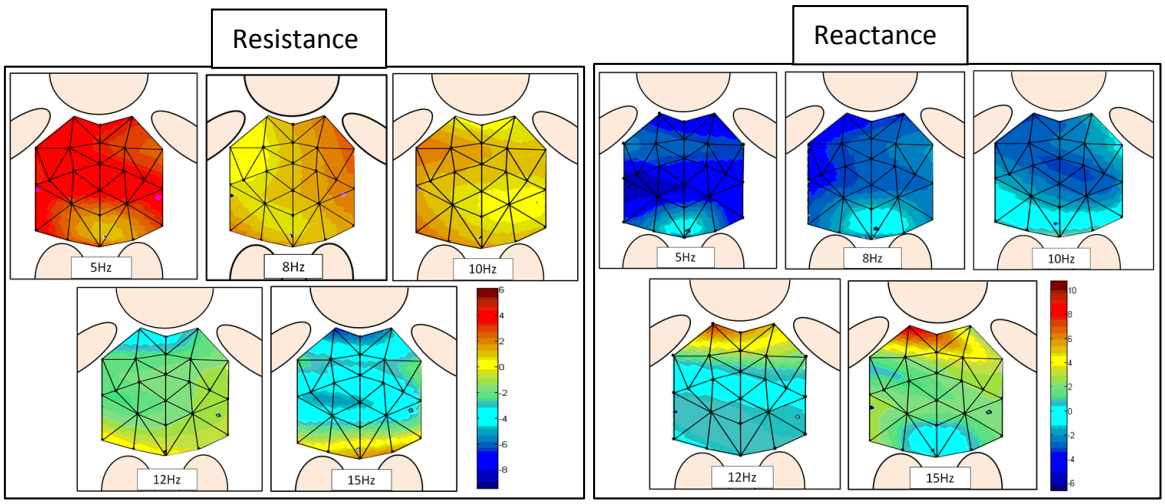

Figure 3 Real (left) and imaginary (right) part of regional transfer impedance [cmH_2O*s/L].

The inhomogeneity of the thoraco-abdominal compartments increases with increasing frequency and in particular at the maximum frequency (15 Hz) different zones have different mechanical behaviours due to their difference tissue composition and stiffness: *i.e.* abdominal compartment is affected by high inertance at high frequencies.

Even if there are inhomogeneities among different zones, there are two evident components of the chest wall: zones belonging to rib cage have similar trend in real and imaginary part and have different frequency behaviours in respect to abdominal zones. For this reason the most suitable division for the infants thoraco-abdominal compartment is two or three compartments, because this areas provide a useful mechanical description and frequency response.

From our results we can conclude that increasing the frequency, the abdominal and rib cage inhomogeneities increase as the result of very different mechanical properties.

While Z_{in} considers the whole respiratory system, Z_{tr} (highly sensitive to peripheral/heterogeneous lung constriction and chest wall restriction) is minimally distorted by shunting of flow into alveolar gas and upper airway walls.

These differences are masked in total Z_{tr} by the much lower modulus of the pulmonary rib cage Z_{tr} that, being in parallel with the abdomen, strongly dominates the resulting total chest wall mechanical behaviour.

For all these reasons, regional alteration in chest wall mechanical properties cannot be identified from the total Z_{tr} but only from local measurements, and OEP technique offers the possibility of studying it.

Finally, the combination of FOT and OEP technique allows to evaluate quantitatively the mechanical response of the respiratory system at different frequencies; the information obtained could be used in clinical practice to choose the optimal frequency and the best way to submit ventilation for the clinician, achieving the maximum mechanical efficiency and, in the same time, reducing the lung distress.
Then, further studies are necessary to draw clinical controlled trials to compare treatment based on quantitative measures with standard treatment, evaluating short term (biochemical) and long term lung damages as outcome.

Sommario

Ogni anno 15 milioni di bambini nascono pre-termine[1]; tuttavia la loro morbilità e mortalità dipendono, nella maggior parte dei casi, da malattie respiratorie. I bambini, infatti, alla nascita devono affrontare un passaggio cruciale verso la vita extrauterina e un sistema respiratorio immaturo aumenta la probabilità di fallire durante transizione e di sviluppare malattie respiratorie.

La ventilazione oscillatoria ad alta frequenza (HFOV) viene utilizzata nella pratica clinica per il trattamento di gravi patologie polmonari nei neonati. Questa è una ventilazione non convenzionale protettiva che utilizza frequenze respiratorie maggiori rispetto a quelle fisiologiche e volumi correnti più piccoli (spesso minori dello spazio morto). Questa tecnica quindi è potenzialmente adatta per ridurre i danni polmonari indotti dal ventilatore ma, per avere una ventilazione efficace, è essenziale una corretta impostazione dei parametri ventilatori.

Mentre per l'individuazione dei valori ottimali di alcuni parametri ventilatori (Continuous Distending Pressure (CDP), pressione picco-picco (P/P), frazione di ossigeno inspirato (FiO2) e rapporto tra tempi di inspirazione ed espirazione (TI/TE)) ci sono procedure standard[2], non ci sono regole per le impostazioni della frequenza di ventilazione.

Tuttavia, fino ad ora non sono disponibili strumenti per la valutazione di f_0 al letto del paziente. Pertanto, nella pratica clinica la frequenza della ventilazione oscillatoria viene normalmente scelta in relazione al peso corporeo del bambino: se il peso è inferiore a 1.5 Kg, la frequenza è impostata a 15 Hz, altrimenti è impostata a 10 Hz.

L'obiettivo di questo studio è quello di valutare la risposta in frequenza del sistema respiratorio nei neonati sottoposti ad HFOV e di capire le caratteristiche della meccanica toraco-addominale, in particolare caratterizzando le eterogeneità regionali con l'uso degli spostamenti della gabbia toracica a differenti frequenze di oscillazione. La valutazione delle proprietà meccaniche globali e compartimentali è ottenuta attraverso il calcolo dell'impedenza d'ingresso (Z_{in}) dalle misure di segnali di pressione e flusso all'apertura delle vie aeree e dell'impedenza di trasferimento (Z_{tr}) dalle misure di pressione alle vie aeree e dalle misure di flusso ottenute con il metodo della Pletismografia OptoElettronica (OEP). Questa tecnica permette di valutare le variazioni di volume sia totale che compartimentali dalle oscillazioni dei marker posizionati sul torace.
Mentre Z_{in} il Sistema respiratorio complessivo, Z_{tr} considera la risposta meccanica regionale e locale una volta applicata l'onda di pressione alle vie aeree.
Infatti, la propagazione dell'onda pressoria alle diverse frequenze è influenzata dalle risposta dei differenti tessuti: ad esempio la risposta in frequenza del torace e dell'addome sono significativamente differenti.

In questo studio, abbiamo sviluppato un set-up sperimentale per l'analisi della meccanica respiratoria globale e regionale di bambini sottoposti ad HFOV. Algoritmi specifici sono stati definiti e sviluppati per la data analysis: in particolare per il calcolo dell'impedenza di ingresso dai segnali di pressione e flusso, per la compensazione dell'effetto passa-basso causato dal sistema di misura e per la flusso dipendenza legata al tubo endotracheale rispetto ai segnali pressori con ampiezza elevata. Inoltre altri algoritmi sono stati pensati per analizzare i movimenti dei singoli marker al fine di ricostruire variazioni regionali causate dall'applicazione di un'onda pressoria di frequenza specifica.
al fine di validare il setup clinico e l'applicazione di questi metodi computazionali uno studio in vitro è stata effettuato. Inoltre il comportamento in frequenza dell'intero setup di tutti i suoi componenti è stato testato, e la risposta del sistema respiratorio dei diversi tipi

di pazienti è stata esaminato utilizzando diversi test lungs che simulano differenti proprietà di resistenza e di compliance. Questo set-up è stato validato in vitro rispetto alla misurazione standard della risposta in frequenza (in cui sono applicate onde pressorie a piccola ampiezza) ed ha dimostrato di essere accurato nella misurazione di un elevato range di proprietà meccaniche.

Nello studio clinico cinque diverse frequenze oscillatorie (5 Hz, 8 Hz, 10 Hz, 12 Hz, 15 Hz) sono state testate in ordine casuale su dodici pazienti (età gestazionale = 29 ± 4 settimane; età postnatale = 5 ± 8 giorni; corpo peso = 1,35 ± 0,8 Kg).
L'impedenza di ingresso è stata descritta come parte reale (resistenza) e parte immaginaria (reattanza del sistema). Mentre la prima rimane quasi costante con la frequenza, la reattanza tende ad aumentare con l'aumento delle frequenze e attraversa la linea dello zero alla frequenza di risonanza, f_0.

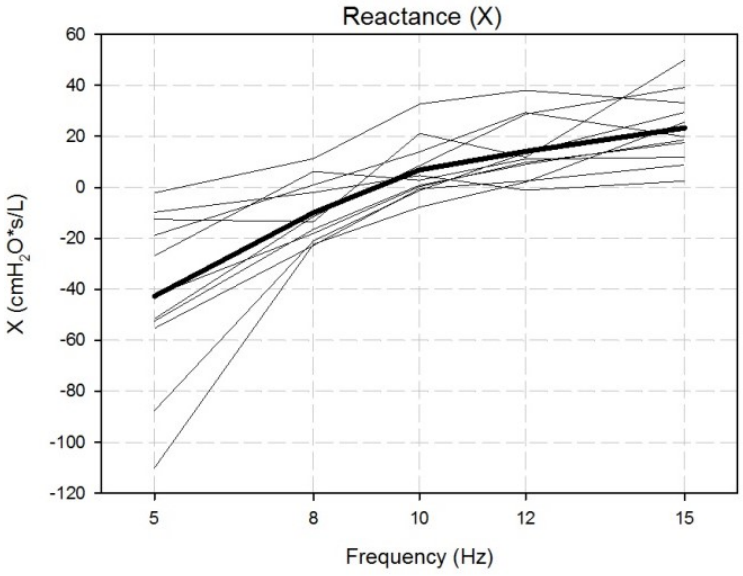

Figura 4 Parte immaginaria dell'impedenza d'ingresso.

La f_0 è definita come la frequenza alla quale la pressione per ottenere i flussi necessari per una corretta ventilazione è minima.
Le frequenze di risonanza, calcolate con una curva di fitting, possono essere considerate le frequenze ottimali di ventilazione in quanto si potrebbe generare la massima efficienza con la minor energia applicata. Le f_0 trovate sono comprese in un intervallo tra 7 Hz a 12 Hz, valori impostabili sul ventilatore per l'HFOV.

L'analisi delle oscillazioni dei singoli marcatori, inoltre, mostra che, mentre la gabbia toracica oscilla quasi uniformemente, nell'addome il ritardo di fase lungo la linea mediana aumenta in direzione cranio-caudale fino ad un massimo a livello della vita. A 15 Hz, il ritardo di fase nelle regioni più distali rispetto alla bocca si avvicina a 180°, indicando movimenti opposti nelle diverse regioni.

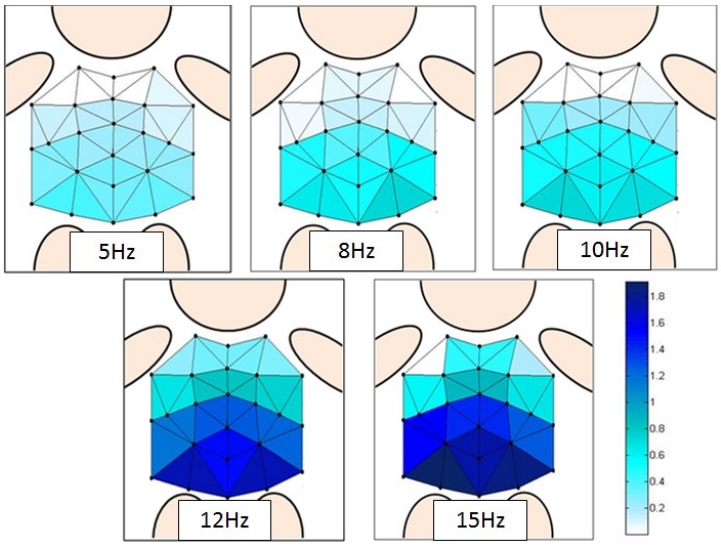

Figura 5 Ritardo di fase nella parete toraco-addominale (misure in rad).

Nei neonati sottoposti ad HFOV, la parete toracica oscilla in modo asincrono e non uniforme. Questo comportamento è più evidente con l'aumentare frequenze oscillatorie, con il compartimento addominale, in media, più sensibile alle variazioni di frequenza.
Poiché il sistema respiratorio del neonato non può essere considerato come un unico singolo compartimento, l'impedenza totale di trasferimento da solo non è in grado di caratterizzare completamente la risposta meccanica del sistema respiratorio ad alte frequenze. La soluzione è quella di considerare il volume della gabbia toracica e il volume addominale separatamente, ma stimolati dallo stesso segnale di pressione imposto alla bocca.

Nove regioni della parete toracica sono state considerate e le 9 funzioni di trasferimento tra il flusso regionale e la pressione sono state stimate per descrivere la distribuzione spaziale dell'impedenza di trasferimento del sistema. Un'informazione aggiuntiva è rappresentata

dalla posizione spaziale dei valori di impedenza regionali sulla superficie toracoaddominale dei neonati, rappresentabile attraverso delle mappe a colori.

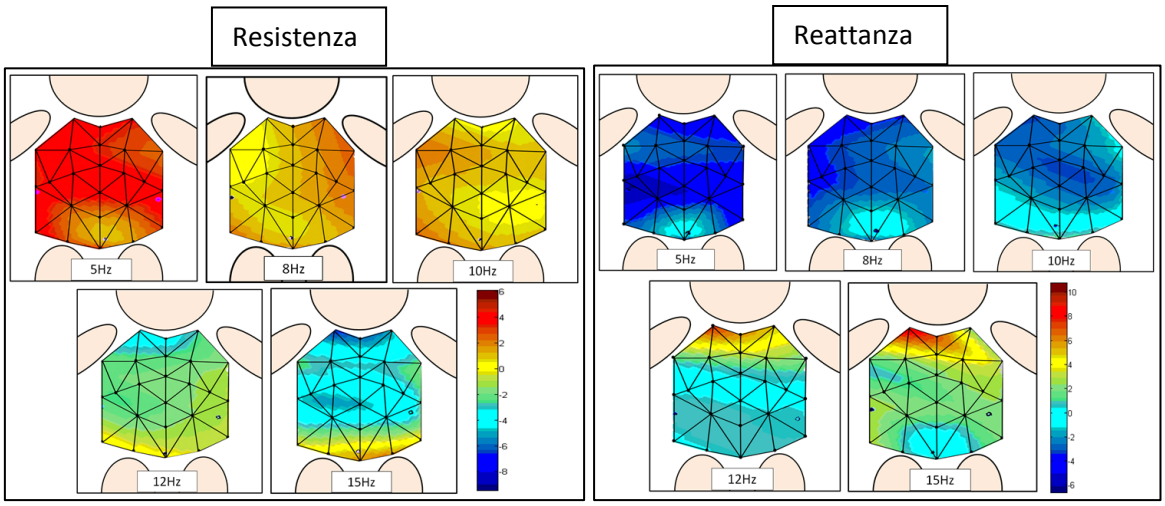

Figura 6 Parte reale e immaginaria delle impedenze di trasferimento regionali (misure in cmH_2O*s/L).

La disomogeneità dei compartimenti toraco-addominali aumenta con l'aumentare della frequenza e, in particolare, alla frequenza massima (15 Hz) le diverse zone mostrano comportamenti meccanici molto diversi dovuti alla loro diversa composizione a livello dei tessuti e quindi alla loro diversa rigidità: il compartimento addominale, ad esempio, è affetto da alta inertanza alle alte frequenze.

Anche se ci sono disomogeneità fra diverse zone, sono individuabili due componenti principali che descrivono la parete toracica: le zone della gabbia toracica hanno infatti lo stesso comportamento e mostrano, invece, un comportamento differente in frequenza rispetto a quelle addominali. Per questo motivo la divisione più adatta per la descrizione della meccanica toraco-addominale nei neonati è due o tre compartimenti.

Dai nostri risultati si può concludere che aumentando la frequenza, le disomogeneità addominali e della gabbia toracica aumentano come risultato di differenti proprietà meccaniche.

Mentre Z_{in} considera l'intero sistema respiratorio, Z_{tr} (molto sensibile all'eterogeneità polmonare) è minimamente distorta dalla presenza delle vie aeree superiori e dalla comprimibilità del gas.

Queste differenze non sono pienamente visibili nella Z_{tr} totale, che risente del compartimento che in un dato momento prevale sull'altro.

Per tutti questi motivi, le proprietà meccaniche della parete toraco-addominale non possono essere identificate come alterazione globale di Z_{tr}, ma solo come misure locali e l'uso dell'OEP offre questa possibilità.

Infine, la combinazione di FOT e OEP permette di valutare quantitativamente la risposta meccanica del sistema respiratorio a differenti frequenze; le informazioni ottenute potrebbero essere utilizzate nella pratica clinica per scegliere la frequenza ottimale e il modo migliore per effettuare la ventilazione, raggiungendo la massima efficienza meccanica e, allo stesso tempo, riducendo eventuali danni polmonari.

Ulteriori studi sono necessari per effettuare studi clinici controllati atti a confrontare il trattamento basato sulle misure quantitative con quello utilizzato in clinica, attraverso la valutazione a breve termine (biochimica) e a lungo termine del polmone.

1. Introduction

IRDS is the most common respiratory disease in pre-term babies because of the structural and functional immaturity of the respiratory system. About 1% of all newborns is affected by IRDS and mortality is also rather high (about 10%) despite of the improvement of IRDS management in last decades.

Signs of respiratory distress such as tachypnea, nasal flaring and cyanosis usually appears few minutes after birth and neonates often need resuscitation at birth, especially if their weight is less than 1000g.

From a structural point of view it means little lungs with thick alveolar walls, difficulties in exchanging gases and little production of surfactant, which leads to low lung compliance, and some difficulties in pulmonary fluid clearance.

High Frequency Oscillatory Ventilation has the potential to be lung protective in patients with severe lung diseases thanks to his unconventional ventilation that employs supra-physiological breathing rates and tidal volumes frequently less than dead space. This lung protective strategy, however, needs a correct setting of ventilator parameters to keep this treatment safe and efficient, reducing lung injuries and traumas.

Many studies have been conducted on the identification of the optimal CDP and lung recruitment, while there are no clinical studies available in literature about the optimal frequency setting. Therefore, theoretical speculations and pre-clinical studies on respiratory mechanics lead clinician decisions in setting ventilatory frequencies.

Nowadays, most clinicians choose the oscillatory frequency based on body-weight:

- about 15 Hz for <1500g body-weight neonates,
- about 10Hz for ≥ 1500g body-weight neonates.

Such tip is based on the idea that a little baby has a little and more rigid lung, so higher frequency are preferred; in opposition a larger lung with a better compliance requires low frequencies to avoid the low-pass filtering effect of the respiratory system.

Moreover, theoretical studies[3] demonstrate that at the resonance frequency (f_0) in the respiratory system the inertial components and the compliant ones are perfectly balanced; therefore minimal energy is required to achieve ventilation. Resonant frequency is very high for a little compromised lung and it reduces with improving compliance. Since a technique to estimate f_0 was not available yet in the clinical setting and since it is supposed that ventilated newborns have a very low compliance (so f_0 too high to be set), it has been recently proposed to set oscillatory frequency at the higher value consistent with adequate tidal volume and pressure amplitude.

The more significant parameters that influence the frequency response of ventilation are mechanical properties described by input impedance and transfer impedance. While the first one (a global estimation of the respiratory system) is easily obtainable in clinical environment with pressure oscillation and flow measurement, the second one, providing information specific to tissues and pulmonary response, so far has been more difficult to obtain by using a body box plethysmography, which describes all the system as an unique compartment.[4]

In infants receiving HFOV, the chest wall oscillates asynchronously and non-uniformly, this behaviour is more evident with increasing oscillatory frequencies and, in the same way, increasing the frequency, increase inhomogeneities as the result of very different mechanical properties.

Since the response of the respiratory system seems to be strictly related to his dynamical features, in this work we aim at studying the mechanical features of newborns' respiratory

system through input and transfer impedance computation to obtain regional information about oscillatory pressure wave propagation.

To achieve this purpose the work has been subdivided into three phases.

First an experimental set-up for the analysis of the global and regional respiratory system mechanics in infants receiving HFOV is developed; specific algorithms are proposed for the computation of input and transfer impedance and for the compensation for the low-pass filtering effect of the measurement system.

An in-vitro study aimed at validating the use of FOT during HFOV at different frequencies is performed. In particular impedance spectra evaluated in response to the squared high amplitude pressure oscillations delivered during ventilation has been validated against standard FOT employing small pressure amplitude waves (about 2-4 cmH_2O).

In order to be able to perform the measurements with the monitoring tools routinely used in the clinical setting without connecting any additional device to the patient, a second in-vitro study was performed to characterize the frequency response of the pressure and flow measuring system employed in the clinical setting and to compensate for the filtering effect that it introduces.

Finally the real clinical study, which considers both the propagation of the pressure wave in the thoraco-abdominal compartments and the analysis in terms of impedance and regional transfer impedance.

The oscillatory pressure wave has to cross different regions with different mechanical properties during its propagation, so the lag between rib cage and abdomen compartments depends on the frequency set on the ventilator and the regional transfer impedance could give information about this mechanical changing in terms of resistance and reactance.

2. Physiopathology and mechanical ventilation

In this chapter is described the physiology of the respiratory system and its mechanical properties, including differences between infants and adults; then the mechanical parameters of interest for this study. This information is useful to understand the mechanical changes in preterm infants affected by different respiratory distress syndromes, described in the second part of the chapter.

Depending on the disease severity, newborns should be ventilated with invasive or non-invasive ventilation. This study focuses on the High Frequency Oscillatory Ventilation technique (HFOV), a protective ventilation way that employs supra-physiological breathing rates and tidal volumes frequently less than dead space.

To assess the lung function in infants receiving HFOV in this study it has been combined the Forced Oscillation Technique (FOT) and the Opto-Electronic Plethysmography (OEP).

The OEP technique measures chest wall displacement, total and compartmental lung volume changes, and, when combined with pressure measurements, allows the estimation of compartmental transfer impedance in a noninvasive way, while the FOT allows the assessment of the mechanical behavior of the respiratory system at the oscillating frequency.

2.1 PHYSIOLOGY OF THE RESPIRATORY SYSTEM IN NEWBORN

2.1.1 Mechanics of breathing

Birth represents a very delicate moment of transition during which some essential changes in cardio-pulmonary physiology happen. At birth, baby's lung is totally collapsed and still full of fluid and so the chest wall is highly compliant due to the poor stiffness of the rib cage. With first breaths a newborn tries to hold some air in his lung.
The typical respiratory pattern, as the adult one, can be divided into an inspiratory (air flowing into the lung) and an expiratory phase (air exits the lung).

Inspiration
Inspiration is determined by the contraction of the inspiratory muscles: the diaphragm and the external intercostal muscles.
The diaphragm is a thin sheet of muscle inserted into the lower ribs. While, at rest, is a dome-shaped muscle, as it contracts during inspiration, it flattens, pushing the abdominal contents downward and forward, therefore increasing the volume of the chest cavity (Figure 2.1). Moreover, the lower ribs are lifted and moved outward, causing an increase of the cross-section diameter of the thorax. The diaphragm acts on the rib cage directly through its insertion and indirectly by increasing abdominal pressure generating forces that tend to elevate and enlarge the lower rib cage. The effectiveness of the diaphragmatic action in changing lung volume depends on the transmission of this action from the lower ribs to the upper ones. This transmission depends on the compliance of the rib cage: if it is very compliant, motion of the lower ribs is not transmitted and paradoxical breathing occurs.
External intercostal muscles are located in between the ribs, extended forward and downward. As they contract the ribs rotate forward and upward and push the sternum in front. In this situation the antero-posterior diameter of the thoracic cage is increased and

therefore the volume of the thoracic cavity grows. The expansion of the thoracic cavity produces negative pressure in the intrapleural space, which induces gas to flow into the lung.

Thus, in the respiratory system there are two pressure generators: the diaphragm and the intercostal muscles. These two mechanical structures have a different behaviour with respect to the pleural pressure, so while one effect on exhalation, the opposite behaviour is had with the other. However, active muscles may respond passively to externally applied forces. The intercostal muscles have force-length characteristics that reduce the compliance of the rib cage and counter the forces resulting from the decrease in intrapleural pressure as the diaphragm contracts.

Expiration

Expiration, during quiet breathing, is a passive event because the main force driving it is the elastic recoil of the chest wall. This recoil refers to the tendency of stretch objects to return to their original shape and depends on surface tension, elastic properties of the tissues and bony elements of the rib cage. When the inspiratory muscles relax during expiration, the elastic elements of the chest wall, diaphragm and lungs, which are stretch during inspiration, recoil to their original shape (Figure 2.1).

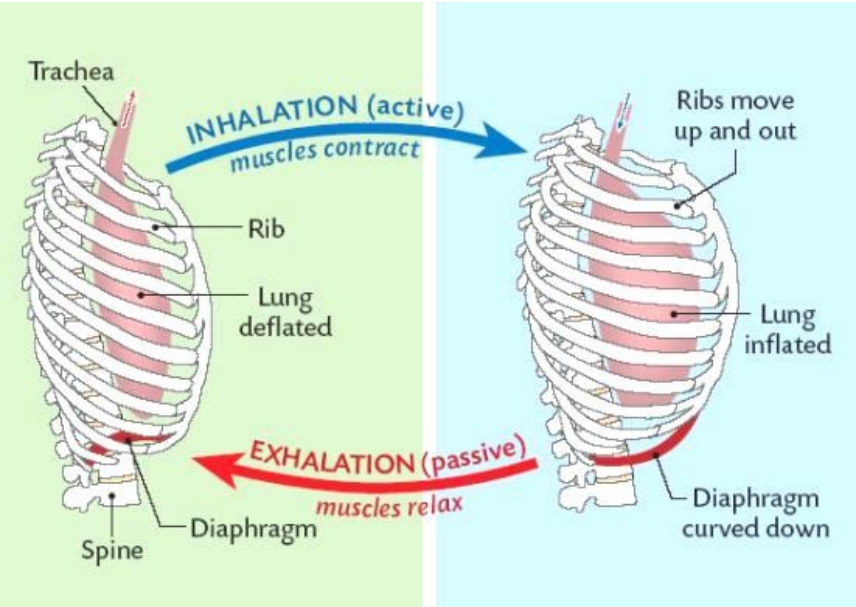

Figure 2.1 Inspiration-expiration cycle.[6]

The lung can expand its volume or decrease it thanks to the up and down movement of the diaphragm which enlarges or decreases the longitudinal axe of the rib cage and also thanks to the elevation of the costal, that changes the antero-posterior diameter of the thorax.
There are different definitions of lung volumes during a breathing manoeuvre (Figure 2.2).

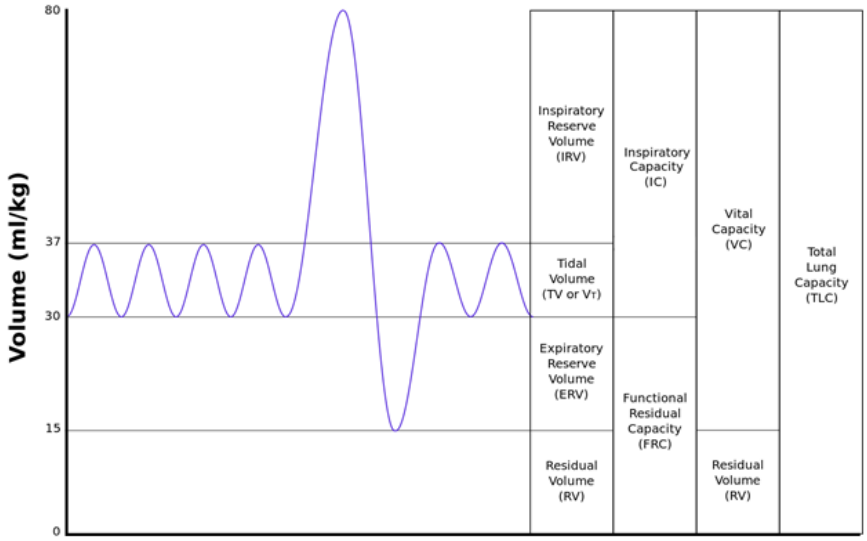

Figure 2.2 Lung volumes during a breathing manoeuvre

• TIDAL VOLUME (V_T) is the volume of a spontaneous breath.

• INSPIRATORY RESERVE VOLUME (IRV) is the maximum volume that can be inspired from an end-tidal inspiratory level.

• EXPIRATORY RESERVE VOLUME (ERV) is the maximum volume that can be expired from the end-expiratory level.

• RESIDUAL VOLUME (RV) is the volume of gas in the lung and airways after as much gas as possible has been exhaled.

• TOTAL LUNG CAPACITY (TLC) is the volume of gas in the lung and airways after as much gas as possible has been inhaled.

• VITAL CAPACITY (VC) is the volume of the deepest breath.

• FUNCTIONAL RESIDUAL CAPACITY (FRC) is the volume of gas in the lungs and airways either at the end of spontaneous expiration or at the resting volume of the respiratory system.

• INSPIRATORY CAPACITY (IC) is the maximum volume that can be inspired from the end-expiratory level.

2.1.2 Mechanical properties of the respiratory system

The mechanical behaviour of the respiratory system is usually described by the relationship between the pressures acting on the different subsystems that compose it, the volumes and the gas flowing inward and outward the system.

The lung increases its volume because of external forces acting on it and tends to return to its resting volume after distension. Elastic and resistive forces of the lung oppose the forces exerted by the respiratory muscles. The static pressure-volume curve describes the relationship between these forces at different levels of lung expansion (Figure 2.3).

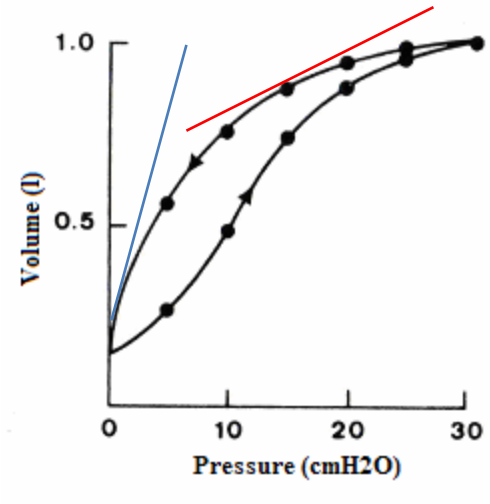

Figure 2.3 Pressure-volume curve of the lung.

The slope of the curve is known as *compliance* and describes the spreading capacity of the lung: the steeper the slope, the grater the 'distensibility'. At the lower end of the curve (low lung volume), the compliance is low, which means that there is a small change in volume for a large change in pressure (blue line). This region is below critical opening pressure so more pressure is required to open terminal airways and atelectatic alveoli. At the centre of the curve the compliance increases resulting in a large change in volume for a small change in pressure (red line).

This is where normal tidal breathing should occur because efficiency is maximal. At the upper end of the curve (high lung volume), the compliance decreases again and the slope gets flatter indicating that the lung gets stiffer. At high expanding pressures, in fact, the

lung is over inflated and opposes to further volume increaments. Applying additional pressure results in little additional volume which can induce airway injuries.

The compliance of the lung depends on its size: the bigger the lung, the higher the compliance.

In the pressure-volume curve of the lung inflation and deflation limbs are different: the lung volume at any given pressure during deflation is larger than during inflation. This behaviour is known as hysteresis and it is due to the fact that small airways close, trapping gas in the alveoli. Lung is expanded by forces generated by the diaphragm and the external intercostal muscles and recoils, thanks to elastic and surface tension forces. Because of its elastic properties, the lung tends to be empty, but this effect is balanced by an equal and opposed force generated by the rib cage.

The equilibrium configurations of the system are shown in the static pressure-volume curve (or relaxation curve), that describes only elastic properties.

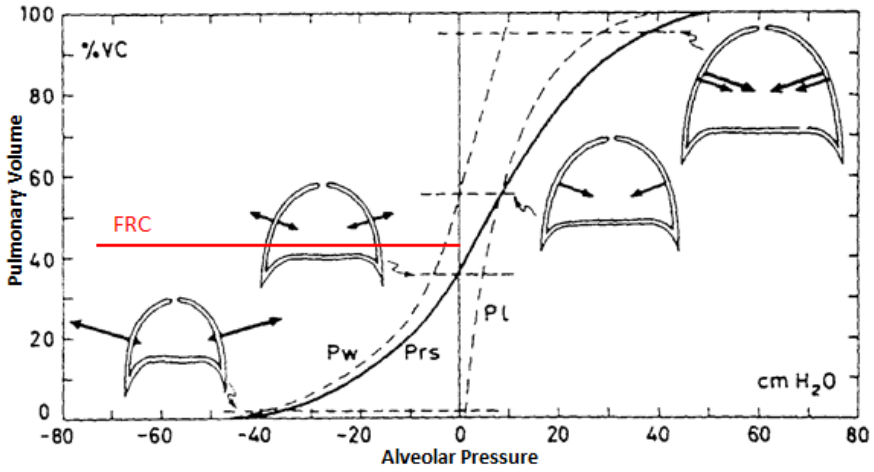

Figure 2.4 Static curves of the lung (PL), of the chest wall (PW) and of the lung-plus-chest wall (Prs). The slope of these curves is related to the compliance of the systems.

During inhalation, the strength generated by inspiratory muscles (diaphragm and external intercostals muscles) exceeds the elastic and surface tension forces (lung recoil), so that alveoli fill with air. During expiration, instead, the muscular component vanishes and lung recoil is greater than the chest wall forces, so that the lung tents to collapse and empty. As expiration is a passive mechanism, air flow stops when $P_{thoracical} = P_{pulmonary}$; it occurs in volumes equal to FRC, the resting point of the whole system.

This functional residual capacity (FRC) represents about 40% of the total lung capacity (TLC) and it allows the alveoli to remain partially extended.

2.1.3 The role of surfactant

An important factor in the pressure-volume behaviour of the lung is the surface tension of the liquid film covering the alveoli. Surface tension arises because the attractive forces between adjacent molecules of the liquid are stronger than those between the liquid and gas, with the result that the liquid surface area becomes as small as possible.

In the lung the surface tension is determined by the presence of the surfactant, a surface-active lipoproteine that improves gas exchange by increasing lung compliance.

Moreover stability of the alveoli is promoted and the work of the respiratory muscles is reduced.

When the lung is full of air, the further reduction of surfactant moves the P-V curves towards high pressures, so that at the same volume the pressure needed to reach that volume is higher than with tensioactive solution.

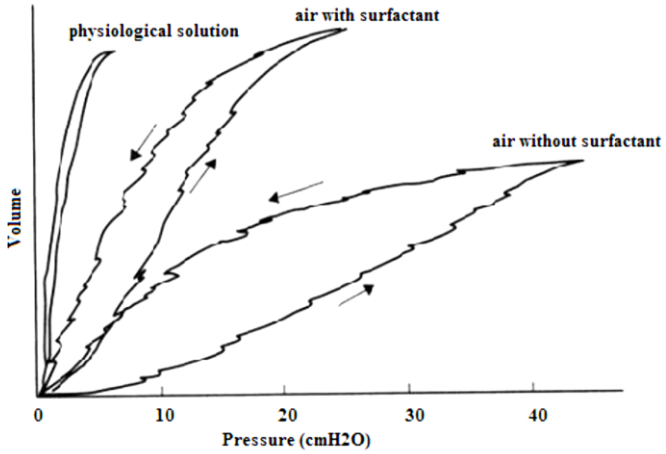

Figure 2.5 Comparison of the pressure-volume curve of the lung filled with physiological solution and with air, with and without surfactant.

Surfactant has another important role: it helps to keep the alveoli dry. In fact, the surface tension tends to collapse alveoli and to adsorb fluid into the alveolar space from the capillaries. The surface tension of alveoli reduces the hydrostatic pressure outside the capillaries by reducing surface forces surfactant prevents the transudation of fluid into the interstitium. So, the consequences of surfactant absence are several: increased surface tension, decreased compliance, presence of atelectatic areas and alveoli filled with transudate. All these are pathophysiological features typical in preterm infant with Respiratory Distress Syndrome (RDS).[7]

2.1.4 Mechanical parameters

Compliance

Compliance (C) is a measure of the change in volume (ΔV) resulting from a given change in pressure (ΔP):

$$C = \frac{\Delta V}{\Delta P} \quad [2.1]$$

Compliance is the mathematical inverse of elastance (E), the amount of pressure required to change the volume of the lung by a given amount.

The lung and chest wall are aligned in series, since pressure applied to the airway is first transmitted to the lung and from the lung, a reduced amount of pressure is transmitted to the chest wall. Because of this arrangement, the pressure to distend the respiratory system is the sum of the pressures required to distend the lung and the chest wall. Thus, the elastance of the respiratory system (E_{RS}) is the sum of lung elastance (E_L) and chest wall elastance (E_{CW}):

$$E_{RS} = E_L + E_{CW} \quad [2.2]$$

While the compliance of the total respiratory system (C_{RS}) can be obtained as follows:

$$\frac{1}{C_{RS}} = \frac{1}{C_L} + \frac{1}{C_{CW}} \quad [2.3]$$

where C_L is lung compliance and C_{CW} chest wall compliance.

Resistance

Resistance represents the opposition to flow due to frictional forces. The resistance of the respiratory system is the sum of viscous resistance and airways resistance. Viscous resistance is the resistance generated within the lung tissue and chest wall during inflation and deflation. Airway resistance is due to the relative movement between the gas molecules and the walls of the respiratory system. It is defined as the pressure gradient required to move gas through the airways at a constant flow rate. The standard formula is the following:

$$R = \frac{\Delta P}{\dot{V}}$$

[2.4]

Airways resistance depends on length and internal diameter of the conducting airways, on viscosity and density of the gas, on flow rate and on whether flow is laminar or turbulent. When flow is laminar, the pressure difference is linearly related to flow by a constant (K_1) being the resistance:

$$\Delta P = K_1 \dot{V}$$

[2.5]

In a single-tube system when flow is laminar, resistance (K_1) can be described by Poiseuille's law:

$$R = \frac{128 \mu L}{\pi I D^4}$$

[2.6]

Where μ is the viscosity of the gas and L and ID are length and internal diameter of the tube respectively. Resistance is directly proportional to the tube length and inversely proportional to the fourth power of the internal diameter, gas viscosity is negligible in the determination of airways resistance; so that, the internal diameter is thus the most significant determinant of resistance. In a multiple tube system, like the human lung, resistance depends on the total cross-sectional area of all the tubes. Although the individual bronchi decrease in diameter as they extend towards the periphery, the cross-sectional area of the airway increases dramatically.

2.1.5 Differences between adults and infants

Mechanics of breathing

Unlike the adult's thorax, which is ellipsoidal, the infant's thorax is almost cylindrical: the ribs extend horizontally from the vertebral column and the cross section of the thorax is circular. Because of these anatomical differences, the intercostal muscles in infants have shorter course and provide less mechanical advantage for elevating the ribs and increasing intrathoracic volume during inspiration than in the adults. Moreover, because the insertion

of the infant's diaphragm is more horizontal than in the adult, the lower ribs tend to move inward rather than upward during inspiration and this deflection is facilitated by the high compliance of the chest wall. The endurance capacity of the diaphragm is determined by muscle mass and the oxidative capacity of muscle fibers. Infants have low muscle mass and a low percentage of type I muscle fibers (slow-twitch, high oxidative fibers) compared to adults so, in order to sustain the work of breathing, the diaphragm must be provided with a continuous supply of oxygen. Respiratory muscles fatigue is a common cause of failure in premature infants. During unlabored inspiration the intercostal and accessory muscles serve primarily to stabilize the rib cage.

In the adult half of the total impedance of the respiratory system is due to the chest wall so about half of the force generated by the respiratory muscles is dissipated in moving it. From this point of view the highly compliant chest wall of the infant appears advantageous. As previously discussed in the respiratory system there are two pressure generators: the diaphragm and the intercostal muscles.

Inspiratory action of either one has an expiratory action on the other. The magnitude of this paradoxical motion depends on the relative compliances of the lung and chest wall, because the diaphragm acts on these in parallel and divides its displacement accordingly. The ratio of the passive compliance of the chest wall to the passive compliance of the lung in preterm infants is very high (about 6.7:1) and results in a division of the displacement of the diaphragm inadequate for ventilation. Distortion of the ribs is another way of stiffening the system and decreasing the active compliance in the very premature infant.

In premature infants elastic recoil is mainly due to surface tension and his synthesis is fast and the turnover rapid. Surfactant is formed relatively late in fetal life and babies without an adequate amount of that develop respiratory distress syndrome.

Functional Residual Capacity (FRC)

It is known that the FRC results from the static passive balance between the outward recoil of the chest wall and the inward recoil of the lung. In the infant the outward recoil of the chest wall is small, because the chest wall is very compliant, while the inward recoil of the lung is slightly lower than in the adult. Consequently, the newborn, especially the premature one, has a low FRC (about 10% of TLC), which seems incompatible with stability of the terminal airways and with adequate gas exchange.

This low FRC and the underdevelopment of the conductive airways structural support are responsible for airway closure and resultant gas trapping. Dynamic end-expiratory volume is substantially above the passively determined FRC and the respiratory system resting volume is close to the closing volume of the lung. The closing volume is the volume at which dependent lung regions cease to ventilate because the airways leading to them have collapsed. In the infant, in contrast to the adult, relaxed expiration is actively interrupted at high flow rates.

Compliance

Lung compliance is related to lung volume: the smaller the lung, the lower the compliance. Because measured compliance depends on the initial lung volume above which the compliance measure is made, comparisons should be normalized to FRC. Lung compliance divided by FRC is called *specific compliance* and is nearly identical for term infants and adults. In term infants, immediately after birth, specific compliance is low but normalizes as fetal lung fluid is absorbed and normal functional residual capacity (FRC) is established. In premature infants specific compliance remains low, due to persistent atelectasis and failure to achieve a normal FRC. Chest wall compliance is very high in the newborn compared to the adult because the ratio of cartilage to rib is higher, the cartilage is thinner and the bone is softer due to incomplete mineralization. In preterm infants (< 32 weeks) the compliance is about 6.4 ml/(cmH_2O*Kg), decreasing to about 4.2 ml/(cmH_2O*Kg) by term.

Resistance

In infants, viscous resistance is much higher than in the adult and may account for as much as 40% of total pulmonary resistance. The relatively elevated viscous resistance is due to higher tissue density (lower ratio of lung volume to lung weight) and to the bigger amount of pulmonary interstitial fluid. Although in absolute terms airways resistance is elevated in the newborn infant, the *relative resistance* (resistance times unit lung volume) is lower than in adults because the newborn's bronchial tree is shorter and that the inspiratory flow velocities are lower. The range of flow rates generated by spontaneous breathing newborns (including term and preterm infants) is approximately 0.6 to 9.9 l/min. Turbulent flow is produced in standard infant endotracheal tubes whenever flow rates exceed approximately

3 l/min in a 2.5 mm tube or 7.5 l/min through 3.0 mm tube. Average values of airways resistance in normal, spontaneous breathing newborn infants are between 20 and 30 cmH_2O*s/L, and these values increase dramatically in disease states.

Nasal airways resistance makes up two thirds of the total upper airways resistance, the glottis and the larynx contribute less than 10% and the trachea and the first four or five generations of bronchi account for the rest.[8 9]

2.2 INFANT RESPIRATORY FAILURE

Neonatal morbidity and mortality are in most cases consequences of respiratory diseases. It is estimated that 10-50% of all preterm newborns develop a respiratory disease. Pre-term babies are more frequently affected by respiratory diseases because of the immaturity of their respiratory system, that increases the probability of failing in adaptation. The most frequent respiratory diseases are Infant Respiratory Distress Syndrome, Meconium Aspiration Syndrome and Connatal Pneumonia.

2.2.1 Infant Respiratory Distress Syndrome (IRDS)

IRDS is the commonest respiratory disease in pre-term babies. It can be also named hyaline membranes disease (HMD) because of its pathologic features and it is due to structural and functional immaturity of the respiratory system.

About 1% of all newborns is affected by IRDS, but its incidence is inversely related to gestational age and birth-weight. Mortality is also rather high (about 10%) despite of the improvement of IRDS management in last decades.

Neonatal IRDS occurs in infants whose lung have not yet fully developed: the surfactant deficiency is the main reason because it causes an high alveolar surface tension, that leads to a failure to attain an adequate FRC and a tendency of the lung to become atelectatic. Moreover, a pre-term has an even more compliant chest wall than a term neonate.

With such a respiratory system, a baby needs very negative pressures at first breaths in order to open alveoli: his PV curve is unfair because of surfactant deficiency, alveoli have so high surface tension that they are unsteady and chest wall can't pull outward the lung because of its collapsibility. This results is an incapability to create and sustain a normal FRC.

Surfactant deficiency, along with small respiratory units and compliant chest-wall, produces also actelectasis and results in perfused but not ventilated alveoli, causing hypoxia. At the same time low lung compliance, small tidal volumes, increased physiologic dead space and insufficient alveolar ventilation induce hypercarbia.

Hypercarbia with the elevate work of respiratory muscles leads to acidosis. The combination of hypoxia, hypercarbia and acidosis produces local arterial vasoconstriction; consequently the increase of pulmonary resistances determines a reduction of lung perfusion that makes the lung susceptible to lung injuries.

Furthermore surfactant distribution is not homogenous in the lung of these neonates. Therefore, the alveoli which contain nearly normal quantity of surfactant can expand and maintain an end-expiratory volume. During following breaths, air flow tends to invest the least resistance way, that is the already opened alveoli. This leads to an hyper-expansion of some alveoli, to a collapse of the others and, in general, to a non-homogenous distribution of the gases in lung which results in tissue injury. Tissue injury, in turn, induces an inflammatory response that leads to produce hyaline membranes through the combination of sloughed epithelium, proteins and edema. Hyaline membranes make all the problems discussed above even more serious, generating a vicious circle.

Signs of respiratory distress (tachypnea, audible grunting, intercostals retractions, nasal flaring and cyanosis) usually appears few minutes after birth. Affected neonates often need resuscitation at birth, especially if their weight is less than 1000g.

The most serious cases are often related to pulmonary hypoplasia that is frequently due to midtrimester preterm premature rupture of membranes: the lack of amniotic liquid causes the impossibility of an adequate development of the lung.

The elements that may help to make IRDS diagnosis are: blood gas and acid-base values and radiographic findings.

Laboratory findings are initially characterized only by hypoxemia, later hypercarbia and acidosis take over.

It is very important that an adequate ventilation and oxygenation are established immediately to avoid vasoconstriction, atelectasis and ventilation-perfusion mismatch. The basic therapy consists of:

- Antenatal steroids: it is rather a preventing therapy.
- Surfactant replacement therapy: it is administrated via an endotracheal tube. It is important that an alveolar recruitment maneuver is done before and after the administration in order to have an adequate distribution of the surfactant.
- Oxygen therapy is very important, but PaO_2 and $Sat\%O_2$ must be controlled.

- Continuous positive airway pressure (CPAP): it is fundamental in order to help the baby to create and sustain a FRC.
- Mechanical Ventilation: the most serious patients must be ventilated mechanically. High Frequency Ventilation (HFV) is gaining more and more importance in the treatment of the early pathology.
- Inhaled Nitric Oxide (INO): if persistent pulmonary hypertension.[10 11]

2.2.2 Meconium Aspiration Syndrome (MAS)

Meconium aspiration syndrome (MAS) is defined as respiratory distress in an infant born through meconium-stained amniotic fluid (MSAF) with characteristic radiological changes and whose symptoms cannot be otherwise explained.

MSAF incidence increases after 42 weeks of gestation, nevertheless, only 2-9% of infants born with MSAF develop meconium aspiration syndrome. MAS accounts for about 10% of all cases of respiratory failure with 39% of mortality rate.

MAS results from aspiration of meconium during intrauterine gasping or during the first few breaths.

MAS pathophysiology is complex and includes several mechanisms:

- Acute airway obstruction: the thicker and the more the aspirated meconium, the more the obstruction. Airway obstruction could lead to both hyperinflation and atelectasis of the alveoli and defines an increase in airway resistances.
- Surfactant dysfunction or inactivation: Presence of meconium in the alveoli can inactivate the endogenous surfactant. This causes atelectasis and defines a lower lung compliance.
- Chemical pneumonia: Meconium is a good chemoattractant for neutrophils and source of proinflammatory mediators.
- Persistent pulmonary hypertension of the newborn (PPHN): 15-20% of infants with MAS are affected by PPHN because of pulmonary vasoconstriction secondary to hypoxia, hypercarbia and acidosis.

Moreover, meconium seems to inhibit the normal process of pulmonary fluid clearance leading to a difficult in lung adaptation to extra-uterine life.
Clinical manifestations are characteristic of respiratory failure: poor oxygenation, hypercarbia, acidosis, signs of respiratory distress.
Neonates with MAS have to be treated in Neonatal Intensive Care Unit. The treatment includes:

- Ventilation: about 40% of newborns with MAS needs mechanical ventilation; 10% requires continuous positive airway pressure (CPAP). High frequency oscillatory ventilation is theoretically advantageous; nevertheless no prospective randomized trials have compared HFOV and conventional ventilation in MAS yet.
- Surfactant therapy: bolus surfactant therapy seems to be associated with reduction in severe respiratory distress.
- Antibiotics: in case of bacterial pulmonary superinfection or sepsis.
- Inhaled Nitric Oxide: in case of PPHN.[12]

2.2.3 Connatal pneumonia

Congenital Pneumonia can be caused by several microorganisms, but the most common are Streptococcus Agalactie and Escherichia Coli.
Infectious pneumonia leads to widespread inflammatory changes in the lung with consolidation, edema and proteinaceous and/or hemorrhagic exudates; all these lead to difficulties in gas exchange.
Pneumonia could be complicated by sepsis that leads to hypotension ad acidosis, causing a reduction in pulmonary blood flow.
To treat these neonates antibiotic therapy and often mechanical ventilation are required.[13]

2.3 MECHANICAL VENTILATION

Irrespective of the technique or mode of ventilation chosen, the goals of mechanical ventilation are to achieve and to maintain an adequate pulmonary gas exchange, to minimize the risk of lung injury and to reduce patient work of breathing. Depending on the disease severity, neonates should be ventilated with invasive or non-invasive ventilation.

In newborn non-invasive ventilation consists of continuous positive airway pressure (CPAP) applied with nasal prongs or tubes (Nasal CPAP) since he is a nasal breather. During CPAP, a continuous positive pressure is applied at the airways: in this way closed alveoli are recruited and kept open. Moreover, CPAP seems to produce a more regular breathing pattern in preterm infants.

Even if non-invasive ventilation is preferred whenever possible, in more serious respiratory failure invasive ventilation is required.

The term "conventional" is used to distinguish this genre of tidal ventilation from high frequency ventilation: the former uses a range of physiological frequencies (lower than 1 Hz) and a gradient of pressure to fill the lungs with air, as in a physiological breath. In this way gas exchange is obtained by convective fluid motion; the latter works on a positive continuous pressure on which pressure oscillations are superimposed at high frequency (8-20 Hz). Convective motion is not the only factor that influences gas exchange (see sub-chapter below).

The main problem of neonatal conventional ventilation is the ventilator induced lung injury (VILI) that can be due to too high pressure or too high tidal volume.[14 15 16]

2.3.1 Ventilator Induced Lung Injury (VILI)

During mechanical ventilation, traumatic injuries are very common in neonates with RDS: normal patients have stable alveoli and ventilation determines small changes in their size. Conversely sick alveoli are unstable and tend to have excessive size changes, which create such a shear stress that leads to alveolar injury.

Four different types of lung injuries can occur:

- Atelectrauma: loss of alveolar recruitment is both a consequence and a cause of lung injury. Surfactant deficient alveolar units are prone to collapse, so, at each breath, they are recruited and derecruited.[17] This implies a moderate shear-stress that conduces to an important signaling and then to the lung injury.[18]
- Barotrauma: manifestation of extra-alveolar air during mechanical ventilation due to high pressure lung injury.[19]
- Volutrauma: it is a lung injury caused by a regional overdistension of alveoli and airways. It is the large tidal volume to determine alveolar stretch and to cause damage to the pulmonary capillary endothelium, the alveolar and airway epithelium and the basement membranes; pressure per se is not involved.
  Preterm's susceptibility to volutrauma is high because of his numerous risk factors: infections, antenatal exposure to inflammatory mediators, surfactant dysfunction, high chest wall compliance, antioxidant deficiency and malnutrition.
- Biotrauma: it is an inflammatory damage supported by cytokines and chemical mediators, whose production is stimulated by mechanical injuries. Therefore, it represents the final common way of all the injures above.[17]

In order to avoid all these injuries scientists and clinicians are working to develop some strategies and ventilator set-up optimization in order to reduce the incidence and the severity of VILIs.

2.3.2 High Frequency Oscillatory Ventilation (HFOV)

High Frequency Oscillatory Ventilation is, right now, the standard of care in patients with severe lung diseases that are hospitalized in NICU (Neonatal Intensive Care Unit). HFOV is a non-conventional ventilation that employs supra-physiological breathing rates and tidal volumes frequently less than dead space.
Around a constant pressure (Continuous Distending Pressure –CDP– or Mean Airway Pressure –MAP–) the ventilator creates oscillations at high frequencies. The active expiratory phase is a unique characteristic.

2.3.3 Gas transport and gas exchange during HFOV

Different mechanisms of gas exchange during HFOV are demonstrated: bulk convection, asymmetric velocity profiles, pendelluft, cardiogenic mixing, Taylor's dispersion, turbulence, molecular diffusion and collateral ventilation.

The role of bulk convection in HFOV is less than in conventional ventilation, but it is quite important to the ventilatory exchange in most proximal gas exchange units.
We talk about convective flux whenever a pressure gradient is imposed on the gas, and it can be described by *Poiseuille's law*:

$$Q = \frac{\pi d^4 \Delta P}{128 \upsilon l} \qquad [2.7]$$

Where: Q is the gas flow rate; d is the airway diameter; ΔP is the pressure difference; υ is the viscosity and l is the airway length.

The bulk of air can move along the airway as a laminar or as a turbulent flow; it depends on Reynolds number (Re).

$$Re = \frac{velocity\ x\ diameter}{viscosity} \qquad [2.8]$$

Moving down along the respiratory tree, the airways diameter reduces and so Re does. Therefore, a turbulence flow develops in upper airways, while a laminar one develops after 4th-generation bronchi.

Table 1: Differences between laminar and turbulent flow

Laminar Flow	*Turbolent Flow*
Parabolic velocity profile.	Flattened velocity profile.
Peak flow velocity 2 times the mean velocity.	Peak flow velocity 1,2 times the mean velocity.
If viscous forces > inertial forces.	If convective inertia > viscous forces.
At low flux velocity.	At high flux velocity.

Regardless of the velocity profile, when the ventilator generates a pressure gradient the bulk of air travels down along the airway with a higher velocity at the center. At the midpoint of the oscillatory cycle the pressure gradient reverses and the bulk of air is pushed back. The final result is that 50% of the air remains centered on the starting point, 25% comes back and 25% goes down. Over many cycles the fresh air is progressively smeared along the airways at their center. Conversely alveolar air gets to the open airways by peripheral travelling. This creates a radial concentration gradient for all gases, mainly oxygen and carbon dioxide, that defines the so called augmented diffusion.

Bifurcations or curvatures of the respiratory tree modify the air flow velocity profile. As fresh air flows through a bend or a bifurcation, it acquires a secondary radial flow that skews the velocity profile making it more prominent closely to the outer airway wall; it doesn't happen to the expiratory velocity profile, therefore an asymmetry between inspiratory and expiratory profile is configured. This phenomenon permits the fresh gas to stream toward the alveoli along the inner airway wall, while the alveolar gas to be streamed away from alveoli along the outer wall.

The combination of augmented diffusion and axial convection defines Taylor's dispersion. Some of the enhancement in gas exchange during HFOV is also attributable to pendelluft: the out-of-phase exchange of gas between parallel compartments. At high ventilatory frequencies, between 7.5 and 20 Hz, alveolar expansion is asynchronous, with phase differences between lobes and between lobe regions: it means that some alveoli are directly

ventilated, while some others are filled out-of-phase with air from in-phase-ventilated alveoli.

A small part of gas transport is also due to collateral ventilation and cardiogenic mixing. The former is permitted by the presence of non-airway connections between neighboring alveoli. The latter happens because of the superimposition of the rhythmic and strong contractions of the heart that promote peripheral gas mixing inducing collateral ventilation. Finally molecular diffusion is the most important gas exchange mechanism in the alveoli. It depends on the ceaseless random motion of the gas molecules (Brownian motion) and the concentration gradients of the gases: the flux is proportional and directionally opposed to gas concentration.[20 21]

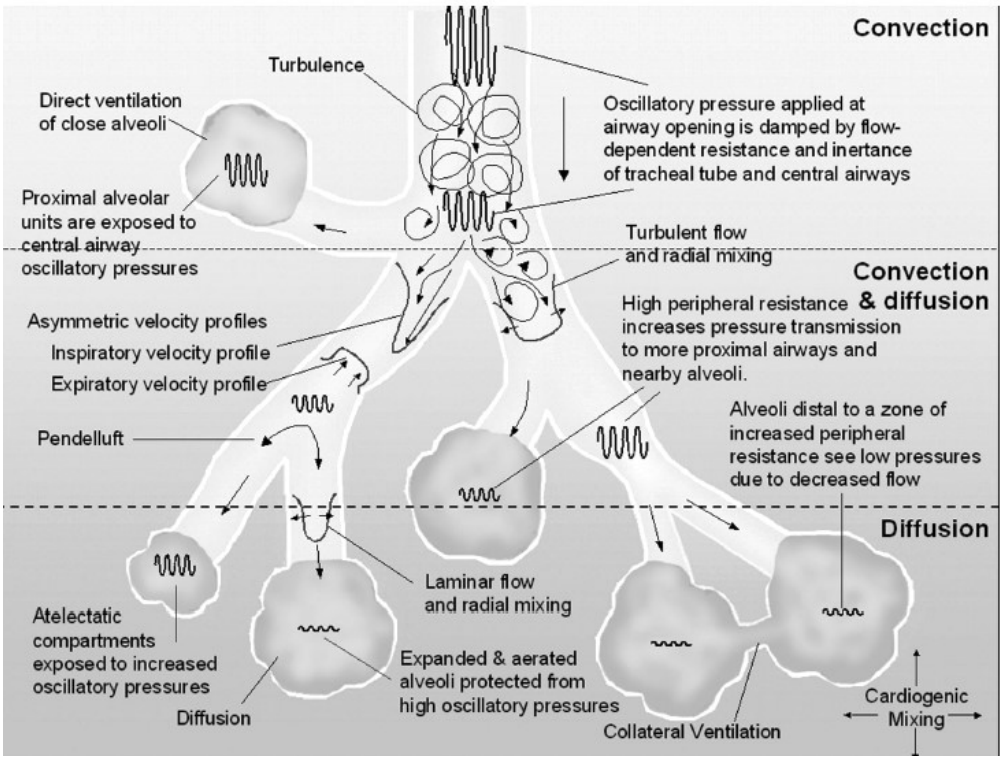

Figure 2.6 Gas transport mechanisms and pressure damping during high-frequency oscillatory ventilation (HFOV). The major gas-transport mechanisms operating during HFOV in convection, convection– diffusion, and diffusion zones include: turbulence, bulk convection (direct ventilation of close alveoli), asymmetric inspiratory and expiratory velocity profiles, pendelluft, cardiogenic mixing, laminar flow with Taylor dispersion, collateral ventilation between neighboring alveoli, and molecular diffusion. The extent to which the oscillatory pressure waveform is damped is influenced by the mechanical characteristics of the respiratory system.[21]

2.3.4 Respiratory mechanics during HFOV and clinical optimization methods

In order to have a successful ventilation a correct setting of the ventilator is fundamental. The clinician has to set up:

- Continuous Distending Pressure (CDP);
- Frequency (f);
- Peak-to-peak pressure (P/P pressure);
- Fraction of inspired oxygen (FiO2);
- Inspiratory/expiratory time ratio (TI/TE).[2]

The aims are:

- Keeping the lung opened and improving oxygenation;
- Obtaining an adequate gas exchange at low intrapulmonary pressure amplitude and low tidal volume.

Keeping the lung opened and improving oxygenation

Continuous Distending Pressure (CDP) recruits alveolar units and maintains lung volume. It must be set at the lower value necessary to maintain alveoli opened; during HFOV the correct CDP value can be obtained through alveolar recruitment maneuver.

Alveolar recruitment maneuver is based on the nonlinear behavior of the lung during inflation and deflation, which configures the hysteresis phenomenon. For the same pressure the lung can have two different volumes depending on the respiratory phase in which pressure is given: according to Young-Laplace law ($P = 2\gamma/r$, where P is pressure, γ is surface tension and r the alveolar radius), once opened, lung units can maintain this state with lower pressures then those required for recruitment (Figure 2.7). This is even more true in RDS diseased lungs.[22]

There are several strategies to define the optimal CDP (CDPO). The most used is the one based on oxygen saturation: during recruitment the lung is over-distended by increasing CDP (till the opening point); then it is deflated till the alveoli collapse (closing point). The optimal CDP is just above the collapse value on the deflation limb.[23]

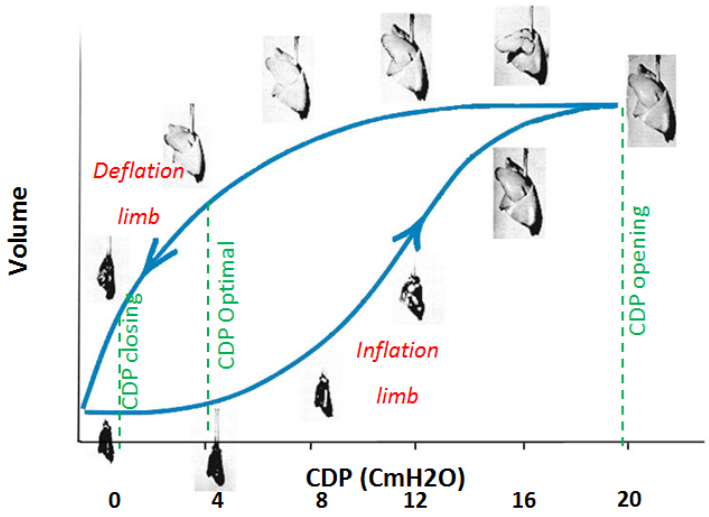

Figure 2.7 Alveolar recruitment.

Other strategies consist of: prediction of CDPO from the static P-V curve (CDPO is 6 cmH_2O above the curve flex)[24]; evaluation of oxygenation index (it reaches a minimum when CDP is optimal because the shunt is very small)[25]; the oscillatory pressure ratio technique (it is the ratio of pressure swings at distal and proximal ends of TT. When this ratio reaches a minimum the lung compliance reaches the maximum and it define the CDPO)[26]; the electrical impedance tomography (it permits to evaluate changes in regional lung aeration and then to define the CDPO)[27]; measurement of inductance by RIP (Respiratory inductance plethysmography)[28]; measurement of reactance by FOT.

An optimal CDP allows the clinician to obtain both a protection from VILIs (barotrauma and atelectrauma) and a better oxygenation: lung recruitment permits to have a low FIO_2 value ($FIO_2 \leq 0.25$), which is important to minimize the incidence of ROS injuries.[29]

Finally, since CDP is closely dependant on lung stiffness and mechanical properties, a frequent review of CDP is required to avoid overdistention or atelectasis with the development (improvement or worsening respectively) of the pathology. Therefore, the future is a continuous monitoring of lung mechanic which permits automatic CDP adjustments in real time.[28]

Adequate gas exchange at low intrapulmonary pressure amplitude and low tidal volume

The use of high frequencies is crucial to obtain both an adequate CO_2 release and a reduction in VILIs. Newborn respiratory system can be defined overdamped, therefore the resonant amplification is attenuated and the proximal pressure swings are always greater than those distending distal alveoli. It provides distal alveoli to be protected from barotrauma.

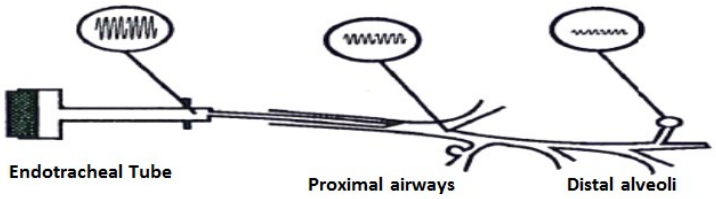

Figure 2.8 Dumping of the oscillations along the respiratory tree.[30]

In order to protect alveoli and small airways located at short distance to the central airways, a low peak-to-peak oscillatory pressure must be set. High frequencies succeed in reducing intrapulmonary pressure amplitude: the amplitude of the swings per unit of flow at the carina is, by definition, the magnitude of the lung impedance (Z). Increasing frequency till the lung resonance frequency ($f0$) a reduction of Z and, then, of the pressure amplitude are obtained. The most of reduction is, however, obtained at lower frequencies than corner frequency (fc), the point at which the lowest pressure-excursion is required to get an optimal ventilation without air-trapping Figure 2.9.[30]

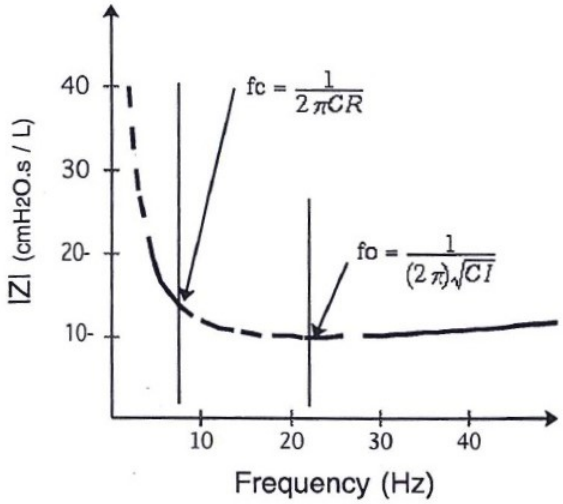

Figure 2.9 Lung impedance (Z) versus frequency for typical parameters in a normal newborn model. Parameters: Compliance, C=0.002 L/cmH_2O; Resistance, R=10 cmH_2O/L·s; Inertance, I=0.025cmH_2O/L·s^2. For these parameters the corner frequency (f_c) and resonance frequency (f_0) are 8 and 22 Hz respectively. Note that Z has a minimum at $f=f_0$, but most of the drop occurs for $f<f_c$.[3]

This strong negative frequency-dependence of Z reflects the decreasing contribution of tissue elasticity to the pressure cost of flow.

During RDS the lung is smaller and stiffer than a normal lung. Since corner frequency depends on lung size and lung compliance, in RDS fc shifts to an higher frequency, so Z reduction continues to be realized at higher frequencies than in normal lungs (Figure 2.10). From this the advantageous possibility of using HFOV to treat RDS.[31]

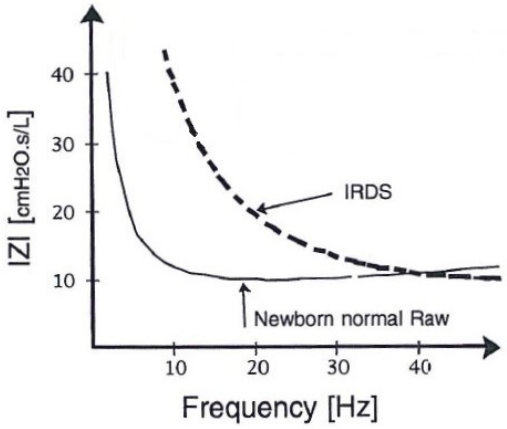

Figure 2.10 Comparison of Z vs. f plots of models of newborns with normal and RDS lungs**.** The solid line represents the curve for a normal baby; the broken line refers to an infant with RDS having only 40% of alveoli recruited.[3]

Finally, CDP has to be considered in order to choose the best frequency because it is the most important determining factor in the lung size.[32] Moreover, as Figure 2.11 shows, Z is low for fewer f -PEEP combinations during RDS than in a normal lung.[32]

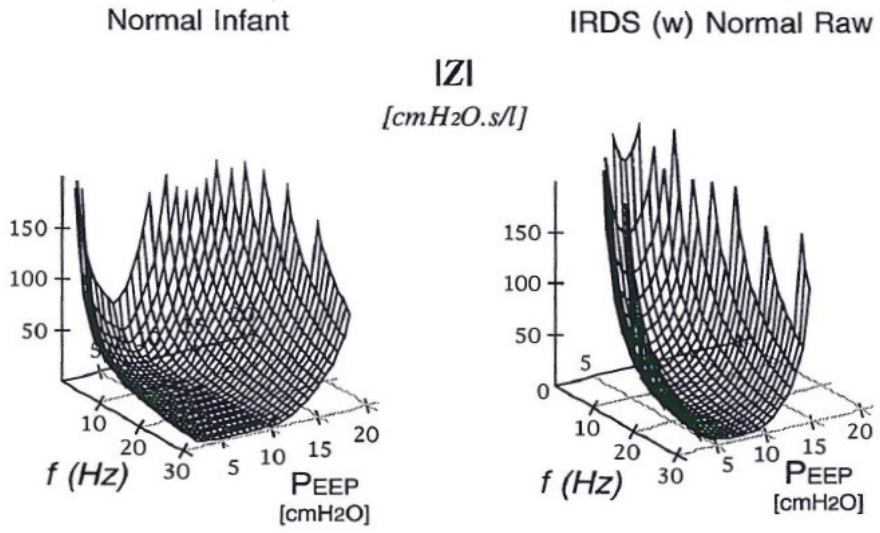

Figure 2.11 Surfaces of carinal oscillatory pressure cost of flow (Z), including the effects of changes in PEEP. Plots are represented for a normal newborn and a RDS affected infant having 40% of alveoli recruited.[3]

Whereas, in order to reduce volutrauma HFOV uses low tidal volume. The target is $VT < 2$ ml/kg (1.5-2.5 ml/kg), that is even less than the dead space volume. Carbon dioxide exchange in HFOV is dominated by tidal volume (VT) and oscillatory frequency (f) according to the equation:

$$DCO_2 = f \times {V_T}^2$$

[2.9]

Equation 2.9 clearly shows that VT has a greater influence on DCO2 than f; it had already been qualitatively demonstrated by Slutsky et al. who compared DCO2 with the oscillatory flow ($\dot{V}_{osc} = V_T \times f$).[33]

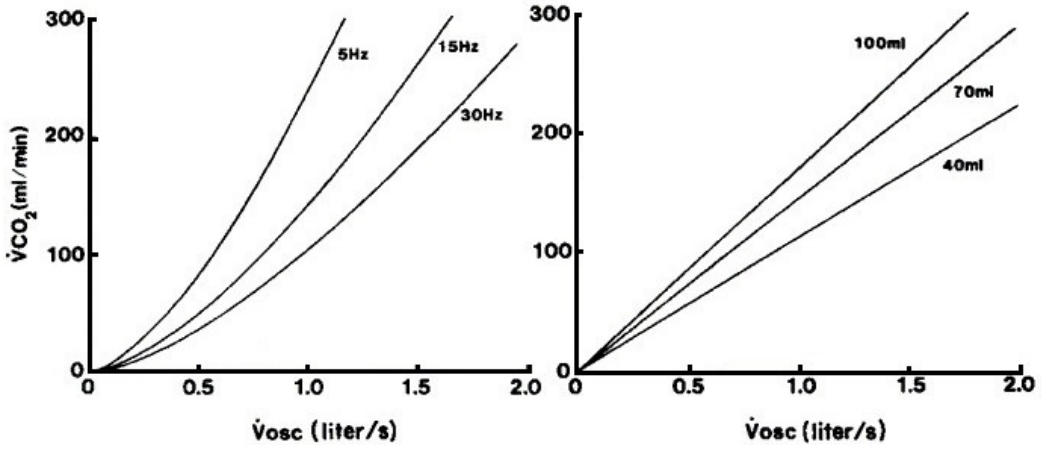

Figure 2.12 : $\dot{V}CO_2$ vs. $\dot{V}osc$ at constant values of frequency (left) and tidal volume (right) in a dog. Note that there is a linear relationship between frequency and $\dot{V}CO_2$ (right panel); while there is an almost exponential relationship with V_T changes (left panel), that is even more relevant for low frequencies.[33]

Therefore, if a low VT is required, an increase in frequency is necessary to maintain an adequate DCO2.

Moreover, studies conducted on dogs demonstrate that a more homogeneous gas distribution is achieved at high frequencies, almost regardless of regional compliance differences. In fact, it seems to be more affected by resistances, respiratory tree geometry and chest wall mechanics than by lung compliance.[34] [35]

In conclusion, frequency is very important in HFOV, it affects other parameters as P/P pressure and VT and it can't be set regardless CDP. For this reasons it seems to be quite difficult to find the optimal frequency in clinical practice, also because there are no clinical

strategies available to estimate fc. Therefore, in clinical practice it seems reasonable to set the frequency at the highest value consistent with adequate peak amplitude and tidal volume. The most common values are: 15 Hz for < 1500 g of weight neonates and 10 Hz for ≥ 1500 g of weight neonates.[36]

Tidal volume is another crucial parameter in HFOV. Only a few ventilators can set a guarantee VT, in the other cases the tidal volume results from the setting of parameters such as:

- Peak-to-peak pressure amplitude: it should be adjusted to the lowest value to obtain normocarbia and visible chest wall vibrations. It is strongly influenced by frequency and, in clinical practice, it is generally accepted that P/P pressure has not to be more than three-times the CDP value.[33]

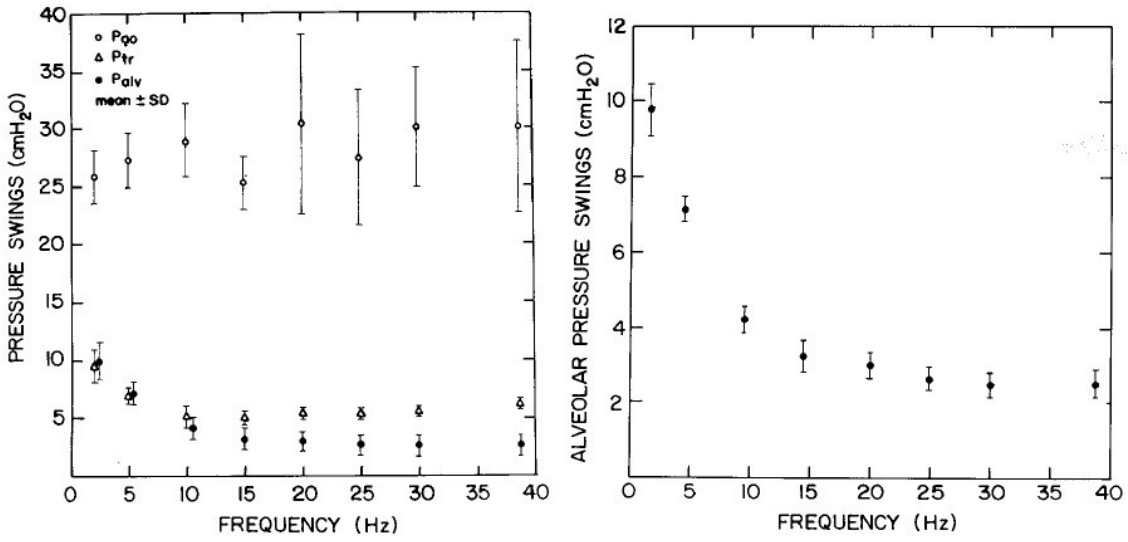

Figure 2.13 Relationship between pressure swings and frequency in rabbits during HFOV. The left panel represents pressure swings at airway opening (Pao), at trachea (Ptr) and in alveoli (Palv). Pressure swings at the airway opening are relatively constant with increasing frequency, while those in trachea and alveoli tend to fall. It is clearer for alveolar pressure swings showed in the right panel, where an increase in frequency is always matched with a reduction in alveolar pressure swings, at least for clinical used frequencies.[37]

- Endo-tracheal Tube diameter (ETT): the smaller is the internal diameter of the tube, the higher is its resistance and the lower V_T will be.

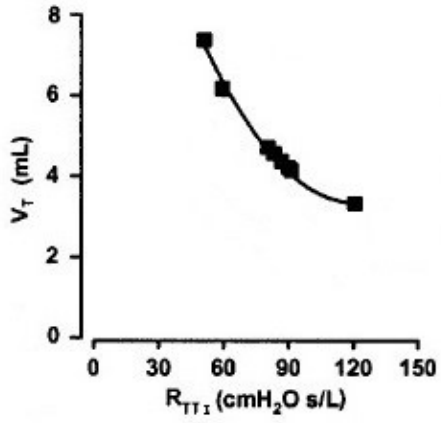

Figure 2.14 Relationship between ETT inspiratory resistances and V_T. In order to obtain an increase in resistance Pillow et al. used ETTs with diameter range between 4 and 2,5 mm. (Modified from Pillow et al.)[30]

Therefore, an adequate choice of ETT diameter and length is fundamental in clinical practice and whenever an unexpected drop in tidal volume occurs, an obstruction of the endotracheal tube have to be supposed: it represents, in fact, the most frequent cause of resistances increase.[30]

- Inspiration / Expiration ratio (I/E): it affects the P/P pressure and so the V_T. Pillow et al. demonstrate that with I:E=1:1 alveolar pressure is substantially equal to airway open pressure; on the contrary the pressure gradient is high when I:E=1:2.

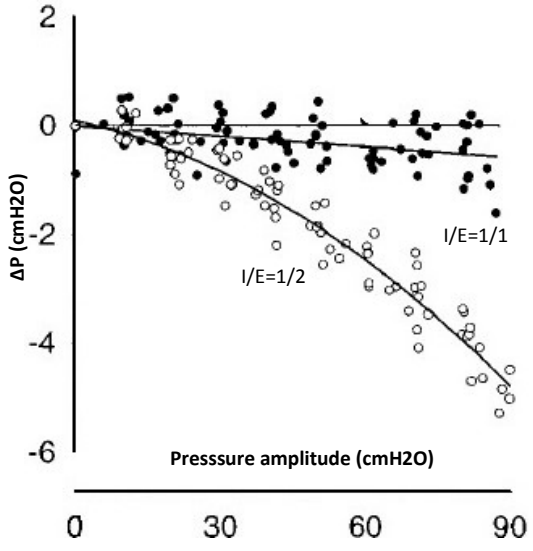

Figure 2.15 Pressure amplitude variations related to I:E ratio in a rabbit lung model. White points represent measurements with I/E=1/2. Black points represent measurements during I/E=1/1 ventilation. ΔP represents the pressure gradient between alveoli and open airways; note that it is much represented for I:E=1:2.[38]

The same study proves that no air trapping is associated with I:E=1:1. Nevertheless, in clinical practice an inspiratory time of 50% is not widely used yet, also because some ventilators have not the possibility of setting the I/E time ratio.[38]

- Piston position: it is usually kept in a central (neutral) position; nevertheless the left position leads to an higher V_T.[39]

Moreover V_T depends on some patient characteristics:

- Peripheral lung resistances: V_T is inversely related to peripheral resistances as Figure 2.16 shows.

  This situation develops in Meconium Aspiration Syndrome (MAS), BPD and interstitial emphysema, during which reductions in frequency and P/P pressure are needed to avoid lung injuries.

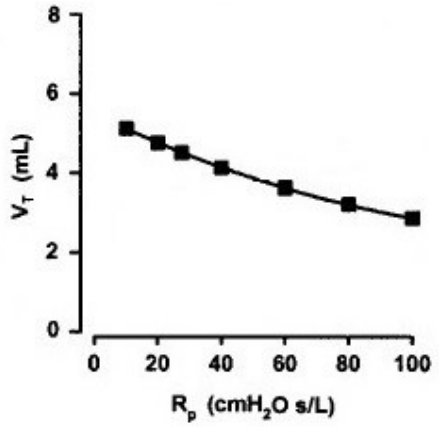

Figure 2.16 Relationship between peripheral resistance and V_T. (Modified from Pillow et al.)**.**[30]

- Lung compliance: compliance doesn't affect V_T so much in HFOV; the higher the frequency, the less the influence of compliance on V_T (Figure 2.17).

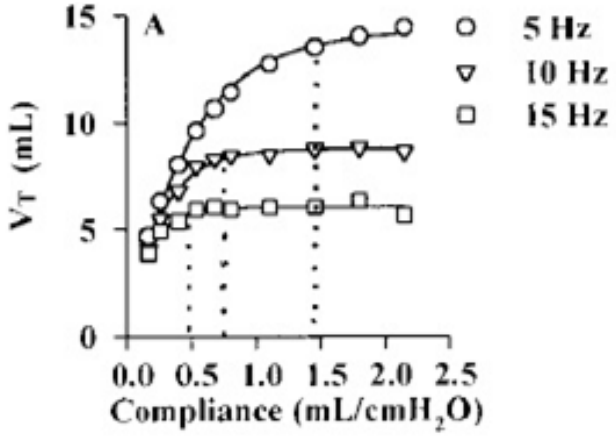

Figure 2.17 Relationship between compliance and V_T.[40]

2.4 MEASUREMENT TECHNIQUES IN RESPIRATORY MECHANICS

Nowadays, several techniques to assess the lung function in ventilated patients are available. Imaging techniques, like Computed Tomography (CT) and Electrical Impedance Tomography (EIT), are useful to evaluate the regional aeration, but the first doesn't allow a continuous monitoring and the latter allow only a regional measurement (a slice view).

Others techniques focus on lung volume measurement: Respiratory Inductive Plethysmography (RIP) and Opto-Electronic Plethysmography (OEP); both are useful to determine the absolute volume changes, but the RIP technique has a lower accuracy than the OEP.

There are several techniques to evaluate the static respiratory mechanics, but they are not suitable to our purpose: they could be used to evaluate the continuous distending pressure, but they are useless to test oscillatory frequency.

Interrupter Techniques (IT) and Forced Oscillation Technique (FOT) are the commonly used techniques to assess the dynamic respiratory mechanics, but the IT is not compatible with high frequency oscillatory ventilation.

For this reason the Forced Oscillation Technique (FOT) and the Opto-Electronic Plethysmography (OEP) are the most suitable techniques to carry out our study.

2.4.1 Forced Oscillation Technique (FOT) and Respiratory Impedance

Given the importance of respiratory system properties, it is right to study them in depth. Forced oscillation technique (FOT) is a simple and minimally invasive method used to study the mechanical properties of the respiratory system by measuring its response to an external applied forcing signal.[41]

When DuBois introduced it in 1956, high-frequency and low-amplitude pressure oscillations (about 2cmH_2O) are required. Recently Dellacà et al. demonstrated that those

measurements can be equally obtained using the oscillations given by the ventilator during HFOV, which are characterized by higher pressure amplitude.[42]

The relationship between pressure and flow is nonlinear in the respiratory system but it can be possible to consider its linearization around a work point in order to analyze the behaviour of the system using tools for studying linear systems.

In this way it is possible to define the transfer function between two variables, one chosen as input and the other one as output and to use it to evaluate the mechanical properties of the respiratory system.

When considering pressure (P) as output and flow ($\dot{V}$) as input we obtain the impedance:

$$Z_{rs}(f) = \frac{P(f)}{\dot{V}(f)}$$

[2.10]

Impedance is a complex term that includes different features: resistance (R), inertance (I), and compliance (C), as described in Equation 2.11:

$$Z_{rs} = \frac{P_{ao}}{\dot{V}_{ao}} = R_{rs} + j\left(\omega I_{rs} - \frac{1}{\omega C_{rs}}\right)$$

[2.11]

where j is an imaginary unit and ω the pulsation.

It can be divided into two parts: a real part that is represented by resistance (R_{RS}), and an imaginary part that is named reactance (X_{RS}) and depends on inertance and compliance. Resistance describes the dissipative mechanical properties of the respiratory system, whereas reactance is related to the energy storage capacity that is determined by both elastic properties and inertive properties of the system.

The same concept expressed in equation 2.12 is also the base of the equation of motion of the respiratory system:

$$\mathrm{P_{ao}} = \frac{1}{\mathrm{C}_{RS}}\mathrm{V} + \mathrm{R_{RS}}\dot{\mathrm{V}} + \mathrm{I}_{RS}\ddot{\mathrm{V}}$$

[2.12]

where V, $\dot{V}$ and $\ddot{V}$ represent end-expiratory lung volume and its time derivates, flow and acceleration, respectively.

Besides, different parts of the respiratory system contribute, with their own properties, to create the general properties of the respiratory system we referred above. Therefore, a deepen speculation should divide at least the contributes from airways and pulmonary parenchyma. DuBois et al. did it by creating an electrical analogous modeled as a T-network. It is a two port system in which one port represents the airway opening, while the other is the body surface.

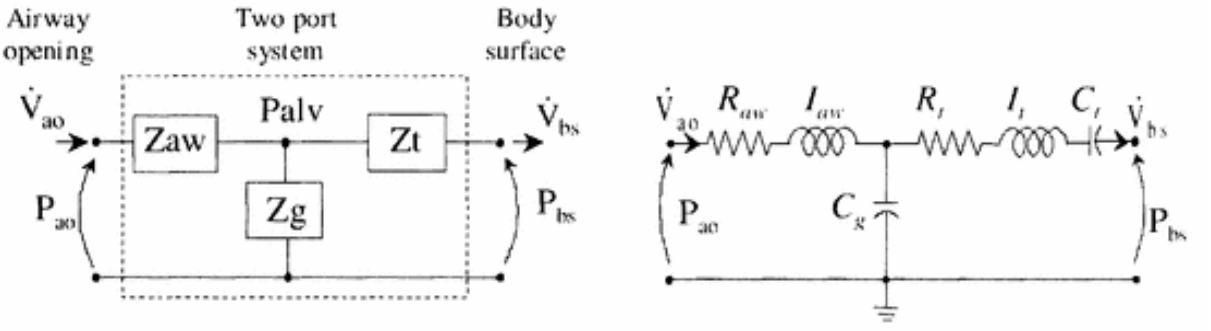

Figure 2.18 Two port T-network model of the total respiratory system and its development. $\dot{V}_{ao}$, airway opening flow; P_{ao}, pressure at the airway opening; P_{alv}, alveolar pressure; $\dot{V}_{bs}$, body surface flow; P_{bs}, body surface pressure; Z_{aw}, impedance of the airways; Z_t, impedance of lung tissues; Z_g, impedance of gas. R_{aw} and I_{aw} are resistance and inertance of airways respectively; C_g is the gas compliance; R_t, I_t, C_t are lung tissue resistance, inertance and compliance.[41]

This is a linear lumped parameter model where the tissue properties are described by the relative resistance, compliance and inertance, *Zaw* is composed of the correspondent resistance and inertance (because in the model the airways compliance can be neglected) while a capacitor element (Cg) accounts for gas compressibility. Lungs and chest wall impedance (Zt) are submitted to the difference between alveolar (PA) and perithoracic pressure (Pbs). The alveolar gas impedance (*Zg*), which is compressible, is submitted to the difference between alveolar and atmospheric pressure. Airways impedance (*Zaw*) are submitted to the difference between airway opening and alveolar pressure.

Each port has its own Z and the total impedance (Z_{RS}) can be computed using this physical formula:

$$Z_{rs} = Z_{aw} + \frac{Z_t \cdot Z_g}{Z_t + Z_g}$$

[2.13]

Figure 2.18 represents the electrical analogue of panel a. Note that different Z has not always the same components: different features are negligible in different districts. Considering the airways (input port), for example, the impedance is composed by resistance and inertance. The former is due to the airways diameter, the latter represents the acceleration of gas along the airways that is closely related to the wall stiffness. At the output port, instead, Z is composed by resistance, inertance and capacity of the lung tissue. Resistance is due to the alveolar diameter, inertance to the alveolar stiffness, while the capacity represents the alveolar compliance which is related to the elastic properties of the alveolus.

Finally, the impedance on the shunt pathway is a capacity that corresponds to the gas compliance in terms of gas compressibility. Because of this pathway, input flow differs from output flow.

Figure 18 also shows that different pressure gradients lead flow in different districts: the airways are submitted to the difference between airway opening and alveolar pressure; the compressible gas is submitted to the difference between alveolar and atmospheric pressure; while the lung tissues are submitted to the difference between alveolar and perithoracic pressure.

For a two port system like that two different mechanical impedances can be defined. The input impedance of the respiratory system Z_{in} is then obtained as the spectral relationship between pressure and flow (defined positive if entering the port) both measured at the airways opening when the stimulus is imposed to the same side, while the transfer impedance (Z_{tr}) is obtained when the oscillations are imposed and pressure and flow are measured at different sites of the respiratory system. The expression for Z_{in} and Z_{tr} are the following:

$$Z_{in}(f) = \frac{P_{RS(f)}}{\dot{V}_{ao}(f)} \qquad [2.14]$$

$$Z_{tr} = \frac{P_{bs}}{\dot{V}_{ao}} \text{ or } Z_{tr} = \frac{P_{ao}}{\dot{V}_{bs}} \qquad [2.15]$$

where Pao and Vao are respectively the pressure and flow measured at the airways opening while Pbs and Vbs are respectively the pressure and flow measured the body surface. Since

Zin and these two variants of Ztr are affected differently by the parallel elements of the respiratory system, such as alveolar gas compressibility and upper airway wall movements, they can be selected or combined to obtain more reliable estimates of the airway and tissue impedance.

If the measured system is linear, the two expressions above for Ztr must be equivalent. During FOT, forcing air through open airways or generating a pressure at the chest wall at different frequencies, it is possible to assess the features of the different compartments.

At low frequencies total compliance (C_{RS}) is much influent than inertance (I_{RS}); this means that the whole system behavior is largely determined by the recoil of the respiratory and parenchymal tissues. In such situation, reactance X_{RS} is negative and the pressure wave is rapidly damped, therefore the proximal airways can be studied.

At high frequencies (as during HFOV), instead, inertance prevails on compliance. Thus, reactance is positive and pressure wave can reach the alveoli. Therefore, the alveolar properties can be studied in this way.

Finally, there is a frequency for which compliance equals inertance (the imaginary part becomes zero) and the pressure cost of flow is related only to the respiratory system resistances. This is called resonant frequency (f_0):

$$\mathrm{f_0} = \frac{1}{2\pi\sqrt{\mathrm{C}_{rs}\mathrm{I_{rs}}}}$$

[2.16]

At the resonant frequency the pressure waveform is not dumped but amplified along the respiratory tree, the impedance reach a minimum and FOT could record an exact measurement of the resistances.[41 43 44]

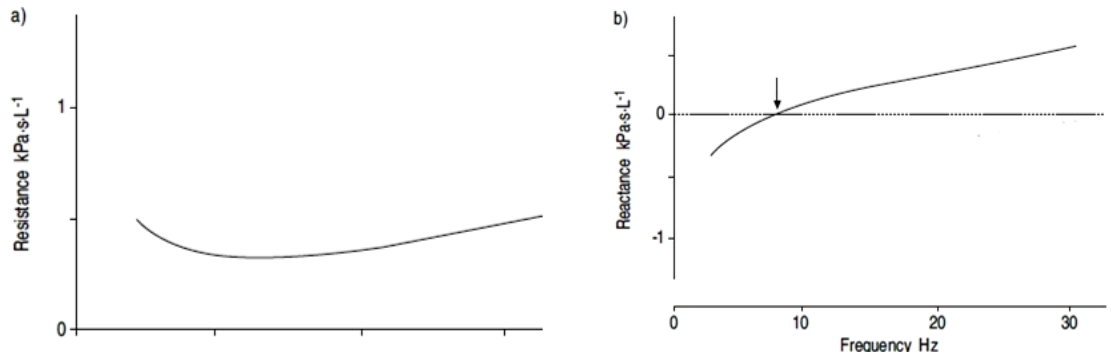

Figure 2.19 Resistance (R) and reactance (X) vs frequency**.** The indicator shows the resonant frequency.[44]

2.4.2 The Opto-Electronic Plethysmography (OEP)

The study of respiratory mechanics and control of breathing ideally requires an accurate and noninvasive measurement of lung volume changes (ΔV_L) not interfering with patients' spontaneous activity. Unfortunately, the currently available methods for the measurement of ΔV_L in infants present several intrinsic and unresolved limitations (see introduction to paragraph 2.4).

Optoelectronic plethysmography (OEP) is a novel noninvasive bedside monitoring technique capable of continuously measuring global and regional changes in lung volumes, which correlate well with intrathoracic changes in air content and ventilation.

OEP (OptoElectronic Plethysmograpy) by *BTS*® is based on the analysis of the movement of a series of reflective markers positioned on the thoraco-abdominal surface of the patient during the breathing. The position of the markers is detected by some infrared cameras and, through the use of advanced algorithms and mathematical models, the system provides an accurate measurement of the thoraco-abdominal wall volume and its variation during breathing.

OEP does not require a connection to the airway opening or subject-specific calibration procedures. It provides an accurate measurement of the chest wall volume and it allows, through the use of subsets of the markers placed on the thorax, the measurement of separate compartments, such as the rib cage, abdomen, or smaller components.

Moreover it can provides information about asynchronies or any asymmetries in the action of the respiratory muscles. Being based on the direct measurement of chest wall volumes, OEP is not affected by integration drift and can be used to track breath-by-breath volume changes.

Recently OEP studies have been performed in respiratory field related to lung volume changes in mechanical ventilated patients and chest wall kinematics during breathing.[45] This technique has proved to be reliable in adults in different postures and conditions[5], in particular Table 2 lists the authors and theirs studies about OEP clinical applications.

Table 2 Clinical studies on patients affected by respiratory disease using optoelectronic plethysmography

Authors	*Aim of the study*
Dellacà et al.	To test the ability of OEP to monitor changes induced by PEEP in lung volumes of mechanically ventilated patients.
Aliverti et al.	To evaluate the feasibility of using OEP in patients admitted to an Intensive Care Unit and report preliminary results regarding the distribution of chest wall volume.
Chiumello et al.	To quantify volume changes and to investigate the mechanisms of pressure-volume curve in patients with acute lung injury and acute respiratory distress syndrome
Aliverti et al.	To analyse the effects of different parameters of pressure support in ventilation pattern, kinematics of the chest wall and its compartments and the work of breathing in patients with acute lung injury.

OEP System solves many problems of traditional plethysmographic technology, because it does not require the body box and the mouth connection, it is a completely noninvasive procedure that allows the analysis in different patient positions and in special situations such as during sleeping and during mechanical ventilation.

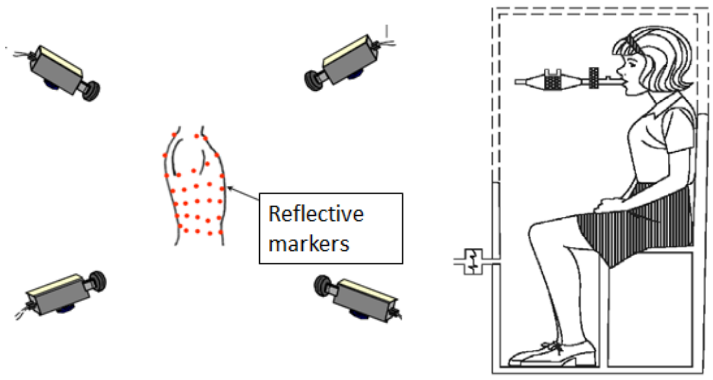

Figure 2.20 Different setup for respiratory mechanics measurement. A) optoelectronic plethysmography, B) traditional plethysmography with the body box.

Moreover, it can be used for measurements on newborns because of its characteristics:

- easy to use and non-invasive for the patient (intensive care, sleep, children...);
- suitable for a prolonged measurement (it doesn't suffer of drift problems);
- can be performed in any posture (sitting, supine,..) and under any experimental condition (rest, exercise, sleep);

- does not require any connection with the patient, like a mouthpiece or a facial mask that could reduce the subject mobility, alter the natural pattern of breathing or introduce additional dead space;
- volume measurement is not influenced by ambient factor (temperature, humidity and gas composition);
- does not require a specific calibration for each patient;
- provides an accurate measurement of the different compartments of the chest wall (pulmonary rib cage, abdominal rib cage, abdomen, eventually split into their right and left parts).[46 47]

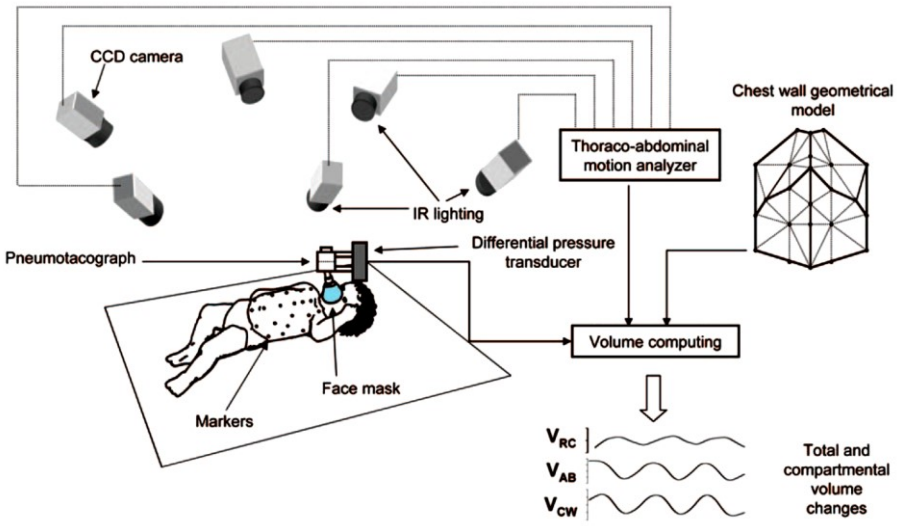

Figure 2.21 Experimental setup for the application of optoelectronic plethysmography in newborns.

3. Instrumental settings and data analysis

The aim of the present study was to map lung mechanics, chest wall kinematics and gas exchange in infants receiving HFOV at different oscillatory frequencies (5 Hz, 8 Hz, 10 Hz, 12 Hz, 15 Hz).
At each frequency the following measurements were performed:

- respiratory system input impedance
- chest wall displacements
- global and regional lung volume changes
- total and regional transfer impedance

The following paragraphs will describe in details the set-ups and the data processing methods that have been used for each of the measurements mentioned above.
Once Optimal CDP has been identified, the next phase is the correlation of the thoraco-abdominal wall kinematics (in terms of pressure oscillations transfer function) to the gas exchange at different oscillatory frequencies.
Five different oscillatory frequencies (5 Hz, 8 Hz, 10 Hz, 12 Hz, 15 Hz) are randomly tested and when a new frequency has been set, the P/P pressure is regulated to adjust V_T in order to maintain DCO_2 constant.

3.1 SET UP

3.1.1 Set up overview

Neonates are studied in supine position on the resurrection cot (Infant Warmer V-505, Atom®). This is provided with a ceramic infrared lamp which permits the baby to be heated during the study.

A schematic representation of the set-up is shown in figure 4: the instrumental settings include the high frequency oscillator (Sensormedics), the flow and pressure monitor (Florian), the transcutaneous monitor (TCMcombiM) and the OEP settings (cameras and workstation). Moreover a standard monitor (DataScope®) is connected to the baby in order to provide SpO_2, HR and blood pressure.

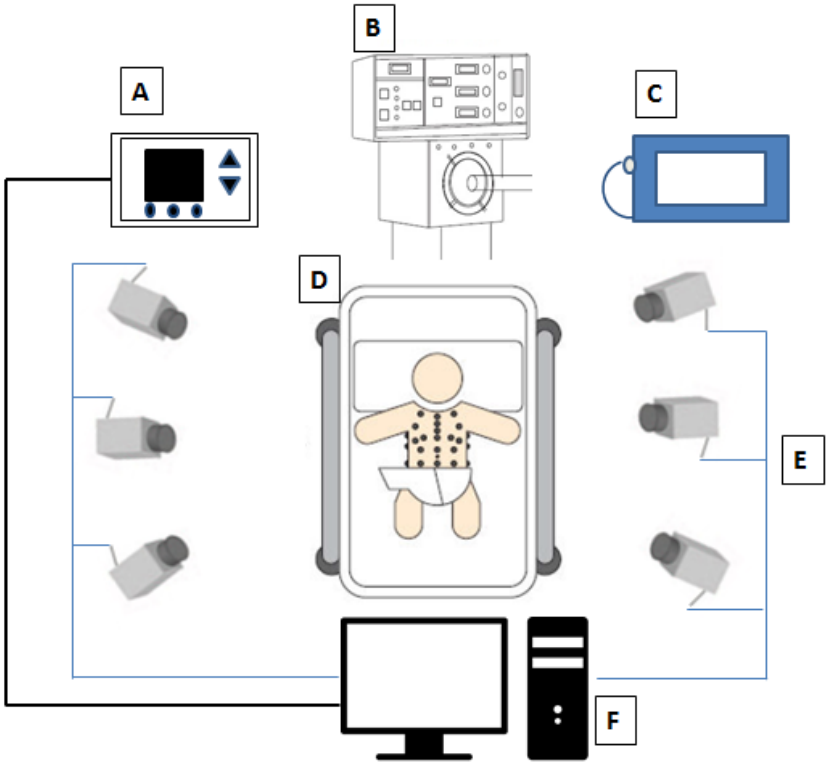

Figure 3.1 Clinical study setting: A) Florian monitor, B) SensorMedics oscillator, C) transcutaneous monitor, D) infa warmer with schematic marker configuration, E) OEP cameras, F) OEP workstation.

The oscillator (SensorMedics)

The pressure oscillations are delivered by the ventilator that supports the respiration. The ventilator choosen for the study is the SensorMedics 3100A which is the most commonly used during neonatal high frequency ventilation. This ventilator uses a linear motor to oscillate a column of bias flow gas. The column of gas is oscillated via the movement of a plate connected to a rubber diaphragm. The plate is attached to a coil which is suspended within a permanent magnet. When the coil is excited, the plate moves because of the electromagnetic effects on the coil and causes an oscillating pressure wave depending on the driving current through the coil and the induced magnetic field.

The driving signal is a square wave of adjustable frequency, amplitude, offset and duty cycle. Frequency can be set between 3 and 15 Hz, pressure amplitude is adjustable to more than 90 cmH_2O, mean air pressure can be set between 3 and 45 cmH_2O and duty cycle can vary between 30% and 50%.

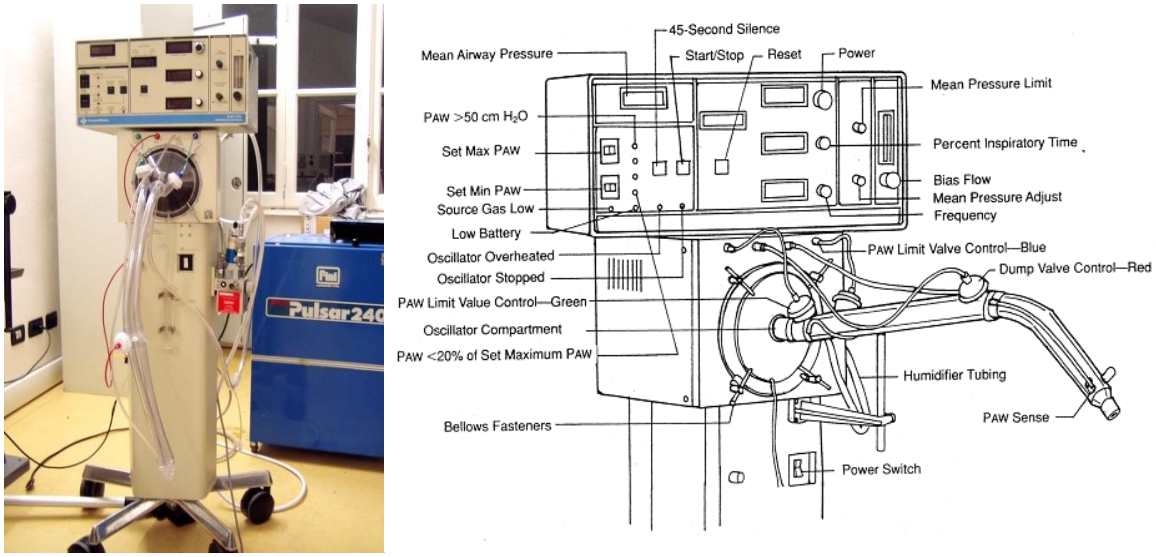

Figure 3.2 The SensorMedics 3100A high-frequency oscillatory ventilator.

The Airway Pressure Monitor processes the instantaneous airway pressure measurements of its pressure transducer to derive the following:

1. Mean airway pressure (P_{aw})
2. Oscillatory peak, minus oscillatory trough pressure (ΔP)

Mean Airway Pressure is essentially an arithmetic mean of the airway pressure measurement. It is obtained by filtering the instantaneous pressure signal with a DC to 0.5 Hz low pass filter.[48]

The ΔP reading is obtained by subtracting the oscillatory pressure from the peak pressure. The pressure data obtained with a T tube near the diaphragm are not reliable because of the low-pass filtering due to the internal tubes and valves that connect the pressure generator to the gas circuit; this mean that the frequency response is altered by the mechanical circuit of the ventilator, which causes a low-pass filter effect. For that reason it has been applied a specific correction explained in the next paragraphs (see Chapter 4).

Florian Monitor

Pressure and flow are measured at the inlet of the tracheal tube with a commercial monitoring system (Florian, Acutronic Medical Systems, Switzerland) commonly used in clinical practice to monitor neonates in HFOV with Sensormedics ventilator.

The airflow is measured by a hot-wire anemometer, while the pressure is measured just above the anemometer where is crated a Y-line leaving from the ventilation circuit and connecting to both Sensormedics and Florian. This configuration permits the ventilator to monitor pressure given to the patients and, in the same time, the Florian to display pressure curve to the clinician.

Figure 3.3 Neonatal respiration monitor Florian, Acutronic Medical Systems.

The Florian uses a small, low dead space plastic sensor that is adapted to the endotracheal tube (ETT) close to the patient and thanks to his high sensitivity even to volumes as small as 0.5 ml it is suitable for monitoring the respiration of neonates.

The advantage of the sensor location is that the inspiratory and the expiratory flow of the breath gases can be picked up completely and thus the exhaled volumes can be measured and displayed. Any continuous flow in the tube system does not affect the measuring method, also influences of compressible volumes (tube system, humidifier, etc.) are excluded.

The LCD screen of the Neonatal Respiration Monitor Florian shows a graphical representation of the patient's breath pattern together with calculated numeric data.[49]

Flow, volume and pressure are displayed and updated in near real-time as Waves or Loops graphics.

On the rear panel there is an analog output to record flow and pressure signals: this output was connected to the OEP working station to record simultaneously the cameras' data and the analogical data, too. The signals are sampled at 240 Hz and recorded by using the analog inlets of the workstation.

Data coming from the Florian monitor are recorded on a personal computer and used to compute respiratory system impedance by the forced oscillation technique. The use of the HFOV ventilatory waveform for the estimation of oscillatory mechanics has been already validated[42] at 5 Hz. In the present study the possibility to use the same approach to study the impedance spectrum has been validated *in vitro* against standard FOT (see chapter 4 for details).

Transcutaneous PaO2 & PaCO2 Monitor

During the whole study oxygen and carbon dioxide are continuously monitored by using a transcutaneous device (TCM CombiM, Radiometer®, Copenaghen, Denmark).

Figure 3.4 TCM CombiM. Transcutaneous device that provides oxygen and carbon dioxide values.

It provides a real-time value of transcutaneous oxygen ($PtcO_2$) and carbon dioxide ($PtcCO_2$) by heating a little patch of skin (till 44.5°C). In this way O_2 and CO_2 flows through the superficial strata of the skin are promoted and they succeed in reaching a cutaneous chemical sensor that measures their arterial partial pressures.

In standard conditions, TCM has an accuracy of 3 mmHg in evaluating $PaCO_2$ and 2.25 mmHg in evaluating PaO_2.[50]

Before the beginning of the study we calibrate the system by comparing monitor values with a capillary blood-gas-analysis. The sensor can be used for 2 hours continuously, then another calibration is needed. Since the duration of the protocol, including the part of the inflation-deflation trial, is greater than 2h, more calibrations have been necessary within the same study.

OEP system

The study of respiratory mechanics in infants requires a non-invasive accurate measurement of the lung volume changes (V_L). Optoelectronic Plethysmography (OEP) is a non-invasive technique, which estimates chest wall volume (V_{cw}) by measuring the three-dimensional position of several reflective markers placed on the patient's thorax.

This acquisition system consists of six cameras for detection of passive markers positioned on the subject. Cameras emit light with IR wavelengths (850 nm) and receive the same wavelengths reflected by passive markers made from hemispheres of 5mm of diameter, covered by aluminum powder. The system workstation allows the acquisition and integration of the kinematic data acquired with a frequency up to 60Hz.

Figure 3.5 BTS Bioingeneer optoelectronic hardware, in particular a) 2 infrared cameras and the computer; b) reflective markers. In this study are used the hemispherical ones (the latters).

Optoelectronic systems are usually supplied with software suitable for biomechanical analysis of the movement. The most important package, created by BTS company is the SMART-SUITE® consisting of 3 programs: SmartCapture, SmartTracker, SmartAnalyzer.
The SmartCapture software allows the acquisition ad storage of 3D marker tracks and it requires a calibration procedure to set the cameras' parameters before starting.
The calibration procedure is necessary whenever the spatial arrangement of cameras is deliberately or accidentally changed and it is usually performed before each acquisition.
The procedure consists of two phases (Figure 3.6):

- Axes Sequence, which fixes the position of the reference triad given by the laboratory, so that subsequent acquisitions have a common origin and the same coordinate system;
- Wand Sequence, in which an axis is moved within the acquisition volume up to the boundaries of the work volume. The work volume is defined as the physical space in which the movement will be made, in our case, the space needed to patient to perform breathing.

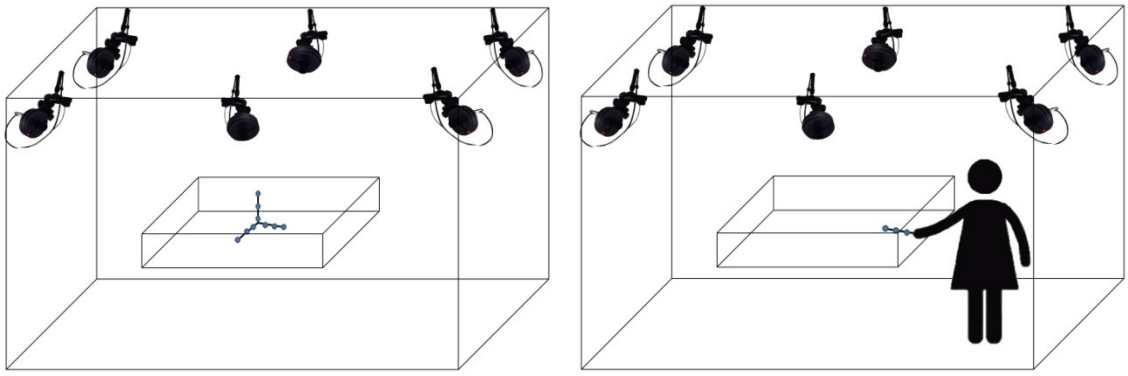

Figure 3.6 Calibration procedure. The left panel represents the axes sequence; on the right the wand sequence.

In the software there is a calculation algorithm which allows to generate the calibration volume, minimizing the error in the determination of the angular position of the markers. After this procedure, the system is ready to capture images: only the signals of markers and their movements will be shown on the screen and the signals coming from outside are considered sources of error.

The maximum acceptable error in the calibration procedure has been decided arbitrarily to have a mean less than 0.4mm and standard deviation less than 0.4mm; in this way it is ensured an optimal accuracy in the field of view of the cameras.

The SmartTracker software is an interactive graphical environment that allows to reconstruct the two-dimensional data acquired by cameras and those from the calibration in order to obtain a three dimensional image, the movement and the path of each single marker. It also allows to label for each marker, established through an appropriate model. Details of tracking procedure and model are described in next paragraph.

Newborn preparation

To apply OEP in supine newborns, 24 hemispheric reflective markers (6 mm diameter) were positioned on the anterior thoraco-abdominal surface from the clavicles to the anterior superior iliac spines at the intersection between predefined vertical and horizontal lines (Figure 3.7).

Six horizontal lines were designated for placing the markers:

a. the clavicular line;
b. the nipples;
c. the xiphoid process;
d. the lower costal margin;
e. umbilicus;
f. superior iliac spine.

With this positioning five vertical lines are formed:

a. a midline (along the sternum and continuing caudally below the xiphoid through the umbilicus),
b. two parasternal lines
c. two midaxillary lines.

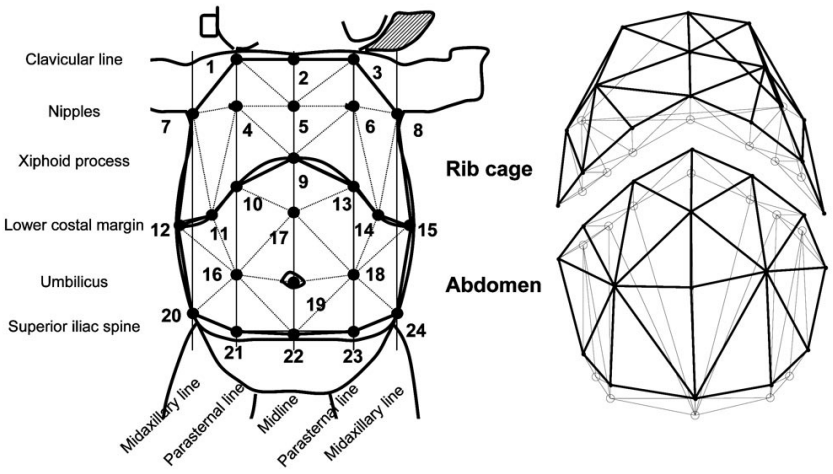

Figure 3.7 Markers positioning and geometrical model for OEP measurement in newborns. *Left panel*: Markers' positioning and chest wall compartments for optical analysis in newborns in supine position. *Transverse lines*: clavicular line; manubriosternal joint, lower costal margin, and anterior superior iliac crest. *Craniocaudal lines*: midsternal line (extended to the abdomen), the midpoints of the interval between the midsternal and the midaxillary lines; and two midaxillary lines. *Right panel*: Three-dimensional model of the chest wall from one representative model. *Black thick lines*: triangles connecting real markers (*solid circles*); *gray lines*: triangles connecting to at least one "virtual" marker (*open circles*). The two compartments are drawn separately by introducing an offset on the craniocaudal direction for clarity.[51]

In order to better outline the costal margin, two markers were added between the parasternal and the midaxillary lines. Similarly, in order to increase marker density in the abdomen, one more marker was added between the xiphoid process and the umbilicus.

The markers were placed on the skin using bi-adhesive hypoallergenic tape.

The three-dimensional position of each marker was measured by an automatic optoelectronic motion analyzer (OEP System, BTS, Milan, Italy) at a frequency rate of 60 Hz using six specially designed infrared video cameras provided with infrared flashing light-emitting diodes.

Cameras were positioned so that each marker was simultaneously seen by at least two cameras to reconstruct their three-dimensional position and displacement during respiration by stereo-photogrammetric methods. Three cameras were placed on one lateral side about 1 m from the bed. Three additional ones were placed symmetrically on the other side of the bed. The four cameras on the corners were placed about 70 cm above the subject while the two in the middle were placed 1.1 m above the subject; all of them were slanted downward. The operative calibrated volume was large enough to include the whole trunk of the infant lying on the bed.[51]

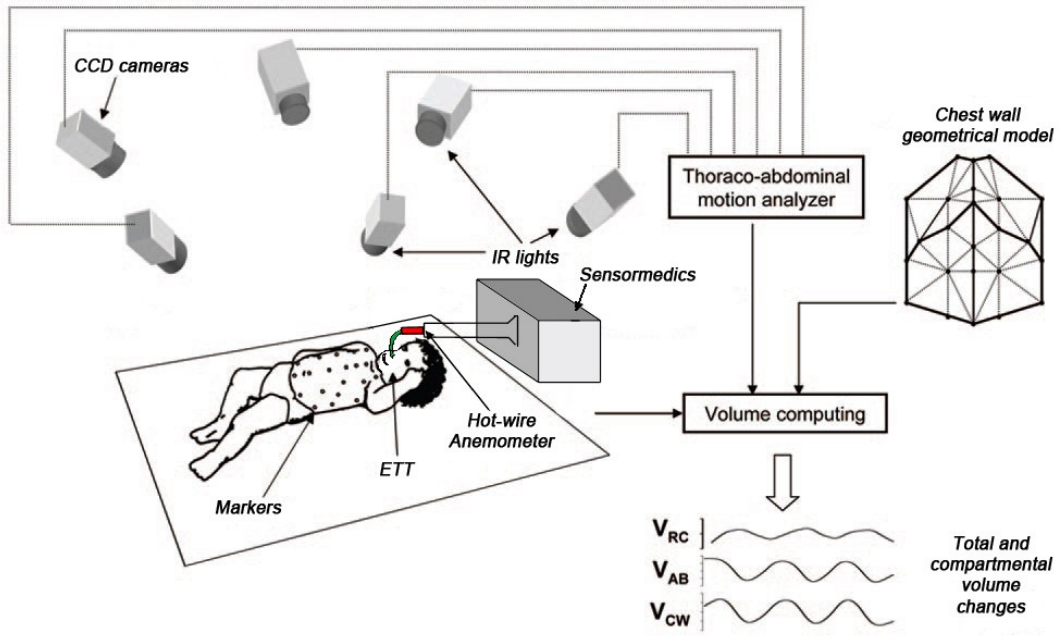

Figure 3.8 Experimental setup for the application of optoelectronic plethysmography in newborns. (Modified from Dellacà et al.)[51]

3.1.2 Set-up shrewdnesses for early preterm neonates

During acquisitions some problems occur if the subject is a very preterm baby. All those problems are related to their very immature skin for which they can be assimilated to burnts victims. So this delicate skin leads the baby to a rapid loss of temperature and the surface-volume ratio is unfavorable; for this reason the major risk for the baby is dehydration if not kept in an adequate environment.

A normal neonatal incubator can maintain baby's body temperature at a physiological value (about 36,8-37°C) and can even reach a relative humidity of 95-97%, but it is a close reflective environment that causes optical distortion phenomena during cameras' acquisition such as refraction or diffraction of IR rays.

These problems are caused by the curved shape of the incubator's cover; so a custom-made cover has been produced to make the cot environment more similar to an incubator, but without the optical distortion and refraction inconveniences thanks to his orthogonal shape. It has been decided to make it with Plexiglas® for its resistance, transparency and its

acceptable weight. Nevertheless, this material has a low transmittance for a large range of infrared waves.

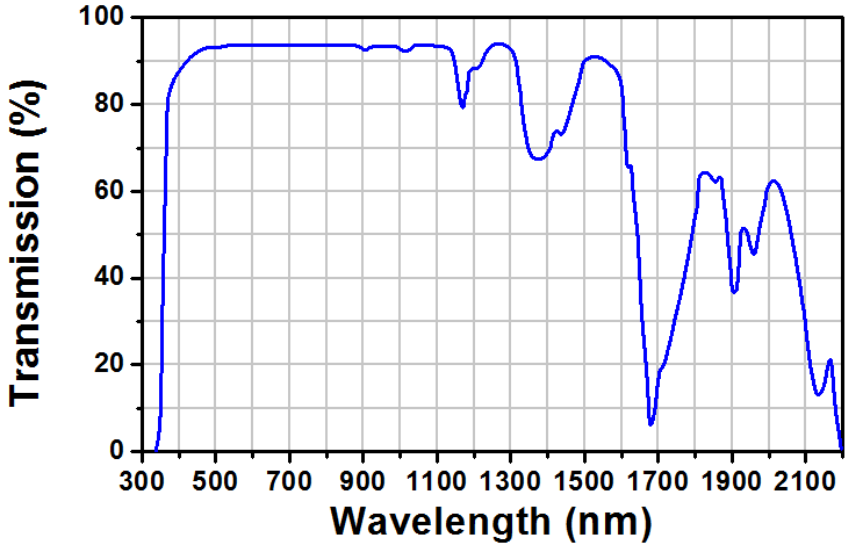

Figure 3.9 Infrared transmittance of colorless 3mm PLEXIGLAS sheet.

Figure 3.9 shows the infrared transmittance to different Plexiglas thicknesses: even for a small thickness (3mm, 0.118 inches) low-wavelength infrared passes through Plexiglas®, but high-wavelength infrareds have a very low transmittance. For this reason Plexiglas® allows the cameras infrared (850nm wavelength) to pass, while not enough thermal infrareds (2000-20000nm) can reach the baby worsening his conditions.

The Plexiglas® cover (3 mm thick) has been produced in order to be able to monitor the baby's condition visually (thanks to his transparency).

The internal environment can be controlled in terms of temperature and humidity through some useful devices.

The neonate is laid down on some reusable hand warmers, which heat the baby by conduction. They consist of little bags made in silicon filled with a supersaturated solution of sodium acetate (therefore non-toxic) which crystallizes if the metallic clip inside is smashed and the whole mass is put in vibration. This reaction gives off heat for several minutes (30 min – 2 hours). The heat exchange is proportional to the temperature difference between the heater and the environment: the bigger the difference, the higher temperature is reached by the hand warmer. This could be a risk for the infant skin, so the

hand warmer hasn't been put in direct contact with the baby's body, but some latex gloves filled with water have been interposed.

Figure 3.10 Hand warmers and humidifier used for environmental control inside the cover.

The environment inside the cover can be humidified with an Ultrasonic Humidifier: in this way a sufficient humidification of the environment can be achieved, setting up another strategy to minimize his loss of temperature.

In order to validate the set-up for critical babies, a series of measurement was performed inside the Plexiglas cover, in particular temperature maintenance and absence of reflexes were verified. For more details see B.1 Plexiglas® cover project.

3.2 DATA ANALYSIS

Data acquired during the study have been computed in order to obtain information about the mechanical properties of the infant respiratory system at different frequencies.
Florian monitor's data, pressure and flow signals measured at the mouth, have been used to determine the total input impedance.
Then pressure signal and flow derived from volume changes have been used for the transfer impedance computation.
The OEP cameras' data also provided information about single marker oscillation, in particular their amplitude and phase shift in craniocaudal direction.

3.2.1 Pressure and flow analysis

Analog data are processed with MatLab®.
Flow data are integrated in order to obtain volume data. Then Vt and P/P are calculated as the absolute difference between maxima and minima of volume and pressure signals respectively.
The total input impedance (Zin) was estimated by the cross-spectrum method:

$$Z_{in} = \frac{G_{pf}}{G_{ff}} \qquad [3.1]$$

where: G_{pf} is the cross-spectrum between pressure and flow signals. G_{ff} is the auto-spectrum of the flow signal.
Both G_{pf} and G_{ff} are estimated by averaging different periodograms computed by applying Fast Fourier Transform to several data segments. In particular the power spectral density estimate of the signals was found using Welch's overlapped segment averaging estimator.

The first step is searching the frequency at which the power spectral density of the pressure signal is the maximum. This frequency is used to identify the correct ventilation frequency and to evaluate the transfer function and the coherence.

The coherence function (γ_{fp}^2), defined as:

$$\gamma_{fp}{}^2 = \frac{|G_{pf}^2|}{G_{ff}G_{pp}} \quad [3.2]$$

is used as a quality index of the obtained data; impedance values with $\gamma_{fp}{}^2 < 0.95$ are discarded.[41]

The result of the transfer function computation is a complex number, which we expressed as either real and imaginary part or modulus and phase.

Equation 3.1 and 3.2 are implemented by the Matlab function "spectrum":

$$[P, F] = spectrum(flow, pressure, 2f_{sampling}, f_{sampling}, [\,], f_{sampling}); \quad [2.4]$$

From the imaginary part of the transfer function it is possible to obtain the resonant frequency as the frequency at which the imaginary part crosses the zero line.

The imaginary part of each newborn has been fitted with the following curve:

$$y = \frac{a}{x} + cx \quad [3.5]$$

Where a and c are characteristic fitting coefficient and change from each newborns.

A possible physical description of the coefficient is represented by the reactance equation:

$$X = (2\pi f * I) - \frac{E}{2\pi f} \quad [3.6]$$

Where I is the inerthance of the system represented by the c coefficient in the previous fitting equation and E is the elastance (the inverse of the compliance), which is represented by the a coefficient.

Finally the frequency dependence behaviour is represented by x in the previous fitting equation (fixed for an accurate fitting at the frequencies established for the present study).

3.2.2 OEP Data Analysis

The operation of tracking is the first stage of data processing: it represents the temporal trend of each single marker during the entire sequence. This is an operation that requires high precision, in order to avoid errors that compromise, as a result, the processing of data. It may happen, in fact, that some markers disappear and then reappear in subsequent frames: this is due to occlusions of the markers that can't be seen by cameras or to mismatches between cameras localizing a single point.

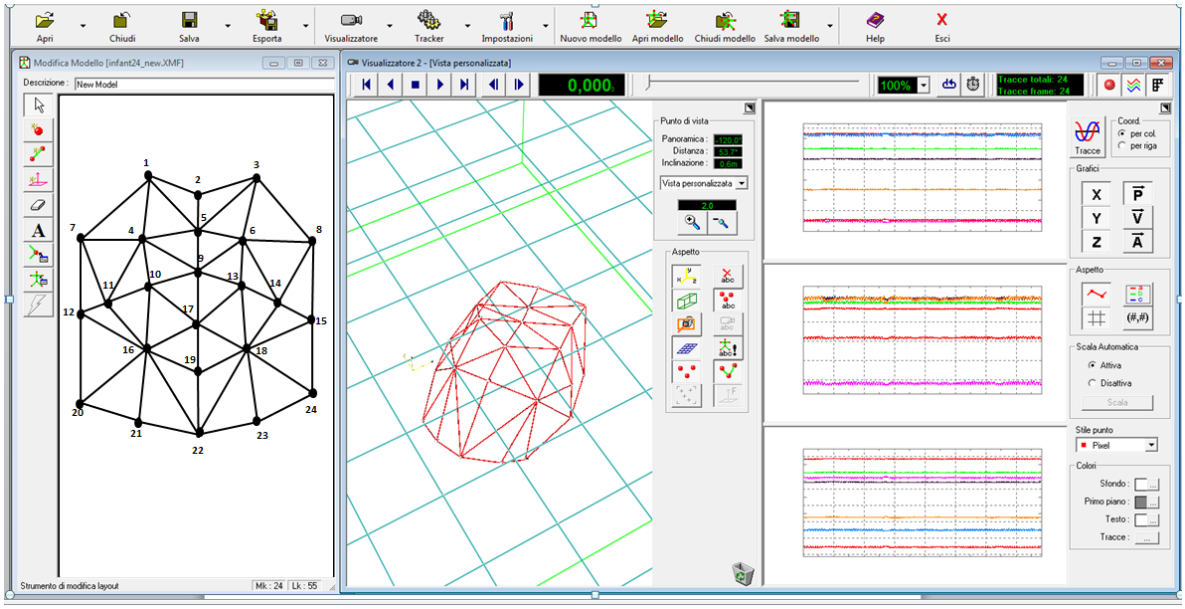

Figure 3.11 Tracking procedure using the SmartTracker software (BTS).

The model used for the tracking procedure is a virtual rapresentation of the clinical marker configuration (see Figure 3.7). Every marker in a correct position seen by almost 2 cameras must be labeled with its respective number in the first frames of the acquisition and it would be recognized by the software till the end of the acquisition. If there are some reflexes around the markers, they should not be included in the labeling phase. Finally, when all the markers seen by the cameras have been labeled during all the acquisition, the file can be saved as a .tdf file. It will contain information about analog signals and camera's acquisitions and it is ready to be elaborated.

Once tracked, OEP data are processed using MatLab® and Smart package (BTS), already used for the acquisition process.

The missing markers are reconstructed by using the function *AddMarker* already implemented in MatLab that allows to add or replace the markers that flicker or are totally absent in the frame sequence (for example in many infant it is not possible to place marker 19 due to the presence of umbilical catheter).
This function is based on the hypothesis of continuity and neighbor mechanical similarity during wave propagation, so it allows to reconstruct the markers by:

- Interpolation: the new marker results as the mean of the two visible markers;
- Estrapolation: Given two known markers, the new marker will be positioned following this rules:
    - Direction: it will belong to the line passing through the two known markers.
    - Versus: it was chosen by giving to the software a wise series of the known markers.
    - Distance: it will be at an equal distance from the second marker in respect to the first marker.
- Symmetry: the new marker is construct from his symmetric in respect to the midline.

Pulmonary volumes have been calculated using an implemented function in the Prompt Command. It returns a .dat file and a .sec file:

- The *.dat* file contains 4 columns that represent time, total volume, rib cage volume and abdominal volume changes;
- The *.sec* contains 69 columns that represent the volume changes of the tetrahedra that composed the total volume: 34 tetrahedra for the frontal part (rib cage and abdomen) and 35 tetrahedra for the back part.

OEP cameras' data are processed in order to obtain information about marker motion analysis and transfer impedance computation. In particular the data obtained are related to:

- Amplitude and phase shift of markers displacement;
- Volume changes;
- Total and regional transfer impedance.

Marker motion analysis

The accurate measurement of 3D marker coordinates during oscillations allowed two different types of analysis: oscillation analysis and regional transfer impedance computation.

The propagation of the forced pressure wave in the craniocaudal direction was studied using the amplitude and phase of the displacement signal in vertical axis of six markers placed on the midline from the sternal notch to the lower abdomen (markers 1-5-9-17-19-22). On this line, in fact, the first hypothesis is that all the displacements are focused in a main vertical direction.

From the tracks of the 3D coordinates the lags between each marker and marker number 2 (the first on the midline) were computed.

The phase shift was estimated as the phase angle of the transfer function between the displacement of the reference marker and the other markers. The transfer function was estimated by computing their Fast Fourier Transforms (respectively, $S_1(f)$ and $S_i(f)$, where f is frequency) and the phase shift was expressed as:

$$phase = arctg \frac{Im[S_1(f)]Re[S_i(f)] - Im[S_i(f)]Re[1(f)]}{Re[S_1(f)]Re[S_i(f)] + Im[S_i(f)]Im[1(f)]} \quad [3.7]$$

The marker from 1 to 9 can be related to rib cage displacements and markers from 10 to 24 can be related to abdominal displacements, so the trend of rib cage lag (RC lag) and abdominal lag (AB lag) at different frequencies can be estimated.

In order to characterize the phase shift in more than 2 regions of the body surface, a virtual division of the surface in smaller subsets was created: 12 zones have been constructed summing up the tetrahedral contributes.

The volume changes detected for the tetrahedra is used to determine the displacement of the surface and this signal is used to the phase shift computation.

In this case the phase shift was estimated as the phase angle of the transfer function between the displacement of the reference area (area 5) and the other areas.

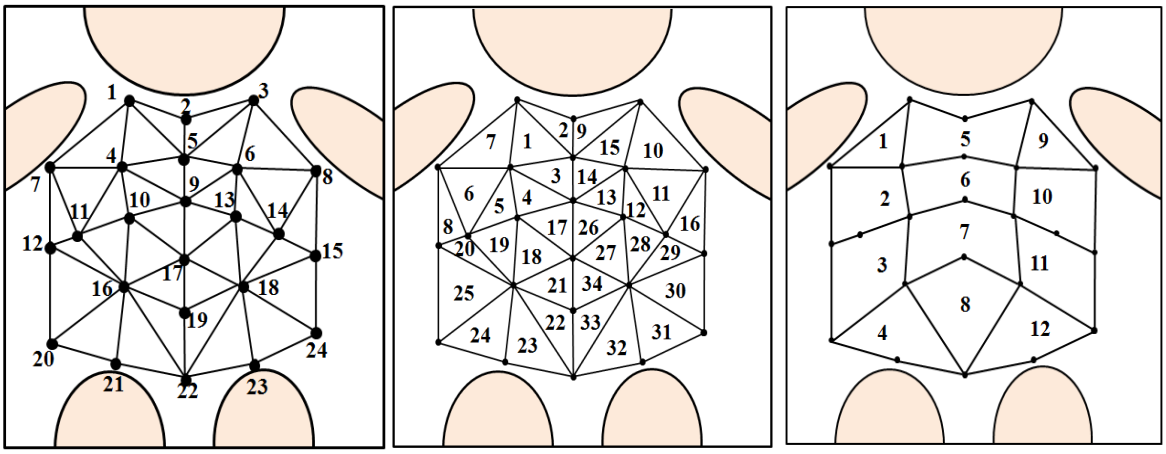

Figure 3.12 Virtual maps used for the phase shift computation: A) marker configuration, B) thetraedra division and enumeration and C) virtual map with 12 areas.

The configuration of the 12 areas has been decided in order to consider the midline separated from the lateral ones, which include the quasi-static closure markers. In fact, the hypothesis was that the propagation of the oscillatory pressure wave occurs mainly in craniocaudal direction, but in order to consider also a lateral propagation contribution, the regional subdivision includes a central midline line and 2 parallel lines on both sides of the body surface which allows to examine both craniocaudal and side-to-side components.

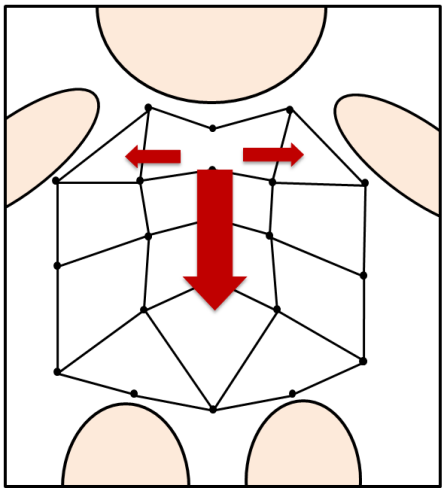

Figure 3.13 Craniocaudal and lateral pressure wave propagation on the thoraco-abdominal surface.

In this way data of the central areas can be compared with another study on phase shift on the midline of the toraco-abdominal surface in adults subjects.[52]

Volume computation

Total chest wall volume (V_{CW}) was determined by approximating chest wall surface by 34 triangles connecting the markers and computing the volume enclosed by all these triangles. The posterior surface of the chest wall (hidden in supine position) was defined by nine "virtual" markers assumed to lie on the supporting plane. The supporting plane was assumed to be parallel to the plane of the bed and 5 mm below the most posterior lateral marker (lateral markers being: 7, 8, 12, 15, 20, and 24, see Figure 3.7). The positions of the virtual markers were determined by projecting onto the reference plane the initial frontal coordinates (from the first image frame) of the following points:

1) the average between marker 4 and 7;
2) the average between marker 6 and 8;
3) marker 11;
4) marker 14;
5) the average between marker 20 and 21;
6) marker 21;
7) marker 22;
8) marker 23;
9) the average between marker 23 and 24.[51]

As mentioned above, the shape of the chest wall was described by connecting the markers to form 34 triangles (Figure 3.7). To quantify local volume variations, the contribution due to the motion of each triangle to the total chest wall volume change was computed in the following way. The coordinates of the mean position point (*P*) for the 24 markers were computed by averaging the 3D coordinates of all the markers. In this way, we obtained the 3D coordinate of *P*, which is always located inside the chest wall. A new projection point for each marker was then defined to be at an arbitrary distance of 5 mm from the original marker in the direction of point *P* (Figure 3.14). The resulting projected points were connected in the same manner as the original markers to form a set of new triangles that defines a second surface internal to the surface described by the original markers placed on the chest wall.

For each period of acquisition, the coordinates of the projected points were computed only for the first acquired frame. These points were then kept fixed for the remaining duration of the acquisition.

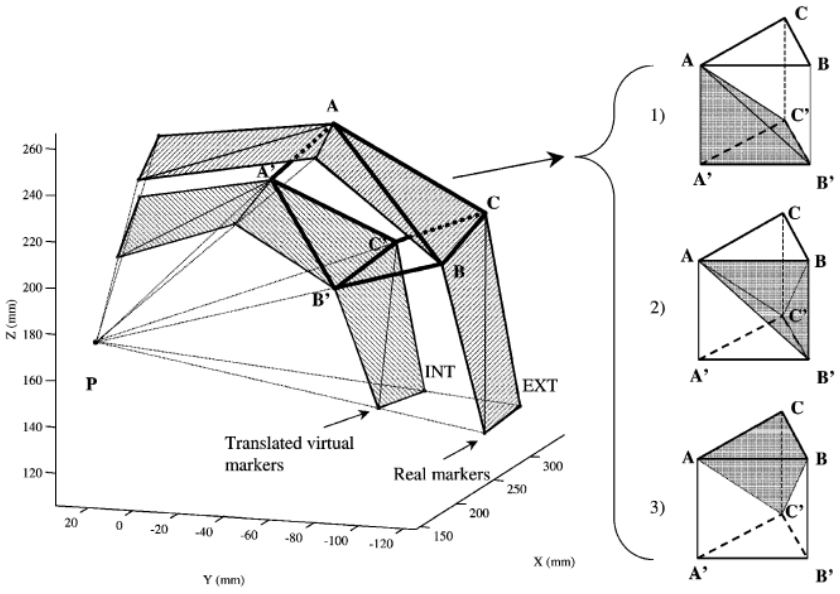

Figure 3.14 Example of the procedure used to compute local volume changes applied on a subset of markers that defines a small region of the chest wall surface (Fig. 1, thick line, here reported as the external surface, (EXT). If we consider each triangle that describes the chest wall surface (for example, the one defined by the markers *A*, *B*, and *C* in Fig.) as the base of a prism with the opposite face defined considering the virtual markers (*A*', *B*', and *C*') it is possible to estimate local volume changes from the measurement of the volume of the prism (left). The virtual markers define the internal surface (INT) and are obtained using the mean point *P* as described in the text. In fact the difference between the prism volume (*V*el) in each frame and the volume computed on the first one gives the element volume change (∇*V*el). The volume of the prism is calculated as the sum of the three tetrahedrons (right) defined as follows: (1) base *A*'-*B*'-*C*', opposite vertex *A*; (2) base *C*'-*B*'-*B*, opposite vertex *A*; (3) base *A*-*B*-*C*, opposite vertex *C*'.

As shown in Figure 3.14, this procedure allows us to associate a volume to each triangle by considering the region of space existing between the external triangle and the corresponding internal one. During the measurement, the pressure signal applied to the mouth induces volume changes in the lung and, consequently, the chest wall surface moves. The markers placed on the chest wall change their position, and the triangles of the external surface move accordingly. This results in a change of the volume subtended by the external moving triangles and the internal fixed ones. The volume comprised between any external triangle and the corresponding internal one was computed as the sum of three tetrahedra, as shown in Figure 3.14 (right).

Regional transfer impedance computation

The forced oscillation technique represents a simple and minimally invasive approach to measure the mechanical impedance of the respiratory system. Two methods are commonly used: input impedance and transfer impedance. While Z_{in} provides a global estimation of the respiratory system mechanical properties, Z_{tr} provides information specific to the tissues and the airways and is less influenced by upper airways shunting.[4]

It comes to "transfer impedance" when pressure and flow are measured at different ports: we use pressure measured at mouth (P_{ao}) and flow measured at the body surface ($\dot{V}_{bs}$), the time derivative of the volume variation ΔV_{el_i}.

To increase the signal-to-noise ratio, we considered regions of the chest wall made by one or more triangles (Figure 3.7), and the volume of these elements was obtained simply from the sum of the volumes associated with all the triangles included in the considered region. Two different schemes of triangle fusion were adopted. Volume variations of the *i*th element (ΔV_{el_i}) were computed for each sample as the difference between each current value and that occurring on the first acquired sample. In this way, the sum of all values (ΔV_{el_i}equaled the total chest wall volume variations (ΔV_{cw}):

$$\Delta V_{cw} = \sum_{i=1}^{n} \Delta V_{el_i} \qquad [3.8]$$

where n, representing the number of the elements, was fixed to 34.

The time derivative of ΔV_{el_i} in the above equation was obtained by dividing the Fourier transform of the volume signal by jω. This procedure is equivalent to differentiating the volume signal with respect to time.

$\dot{V}_{bs}$ is calculated as the time derivative of the chest wall volume and Ztr is calculated as:

$$Z_{tr} = \frac{P_{ao}}{\dot{V}_{bs}} \qquad [3.9]$$

Transfer impedance is expressed as real and imaginary parts.

Transfer impedance has been initially computed on the total volume, but it represents the mean of several different mechanical behaviours, so it has been decided to split the surface in more compartments, such as rib cage and abdomen.

In 1989 Barnas et al. studied transfer impedance of the rib cage and the abdominal compartments at low frequencies (0.5–4 Hz) and they found that these two compartments are characterized by different transfer impedances, confirming the hypothesis that chest wall mechanical properties are not homogeneously distributed. Therefore, that a complete description of respiratory mechanics requires the chest wall to be divided into two or more compartments.[41]

It is possible to define the compartmental transfer impedances, as the complex ratio between airway opening pressure and time derivative (or frequency derivative) of the compartmental volumes. Because the compartments are submitted to the same pressure (P_{ao}), they result connected in parallel.

Recently, Optoelectronic Plethysmography has been used to measure the transfer impedance of adults chest wall partitioned into three compartments (pulmonary rib cage, abdominal rib cage, and abdomen) and the results confirmed that the contribution of these three compartments to the total transfer impedance change significantly.[4]

Considering different subsets of optical markers on the thorax, it is possible to partition the transfer impedance by measuring the contribution of these distinct components on the chest wall to the total transfer impedance.

To perform this computational method single markers displacements were considered in respect to the barycentre of the areas, and to increase the signal-to-noise ratio, the displacements of the markers in the same areas were merged in order to obtain 34 triangles, maximum division allowed by the model used in this study.

The transfer function between the mean displacements (multiplied for the triangle area) and the pressure signal has been computed through the Spectrum Matlab function (as for the input impedance). The final steps have been the frequency derivative calculation and the pressure correction through the transfer function described in the next chapter (in vitro study).

The resulting transfer impedance is a complex number which can be expressed either as modulus and phase or real and imaginary part. In the complex domain the most common risk is a mismatching in the phase component:

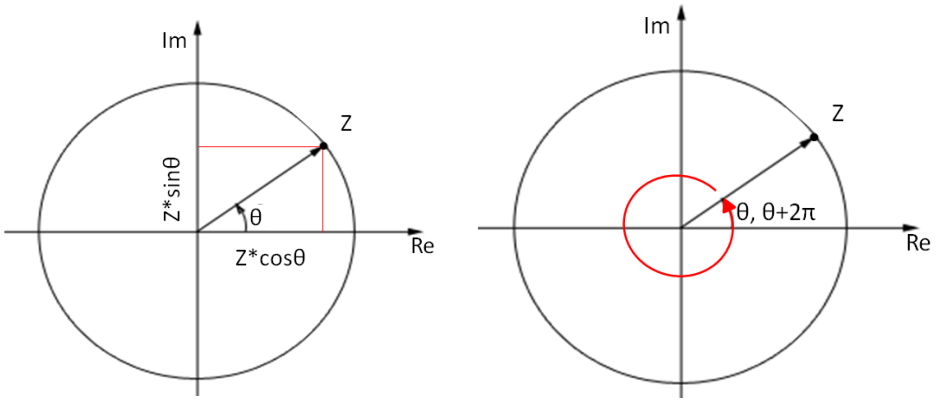

Figure 3.15 Representation of a complex number in the complex plane with its phase component. The phase mismatching occurs when the matlab code returns θ instead of $(\theta + 2 * \pi)$.

The phase components have been checked and 2*π has been summed up where needed.

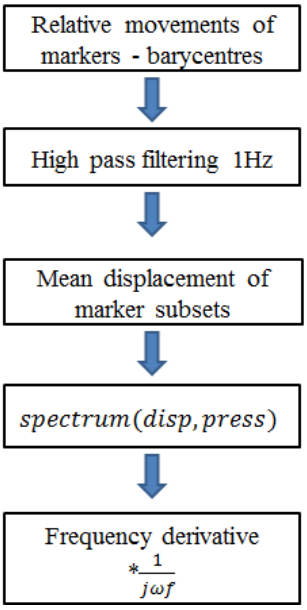

Figure 3.16 Flow chart of the transfer impedance computation for different zones of the body surface: displacements of markers belonging to the same area have been referred to their barycentre; then both pressure and marker traces have been filterd (1Hz high pass filter); markers belonging to the same area have been averaged; transfer function between pressure and displacement has been computed and the frequency derivative has been applied.

Moreover the estimation of the heterogeneity of the transfer impedances over the chest wall surface could be useful to study, evaluate, and quantify changes in respiratory mechanics.

The description of the heterogeneity with 34 triangles is too large for the small volume of newborns and data are affected by high noise. The subdivision should be reduced in order to merge the triangles with similar behavior and increase the signal-to-noise ratio.

The total chest wall can be considered as at least 2 compartments, as explained before, but each compartment can be divided in left and right side in order to point out any asymmetry. Moreover the lower costal margin has a different stiffness than clavicular line and abdominal compartment, so another division should consider high-low rib cage and high-low abdomen. Finally, closure markers' displacement is very small, because they are placed in quasi-static zones of the body surface, so these markers 'dump' the area's displacement. In particular the umbilicus zone is separated from the superior iliac spine because of its high elasticity and consequently its elevated displacement.

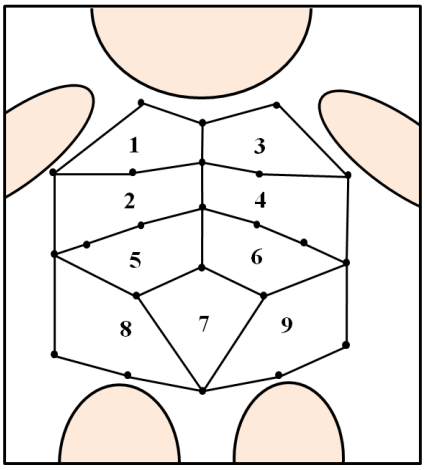

Figure 3.17 Virtual map used after merging mechanical similar behaviour markers for transfer impedance computation.

In the present study, the final computation method provides the transfer impedance on 9 different zones on the body surface: 4 zones for the rib cage and 5 zones for the abdominal surface. This choice represents a compromise between a large number of zones and a good signal-to-noise ratio: the quality index that has been use is the coherence function, that was maintained over 0.9.

The regional transfer impedance data have been combined with three-dimensional location of each triangle (tetrahedron) and their barycentre, allowing the construction of colour maps of modulus, reactance and resistance of Z_{tr} distribution over the chest wall surface. This computation has been made through the Matlab's *surf* maps.

4. In vitro study

Before starting our clinical study an in-vitro study was performed. To understand the behaviour of the respiratory system at different frequencies, the mechanical properties of different types of patients have been simulated creating some in-vitro models using glass inextensible bottles and endotracheal tubes of different size and diameters.

The principal aim was to validate the set-up used for the measurement of respiratory impedances in newborn undergoing HFOV. Secondarily, since few articles about frequency are available in literature, it has been verified how mechanical properties affect the respiratory system behaviour at increasing frequencies.

To validate the clinical setup, different pressure generators are tested: small signal generator was compared with the high frequency ventilator used in clinical practice.

Pressure measurements have been corrected in order to compensate the low pass filter effect of the clinical ventilator circuit and endotracheal tube (ETT) tube resistance has been evaluated to perform a flow dependence compensation on the real part of the input impedance.

4.1 FREQUENCY BEHAVIOUR

In order to better understand how the frequency-dependence behaviour of the respiratory system is affected by the mechanical characteristics of the patient, the mechanical properties of different types of patients have been simulated creating six in-vitro models. Respiratory resistance (R) and compliance (C) are the most influent variables that define the respiratory mechanics; therefore to change the mechanical features we changed R or C of our lung model.

The mechanical model of the infant respiratory system was realized by a resistance, an inertance and a compliance arranged in series. However, inertance is very small anyway and contributes very little to the system impedance, thus the difference between the desired value and the real one does not significantly affect the reactance value of the whole model. Finally, the volume of the bottle was calculated assuming that the compression is adiabatic. In such a model the most of the resistances are represented by the endotracheal tube (ETT). Therefore we tested three different ETT sizes commonly used in clinical settings: 2, 2.5 and 3 mm diameter with a length of 15.5, 16.3 and 17 cm respectively.

On the contrary, the elastic characteristics (C) of the respiratory system are modelled by the compressibility of the gas included in an inextensible glass bottle. Therefore, in order to change C we use two different-volume bottles (0.5 and 1 L).

Since lung compliance depends on lung volume, neonates with a smaller lung size (lower weight or gestational-age) or with a smaller number of recruited alveoli (more serious clinical condition) are represented by the smaller bottle (0.5 L) that has a compliance of about 0.5 ml/cmH_2O. Whereas, 1 L bottle is a neonate in a less serious condition with a compliance of about 0.96 ml/cmH_2O.

Figure 4.1 Different size bottle and ETT tube used for the in vitro study.

Ventilation is provided by the same ventilator used for the clinical study (SensorMedics 3100A). The acquisition system is composed by a pneumotachograph connected to a personal computer running LabVIEW® (National Instruments).

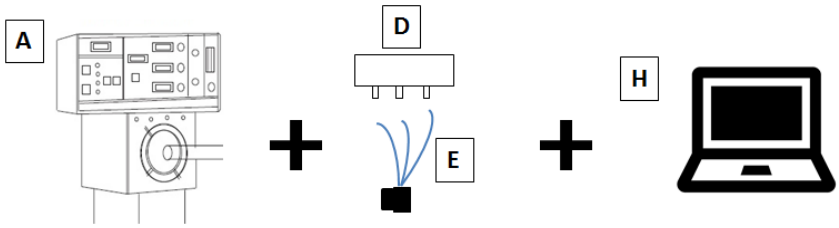

Figure 4.2 Setup for test lung and ETT frequency characterization.

For each combination bottle-endotracheal tube the frequencies (5, 8, 10, 12, 15 Hz) are tested in sequence keeping pressure amplitude (ΔP) constant at 25 cmH_2O. Continuous Distending Pressure (CDP), Inspiration/Expiration Ratio = 50% and the central piston position were not modified.

At each frequency-step 30s pressure and flow waves are acquired. Data are sampled by National Instruments acquisition board and record on LabVIEW on the PC. The recorded data are processed in order to obtain impedance, its real (resistance) and imaginary part (reactance) as for the clinical study data.

Mechanical property	Mechanical analogue	Elemental equation	Impedance $Z(\omega) = P_{21}/V$	
Inertance (I)	Fluid	$P_{21} = I\frac{d}{dt}V$	$Z = j\omega I$	$I = n\rho L / A$
Elastance (E)	Chamber with rigid walls	$\frac{d}{dt}P_{21} = EV$	$Z = -j\frac{E}{\omega}$	$E = \beta P_0 / V_0$
Resistance (R)	Fluid	$P_{21} = RV$	$Z = R$	$R = \frac{8\pi\mu L}{A^2}$ $R = \frac{8\pi\mu L}{A^2} + \frac{\sqrt{2}}{\pi r^4}\mu\left(\frac{r^2\omega}{\nu}\right)^{\frac{1}{2}}L$

Figure 4.3 Elemental relations for passive mechanical elements representing the properties of the respiratory system.

Theoretical values of resistance for each tube and the value of compliance for each bottle have been computed. According to Poiseuille's law, the resistance's value is independent from the frequency and depend only from the cross section of the endotracheal tube.
As expected, the value doesn't change with the bottle size, because all the resistance of this system can be totally attributed to the tube.
Resistance values [cmH2O*s/L] are resumed in table 4:

Table 3 Theoretical resistance values of different ETT tube

Tube diameter	***R [cmH2O*s/L]***
2 mm	75.76
2,5 mm	31.03
3 mm	14.97

Compliance values, instead, are strongly dependent on the bottle size, as show in this computational formula:

$$C = \frac{V_{bott}}{B \cdot P_{atm}} \qquad [4.1]$$

Where V_{bott} is the glass bottle volume (0,5 L or 1L); P_{atm} is the atmospheric pressure (1033.2559 cmH_2O) and B is a coefficient set to 1 if the compression is isotherm and 1.4 if the compression is adiabatic.
Compliance values [L/cmH_2O] are reported in table 5:

Table 4 Theoretical compliance values of different size bottles

Bottle size	***C [L/cmH_2O]***
0.5 L	$4.83 * 10^{-4}$
1L	$9.68 * 10^{-4}$

The theoretical inertance was also calculated as:

$$I = \frac{\rho L_{tube}}{A} \qquad [4.2]$$

Where ρ is the density of the gas, L_{tube} is the tube length and A is the cross section area of the tube.

The inertance value [cmH_2O*s^2/L] are reported in table 6:

Table 5 Theoretical inertance values

Tube diameter	***I [cmH_2O*s^2/L]***
2 mm	0,6481
2,5 mm	0,4148
3 mm	0,2880

With these elements we have also computed the theoretical values of the total imaginary part of the transfer function:

$$X = (2\pi f I) - \frac{1}{2\pi f C} \qquad [4.3]$$

Where f is the frequency set on the ventilator (5Hz, 8Hz, 10Hz, 12Hz and 15Hz).

The reactance value [cm$H_2O*s\ /L$] are reported in table 7:

Table 6 Reactance values from 5Hz to 15Hz for all the studied test lungs.

Bottle size	***Tube diameter***	***5Hz***	***8Hz***	***10Hz***	***12Hz***	***15Hz***
0,5 L	2 mm	-45,41	-8,53	7,83	21,46	39,15
	2,5 mm	-52,74	-20,26	-6,82	3,867	17,16
	3 mm	-56,72	-26,63	-14,79	-5,68	5,22
1 L	2 mm	-12,52	12,02	24,27	35,16	50,12
	2,5 mm	-19,85	0,294	9,61	17,57	28,13
	3 mm	-23,83	-6,07	1,65	8,01	16,18

The theoretical values of resistance and reactance calculated on different ETT tube and different size bottles differ from the real measured values and this is probably due to the preliminary hypothesis on the materials and conditions that have not been respected.

The experimental values of resistance and compliance differ from the calculated one. This may be due to the fact that the underlying assumptions of the used equations have not

occurred. The higher resistance values can be due to the junctions and to the turbulent flow into the capillary tube, in fact the calculated value using Poiseuille's law accounts only for the linear term of resistance.

The reactance is less negative or more positive than the expected one. This is probably due to an underestimation of the calculated compliance. In fact the theoretical compliance only includes the compressibility of the air into the bottle and does not consider the air in all the connecting tubes. Moreover an underestimation in the calculated compliance values may occur also if the hypothesis of adiabatic transformation is not verified.

4.2 OSCILLATORY PRESSURE SIGNALS

In the clinical study the high frequency ventilator generates the pressure wave used for the impedance computation. FOT classically uses little pressure amplitude waves (about 2-4 cmH_2O), that are far smaller than pressure amplitudes generally applied by clinicians (10-50 cmH_2O). Measuring total impedance by applying high-amplitude waveforms (in the same way as during HFOV) may lead to artifactual results[21] associated with the nonlinearity of the respiratory system. For this reason, in previous studies assessing subjects receiving HFOV, FOT measurements were performed by connecting the subjects to a dedicated device delivering small-amplitude forcing signals.

Recently it was demonstrated that HFOV could provide the opportunity to measure Z_{rs} simply by processing the flow and pressure signals in a noninvasive way.
Dellacà et al. have already validated the use of the ventilator as wave generator to apply FOT: it was found that, even if the impedance values obtained cannot be considered realistic, the imaginary part trend is comparable to data obtained in standard conditions. On the contrary, real part cannot be considered reliable enough.[42] In fact, while the resistance of the respiratory system (R_{rs}) measured during HFOV is greatly affected by the nonlinearity of the respiratory system, the measurement of reactance of the respiratory system (X_{rs}) still provides accurate results when compared with standard FOT.[42]
Nevertheless, only 5 Hz frequency input waves were tested.

The aim of this in vitro study is to evaluate the accuracy of impedance measurements obtained when HFOV waveforms at different frequencies, applied in place of standard low-amplitude FOT with an experimental set-up that simulate the infant respiratory system.
In order to validate the clinical setup different combination of the source generators, transducers and acquisition system are tested and compared.

4.2.1 Validation Setup

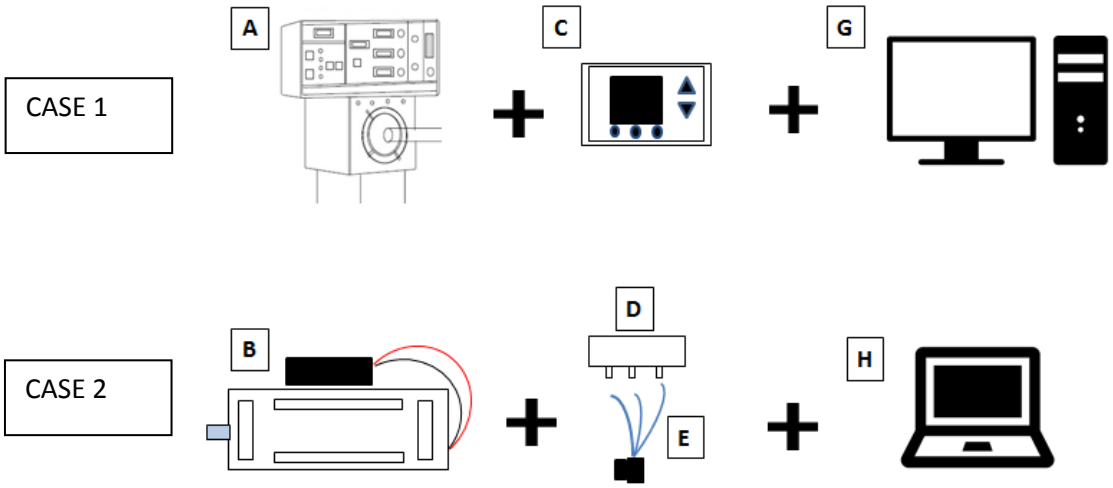

Figure 4.4 Setup for the validation study: Case 1) Sensormedics, Florian, OEP system; Case 2) Syringe pump, pressure transducer, personal laptop.

The system is composed by a pressure wave source to generate the oscillation signal:

- High frequency mechanical ventilator used in clinical practice (SensorMedics 3100A) that produces high amplitude pressure signals (10-50 cmH_2O);
- Small amplitude pressure oscillator realized by a syringe driven by a servo-controlled linear motor (2-4 cmH_2O).

Then the oscillatory pressure generator is connected to pressure and flow sensors:

- Florian monitor, which is the common flow and pressure monitor used in the clinical settings;
- Pressure transducer and a differential pressure transducer connected to the pressure taps of a mesh-type pneumotachograph.

The last step in the chain is the acquisition system:

- OEP workstation, that allows to acquire analogical signals with a sample frequency of 240 Hz;
- LabVIEW on a personal laptop, with a general-purpose acquisition board (DAQCard6036E, National Instruments, Austin, TX) linked to a BNC connector

block to which the transducers are connected: signals are recorded with a sample frequency of 600 Hz.

The respiratory system is modelled as a resistance and a compliance in series:

- Endotracheal tube: it represents the resistance of the respiratory system and its value mainly depends on the diameter of the tube (2mm, 2.5mm, 3mm and 3.5mm);
- Glass bottle: it represents the compliance of the system and the value depends on the volume of the bottle (0.5L and 1L).

Case 1 is composed by Sensormedics, Florian monitor and OEP acquisition system and represents the clinical conditions.
Case 2, instead, is composed by syringe pump, pressure transducer, pneumotachograph and a National Instrument acquisition board on a laptop (with Labview).

For each combination all frequencies (5, 8, 10, 12, 15 Hz) were tested in sequence with 30 second recordings of pressure and flow waves.
When Sensormedics is used as oscillatory generator a pressure amplitude (ΔP) of 25-26 cmH_2O was kept constant; on the contrary, with the syringe a constant ΔP of about 2-4 cmH_2O was used.
The recorded data are processed in order to obtain impedance, expressed as real part (resistance) and imaginary part (reactance) as for the clinical study data.

4.2.2 Validation results

In order to validate the use of high amplitude pressure signals instead of low amplitude pressure waves used in standard FOT, both setups are compared in the same condition: peak to peak pressure remains constant (0.4 cmH_2O for syringe pump and 25 cmH_2O for Sensormedics) and the frequency tested are the same as in the clinical study (5 Hz, 8 Hz, 10 Hz, 12 Hz, 15 Hz).

This graphs show the input impedance, composed by real and imaginary part, of a test lung (glass bottle 0.5L connected through a 2.5mm endotracheal tube) measured with different setups. The clinical setup (Sensormedics, Florian, OEP) needs a pressure correction as explained in the next paragraphs.

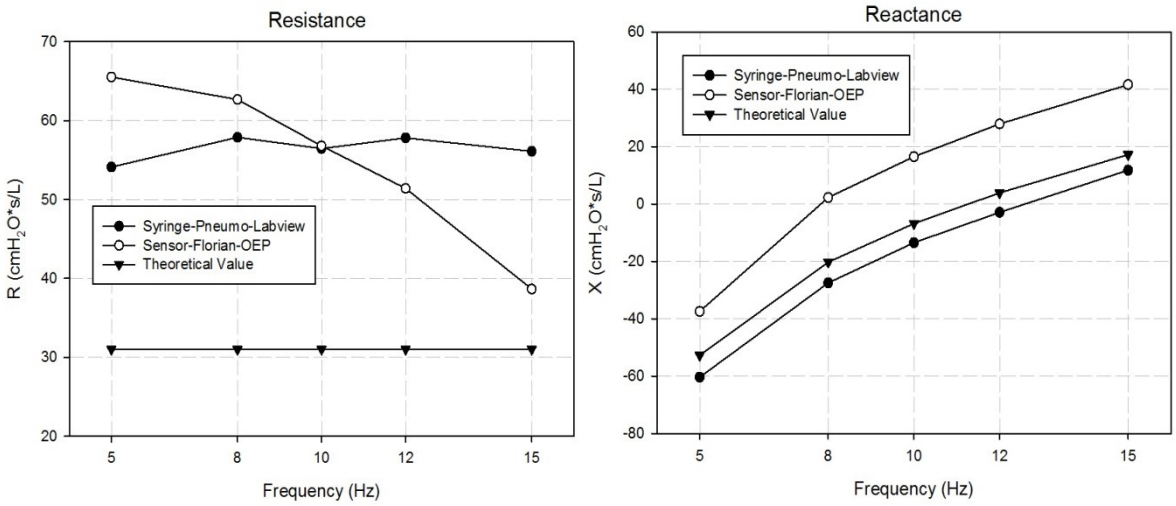

Figure 4.5 A) Real part and B) Imaginary part of the transfer function between pressure and flow measured with different setup. The -●- line is the low amplitude pressure signal, the -○- line is the clinical setup and the -▼- is the theoretical value.

Figure 4.5 shows how measurements with both setup are similar in the same conditions: a line represents measurements with the syringe pump-pneumotachograph-Labview setup, the second line represents the Sensormedics-Florian-OEP setup and the third is the theoretical value of resistance (panel A) and reactance (panel B) computed with mechanical laws described before.

While the real part has a different trend, the trend of the imaginary part is the same showing a similar response with an error that remains almost constant at increasing frequency.

In order to verify the linear dependence of the measurements, a linear regression has been performed on both real and imaginary part of the transfer function between pressure and flow.

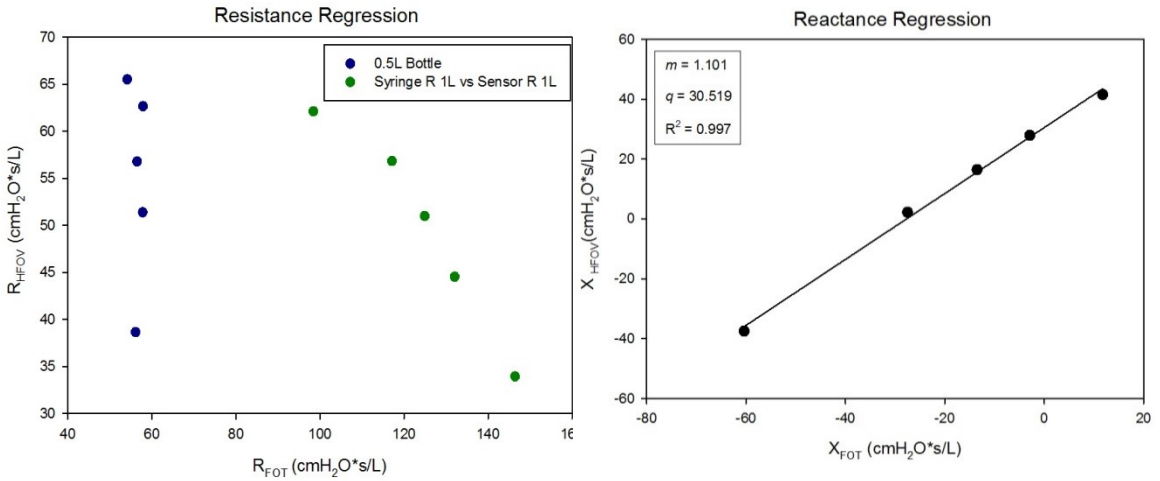

Figure 4.6 Linear regression between measurement with standard FOT setup (resistance and reactance LAB) and with clinical setup (resistance and reactance OEP). A) Real part with different lines for 0.5L and 1L size bottle; B) Imaginary part.

The regression shows a linear dependence of the measurements for the imaginary part (m=1.01), but not for the real part (no linear regression has been performed).

Another commonly used test is the Bland-Altman analysis:

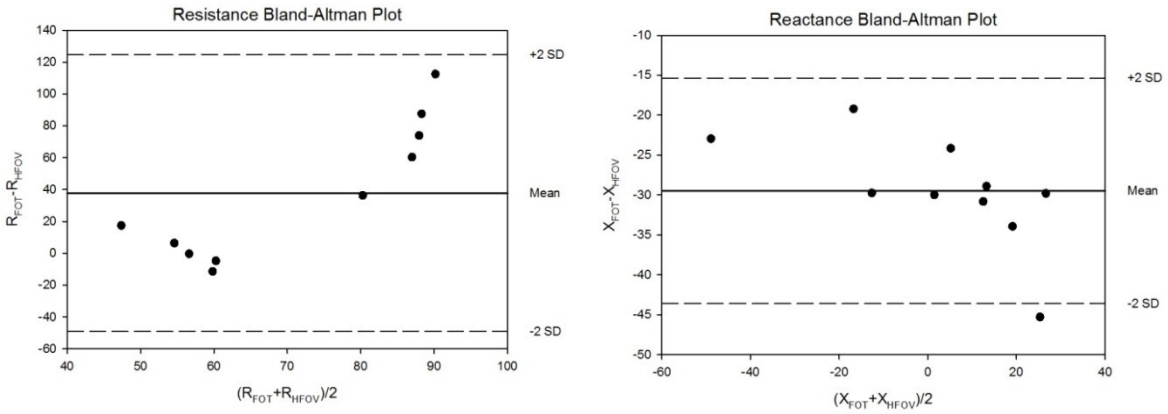

Figure 4.7 Bland-Altman analysis for the real and imaginary part of the transfer function between pressure and flow measure with different setup (standard FOT and clinical setup). A) Real part, B)Imaginary part.

The values reported in figure 4.8 are included in the region of ±2σ and there is no evidence of trends in the cloud distribution of the values

4.3 PRESSURE COMPENSATION

Once the high pressure signal setup has been validated, the next step was to validate the clinical setup, and in particular the pressure measurements: preliminary measurements found out frequency and amplitude-dependent errors in pressure measurement that needed the following validation to be corrected. In clinical practice pressure is measured through a tube connected in parallel to the ventilator circuit, which introduces a low pass filter on pressure signal.

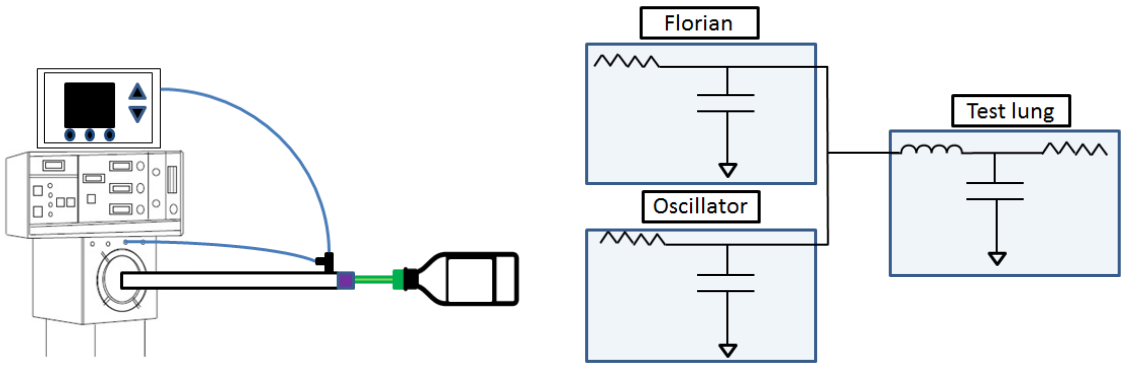

Figure 4.8 A) Parallel connection between the oscillator circuit and Florian monitor. B) Electrical equivalent of the connections, in particular the oscillator is represented as a low pass filter.

During HFOV, inspiration and expiration are both active (proximal airway pressures are negative during expiration). Oscillators produce little bulk gas delivery: continuous flow of fresh gas rushes past the source, generating or powering the oscillations. A controlled leak allows gas to exit the system and the gas valve allows to keep the circuit open to the gas flow, but this introduces a low-pass filter to the gas circuit. Moreover, the air tubing that runs to the pressure port for the purpose of transmitting the airway pressure signal to the pressure transducer, has a large diameter and thus introduces a compliance that affects pressure measurements. The combination of these factors influenced the measurement circuit that has been connected in parallel to the ventilator and for this reason pressure should be corrected.

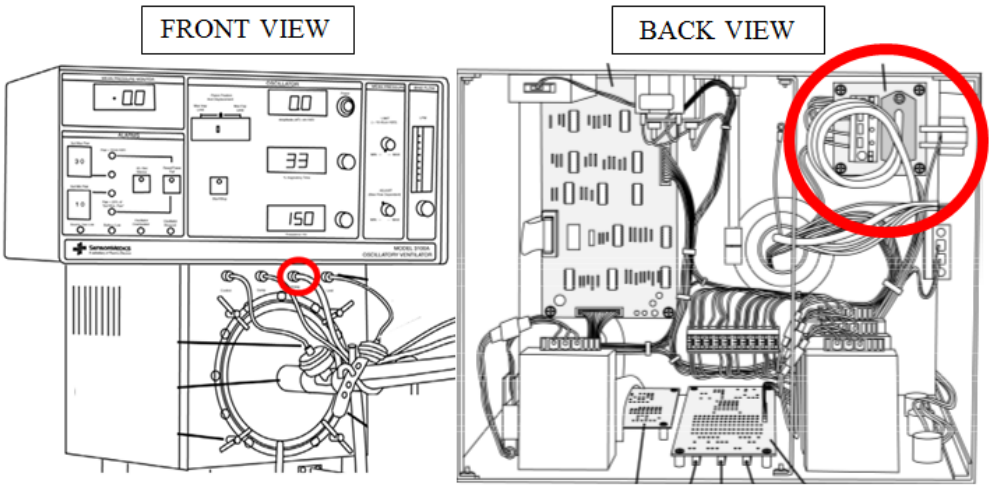

Figure 4.9 Sensormedics circuit. A) Front view of the ventilator, the red circle indicates the air pressure inlet; B) Back view of the circuit, the red circle indicates the internal tube and the gas valve.

4.3.1 Pressure correction setup

In order to measure both 'right' and 'wrong' pressure, it was set a single measurement circuit with a double pressure outlet.

The set-up was composed of:

- Sensormedics: it provides HFOV to the test lung;
- Pressure transducer and Florian: as pressure sampling systems;
- Flow measurement;
- OEP System: as acquisition and recording system.

(For more details on Sensormedics and Florian refer to sub-chapter 3.1.1 Set up overview).

The pressure sensor was connected right out of the ETT and provided the right pressure. Since the sensor was placed near the airway opening, the 'right' measured pressure is called P_{nao}. Florian was connected in parallel to the oscillator as in the clinical study and provided the 'wrong' pressure. Since it was placed away from the airway opening, the 'wrong' pressure is called P_{aoo}.

In this part of the in-vitro study different test lungs have been used: as before, they are composed of a 0.5L and 1L inextensible glass bottles and different diameter endotracheal tubes (ETT): 2, 2.5, 3 and 3.5 mm.

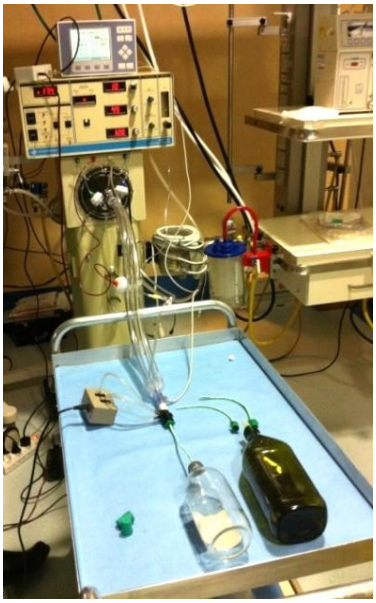

Figure 4.10 Different combination of endotracheal tubes and bottles as test lungs.

Using this setting we tested 5, 8, 10, 12, 15 Hz of oscillatory frequencies at five different pressure amplitudes: 10, 18, 25, 33, and 40 cmH_2O; other ventilator parameters (continuous distending pressure and E/I ratio) were not changed. For each step 30'' pressure and flow waves are acquired. Data are saved on the OEP workstation.

The recorded data were processed in order to obtain the transfer function between the two measured pressures ΔP_{nao} and ΔP_{aao}:

$$tf = \frac{\Delta P_{nao}}{\Delta P_{aao}} \qquad [4.4]$$

The transfer function was obtained for all different combinations of ETT and compliances, at all oscillatory frequencies, for all different pressure amplitudes.

The correction was made through a product between the input or transfer impedance calculated with the "wrong" pressure, and the transfer function between the right and the wrong pressure.

$$Z_{new} = tf \cdot Z_{old} \qquad [4.5]$$

4.3.2 Pressure correction results

With the in vitro setup it was possible to find out the difference between impedance with pressure signal evaluated near the bottle and pressure signal evaluated with normal setup (near the diaphragm of the ventilator).

The transfer function between pressure near the endotracheal tube and near the diaphragm of the ventilator and has been computed for each frequency at each pressure amplitude value. From these measure we obtain magnitude, phase, real part and imaginary part of the transfer function. The results can be summed up in Figure 4.11 (A,B,C,D):

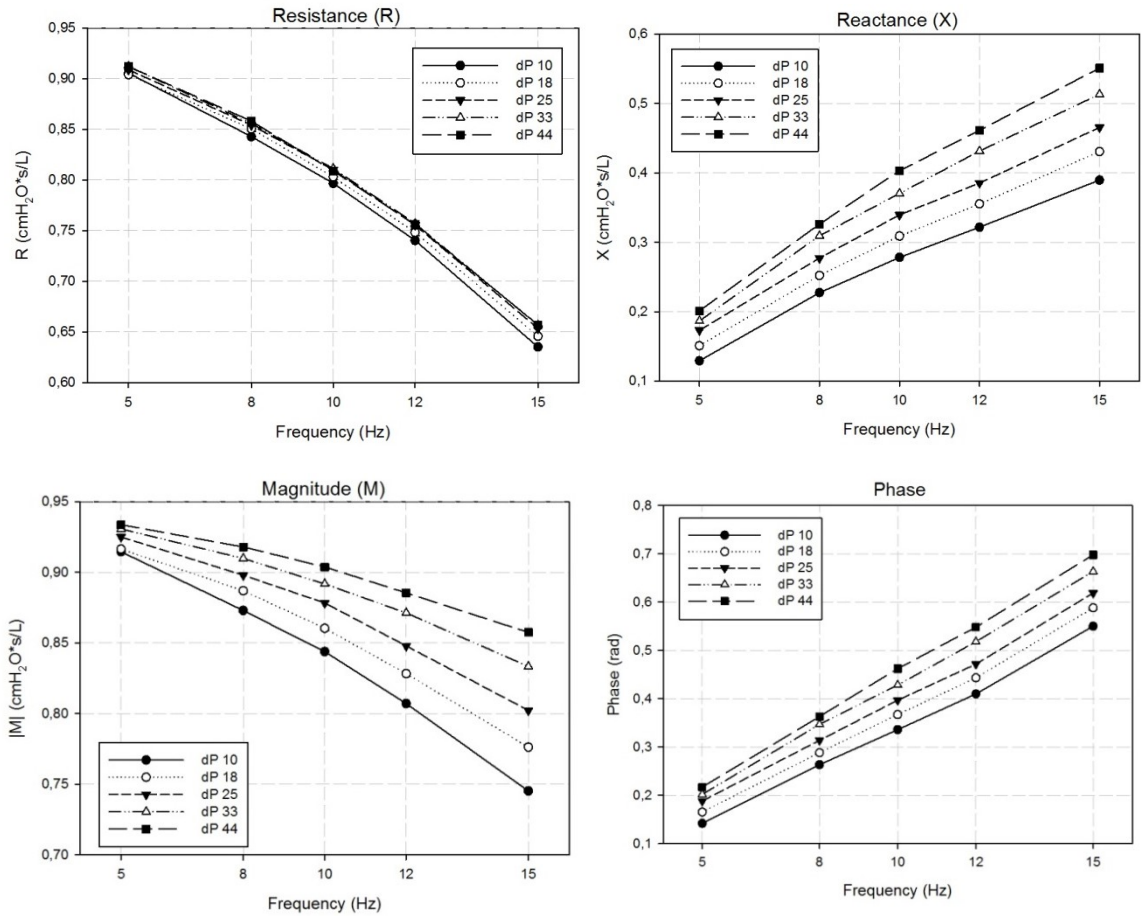

Figure 4.11 Corrective transfer functions. The graph shows the corrective values for impedances resistance (A), reactance (B), magnitude (C) and phase (D) at each frequency (5, 8, 10, 12 and 15 Hz) for different pressure amplitudes (10, 18, 25, 33 and 40 cmH_2O).

While resistance values are very similar between the ΔP tested and they decrease from 0.9 cmH2O*s/L at 5 Hz to 0.65 at 15 Hz, the reactance values increase from 0.12-0.2 at 5 Hz to 0.38-0.55 at 15 Hz. The magnitude values increase from 0.92 at 5 Hz to 0.74-0.85 at 15 Hz; the phase values increase from 0.14-0.21 at 5 Hz to 0.55-0.7 at 15 Hz.

The real part (R) of the correction transfer function seems to be frequency dependent, but not amplitude dependent, while imaginary part (X) shows a behaviour that is strongly dependent from the amplitude of the oscillatory pressure wave. The phase component, instead is characterized by 5 parallel lines, one for each pressure amplitude tested.

These measurements permit to find out corrective factors for impedances: a correction function has been implemented in Matlab ad it allows to correct the impedance in frequency domain, giving the vector of pressure amplitude at increasing frequency as input.

The correction is obtained by a multiplication of the impedance function (Z) of each baby with the correspondent transfer function (Z_{corr}) in terms of frequency and pressure amplitude. Real part (R) and imaginary part (X) of the impedance function, therefore, can be corrected with one only computation.

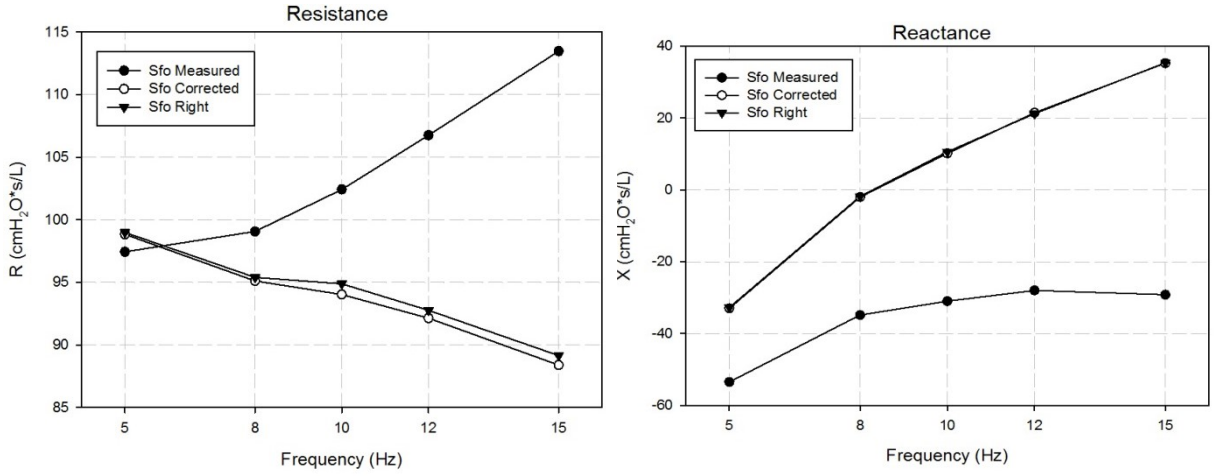

Figure 4.12 Example of pressure correction in terms of real and imaginary part of input impedance of a test lung (0.5L) ventilated at 5 different frequencies with a peak to peak pressure of 25 cmH_2O.

Figure 4.12 shows an example of pressure correction in terms of real and imaginary part of the input impedance of a 0.5L glass bottle ventilated at 5 different frequencies with a peak to peak pressure of 25 cmH_2O.

The imaginary part of the input impedance was perfectly corrected (in panel B the 'right' and 'corrected' curves are superimposed), and for the real part there is an error less than 2% of the 'right' resistance values.

In some clinical studies (patient 8 and 9), the evaluation of pressure signals was made in two different point (near the mouth of the newborn and near the Sensormedics) in order to verify that the correction worked in the right way.

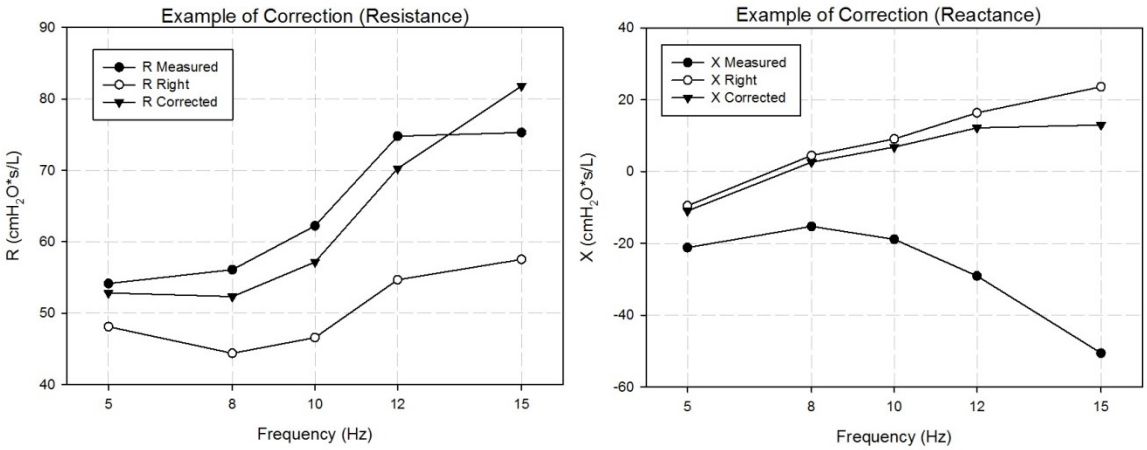

Figure 4.13 Correction of a newborn impedance.The -●- line represents the measure before correction and -▼- line represents the measure after correction of (A) real part, (B) imaginary part.

Figure 4.13 shows an example of input impedance correction on a newborn data. The effect of the correction is strongly visible on the imaginary part, which approximated the right measurements, even if the error increases with increasing frequencies. After correction the low pass filter limitation is solved and the reactance curve cross the zero line at a resonant frequency almost equal to the reference one.

For the real part the correction is not so evident, but this is probably due to the absence of flow compensation described in further paragraphs.

4.4 FLOW COMPENSATION

The phenomenon of airway resistance to inflow is complex and has different behaviors as the fluid flows. A fluid moves through a conduit due to the pressure difference (ΔP) that overcomes the attrition after the flow ($\dot{V}$). Thus, $\dot{V}$ depends on the existence of ΔP between the extremities of the conduit and the larger or smaller difficulty to the passage of this flow is understood as larger or smaller resistance (R), which is directly proportional to ΔP and inversely proportional to $\dot{V}$, as demonstrated in the following equation[53]:

$$R_{aw} = \frac{\Delta \mathrm{P}}{\dot{V}} \qquad [4.6]$$

where R_{aw} is airway resistance.

When the phenomenon is observed with low flows, it occurs the so called laminar flow, an occurrence that can be described by a first grade equation (eq. 4.7). If the flow is increased, the phenomenon will become turbulent, and the equation to describe this phenomenon will be the following second-grade equation, as described by Rohrer equation (eq. 4.8):

$$\Delta \mathrm{P} = K_1 \dot{V} \qquad [4.7]$$

$$\Delta \mathrm{P} = K_1 \dot{V} + K_2 \dot{V}^2 \qquad [4.8]$$

where K_1 is the linear coefficient and K_2 is the angular coefficient of the straight line.[53]

By dividing all the terms of the last equation by $\dot{\mathrm{V}}$ and substituting with eq. 4.6 one can observe that system R is linearly related to $\dot{\mathrm{V}}$, as follows:

$$R_{aw} = K_1 + K_2 \dot{V} \qquad [4.9]$$

In the clinical study were used different size endotracheal tubes (ETT) and their resistance behaviour is flow dependent because at different frequencies correspond different flows.

For this reason the real part of the transfer function between pressure and flow, which represents the resistance of the system, should be corrected in order to estimate the resistance of the respiratory system without ETT resistance contributes.

4.4.1 Flow dependent measurement setup

In order to measure flow dependence the set-up used was very similar to the one described before.
It was composed of:

- Sensormedics providing HFOV to the test lung;
- Pressure and flow sampling system (Florian);
- OEP System for acquisition and record.

Also the same test lungs have been used; they were composed of a 0.5L and 1L bottles and different endotracheal tubes (ETT): 2, 2.5, 3 and 3.5 mm. A further precaution was the use of different size corks with which it was possible to 'intubate' the bottles in order to avoid any additional resistive phenomenon due to the ETT connection.
Figure 4.14 shows the setup.

Figure 4.14 Test lungs setup to flow-dependent resistance compensation. A) Intubated test lung with a cork, B) different size bottle and ETT used for the in vitro study.

Using this setting we tested 5, 8, 10, 12, 15 Hz of oscillatory frequencies at five different pressure amplitudes: 10, 18, 25, 33, and 40 CmH_2O; other ventilator parameters (continuous distending pressure and E/I ratio) were not changed. For each step 30'' pressure and flow waves are acquired. Data are saved on the OEP workstation.

If the airway opening pressure is measured near the endotracheal-tube (ETT), the input resistance includes the ETT resistance, which is strongly flow dependent. In order to determine the real resistance of the newborns, a correction is applied on the real part of the impedance (and transfer impedance): endotracheal tube resistance was subtracted from total resistance to obtain respiratory resistance.

$$R_{new} = R_{old} - R_{ETT} \tag{4.10}$$

The evaluation of the real part of the transfer function between pressure measured near the ETT and the flow measured through the Florian's and the hot wire anemometer was made in this part of the study.

$$tf = \frac{\Delta P_{nao}}{\dot{V}} \tag{4.11}$$

$$R_{ETT} = Real(tf) \tag{4.12}$$

In this case it was found that the resistance of the ETT is not affected by the size of the bottle, so the correction depends only on the diameter of the tube and so on the flow, as expected from equation 4.8 (Rohrer's equation).

4.4.2 Flow correction

The second part of the in vitro study focused on the value of resistance of ETT tube and compliance of the bottles. These measure allow us to correct the value obtained in the clinical study to compute a value of impedance that is not affected by endotracheal tube flow-dependent resistance.

The following graphs report the real and imaginary part of the input impedance of 2 different test lungs composed by 0.5L and 1L glass bottle and 4 different ETT (2mm, 2.5mm, 3mm and 3.5mm).

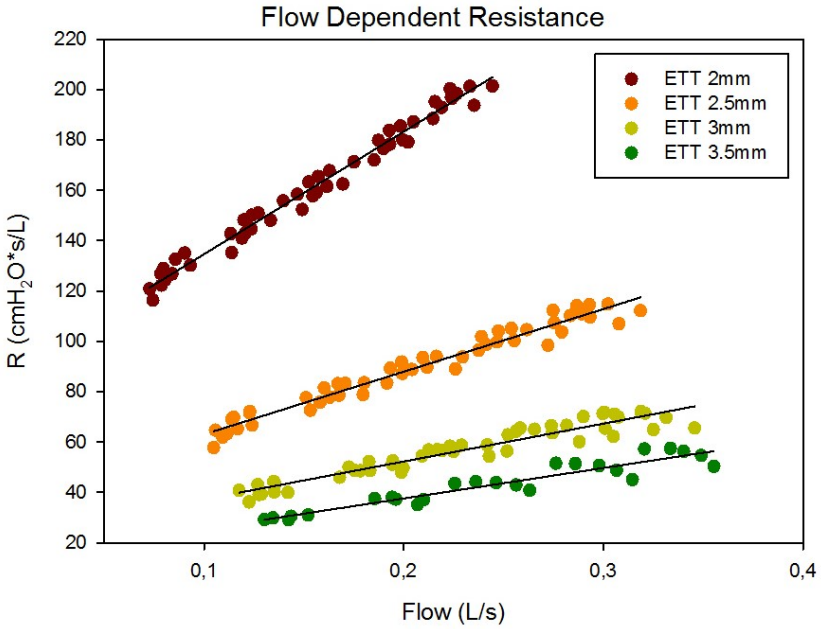

Figure 4.15 Real part versus flow of the transfer function between pressure and flow of a series of test lungs and endotracheal tubes.

The linearly flow-dependence of ETT resistance has been explained in previous paragraphs through the Rohrer's equation and it is demonstrate in this plot: each line represents a different endotracheal tube, from 2mm (green dots) to 3.5mm (red dots). The tested frequencies are the same of the clinical study and for each frequency have been tested 5 pressure amplitude (from 10 cmH_2O to 40 cmH_2O): frequencies are represented as 5 cloud of point and each cloud corresponds to a pressure amplitude. This means that at increasing pressure (and so at increasing flow) the correction of the real parte is more evident.

As endotracheal tube diameter increases, the linear coefficient decreases and the trend is not influenced by the load (i.e. glass bottle size).

The linear coefficients, intercepts and r^2 values are reported in table 7:

Table 7 Regression values

Tube diameter	*m*	*q*	r^2
2 mm	486.5	85.9	0.982
2,5 mm	248.8	38.2	0.959
3 mm	150.3	22.2	0.913
3.5 mm	120.9	13.4	0.896

Also the imaginary part shows a trend for each tube, but in this case the linear dependence is not supported by any physical low.

The following graphs show the imaginary part of the input impedance of the same test lung combination used to determine the real part, but the representation is focused on the frequency dependent behaviour.

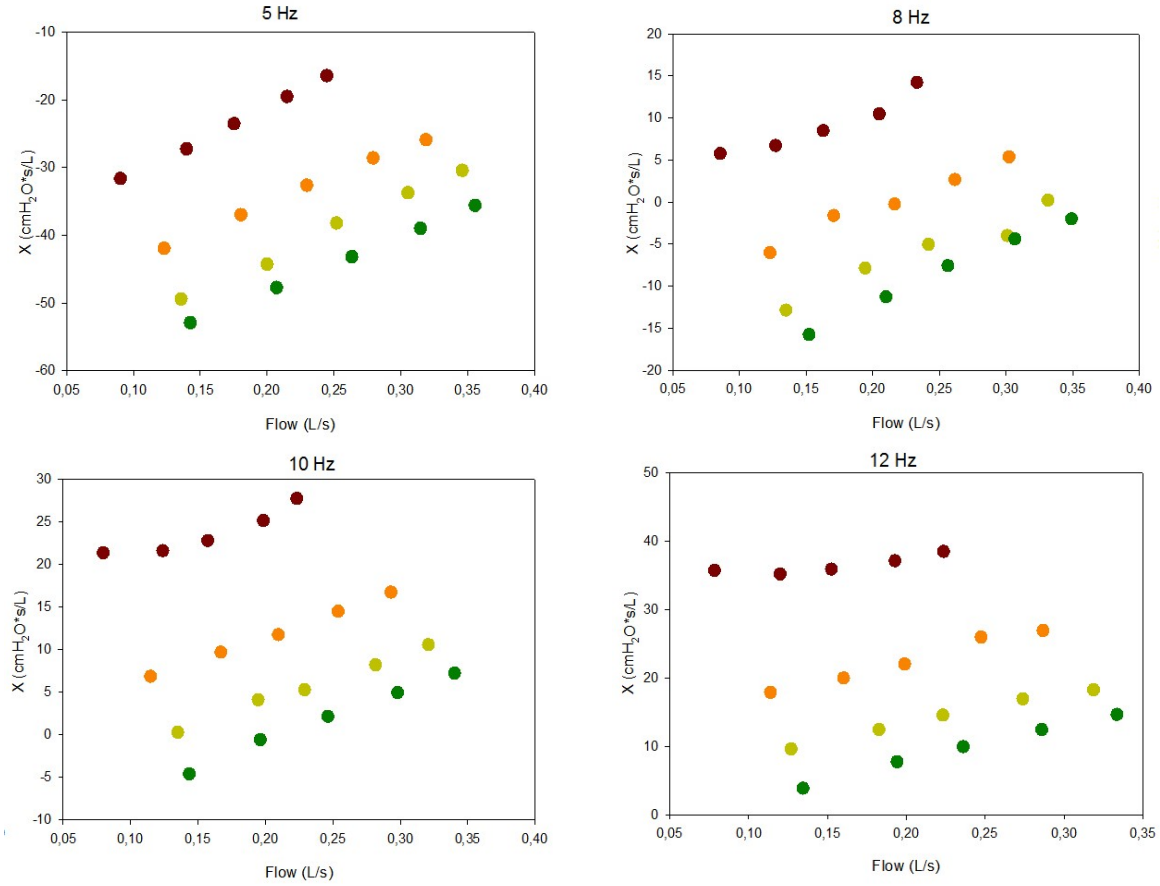

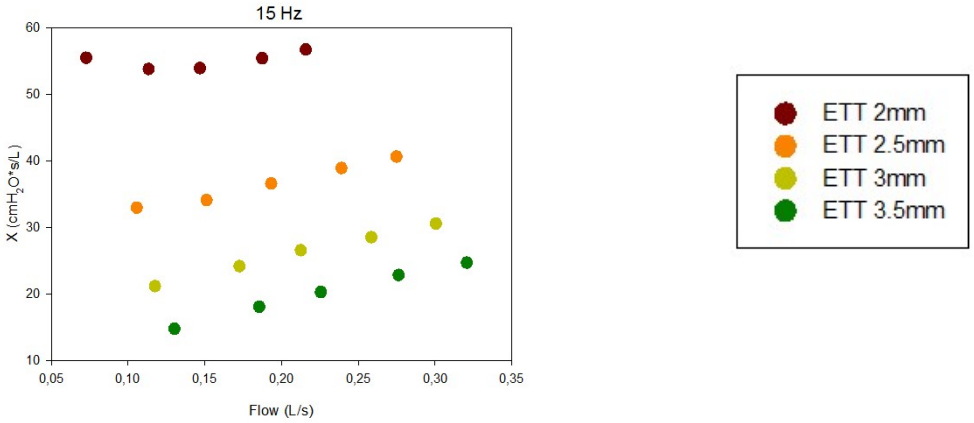

Figure 4.16 Imaginary part versus flow of the input impedance of a series of test lungs and endotracheal tubes.

At each frequency the imaginary part of different ETT shows a linear dependence from flow but, unlike the real part, the coefficient seems to remain constant: the lines that represent different ETT diameters are almost parallel and there is a vertical shift at increasing frequencies. The zero crossing point in frequency (resonant frequency) increases with increasing diameters.

More tests would be useful to understand how the imaginary part compensation should be performed, for example making different protocols in terms of pressure amplitude or testing different size and materials test lungs.

5. Clinical study

This chapter reports the experimental protocol, population and results of the clinical study. The combination of Optoelectronic Plethysmography (OEP) and Forced Oscillation Technique (FOT) allows collecting information about the mechanical behaviour of the chest wall and pressure wave propagation in different thoraco-abdominal compartments. The clinical results provide information about the frequency dependent response of different compartments in terms of resistance and reactance, in particular referring to the resonant frequency. Moreover total and regional transfer impedance of the respiratory system have been computed and compared in order to propose a suitable compartment subdivision of the chest wall.

5.1 CLINICAL STUDY DESIGN

The whole study was carried out in the Neonatal Intensive Care Unit (NICU) of FMBBM San Gerardo Hospital, Monza.

The clinical study protocol has been approved by the Ethics Committee of the province of Monza and Brianza and all data are collected pursuant to the Personal Data Protection Code – Legislative Decree n. 196/2003.

This is a prospective/observational study, so there are no potential risks associated with the performance of both phases.

The recruitment maneuver and identification of the optimal CDP is part of the common clinical protocol applied in the neonatal intensive care unit and the oscillatory frequencies are varied in the range already proved suitable for the application of HFOV. This is a preliminary maneuver that allows the clinical optimization of the oscillatory parameters.

The frequency study involves the acquisition of the thoraco-abdominal wall kinematics in terms of pressure oscillations transfer function and gas exchange at different oscillatory frequencies.

5.1.1Clinical optimization of the oscillatory parameters.

The clinical protocol currently in use in S. Gerardo's Hospital Neonatal Intensive Care Unit (NICU) is followed in this phase.

If not already done, a recruitment maneuver is performed in order to identify the Optimal Continuous Distending Pressure (CDP) by using the "incremental decremental CDP trial" based on SpO2 proposed by DeJaegere.[23]

The starting settings are the following:

- CDP: 6-8 cmH_2O
- FiO_2: adjusted to obtain a correct oxygenation (FiO_2 form 0.21 to 0.5)
- P/P pressure: at minimum to obtain normocarbia
- Oscillatory frequency: 10-15 Hz.

A stepwise recruitment maneuver is performed following this procedure:

1. CDP is increased stepwise: 2 cmH_2O every 3 minutes. At each step an increase in oxygenation (SpO_2 and $PtcO_2$) occurs; SpO_2 must be kept between 86% and 94% by adjusting FiO_2. The lung inflation is carried on till we observe a worsening in oxygen saturation or FiO_2 becomes less than 30%. It identifies the apex of the lung hysteresis curve: the so called CDP Opening.
2. CDP is decreased stepwise with steps of 2 cmH_2O every 3 minutes. The lung deflation is carried on till we reach the CDP Closing: the CDP value at which a worsening in SpO_2 is registered (because of the alveolar closing), that is a drop in SpO_2 equal or more than 5% of the SpO_2 measured at CDP Opening or an absolute SpO_2 value inferior to 86%.
3. The CDP is set at CDP Opening for 2-3 minutes in order to re-open the lung.
4. The CDP is set at CDP Optimal, that is 2 cmH_2O above the CDP Closing on the deflation limb.

P/P pressure is kept constant during the whole maneuver.

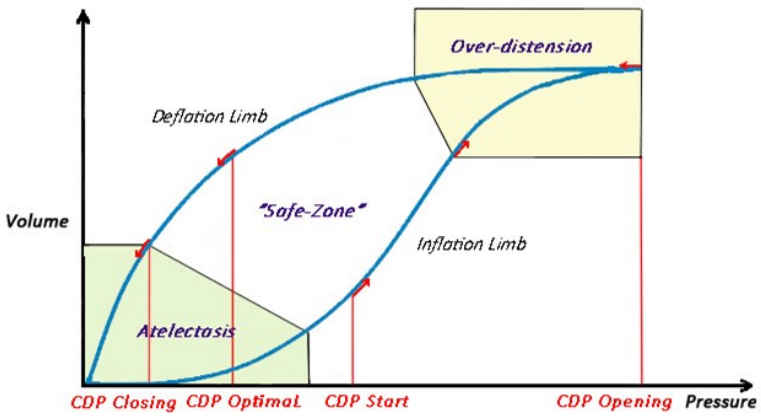

Figure 5.1 Incremental-Decremental CDP trial. (Modified from A.T. Rotta et al[54]).

5.1.2 Frequency Study

Once optimal CDP has been identified, pressure amplitude is adjusted to ensure a $VT <$ 2.5 ml/kg and a partial pressure of CO_2 (PtcCO2) between 40 and 60 cmH2O*s/L.

In this condition the DCO_2 value is calculated using the following formula:

$$DCO_2 = f_{HFOV} \left(\frac{V_T}{Kg}\right)^2$$

[4.1]

Five different oscillatory frequencies (5 Hz, 8 Hz, 10 Hz, 12 Hz, 15 Hz) are randomly tested.

When a new frequency is set, the P/P pressure is regulated to adjust VT in order to maintain DCO_2 constant.

After 10 minutes all parameters are recorded: clinical values, thoraco-abdominal wall movements, air flow and pressure waves (1-2 minutes acquisition). All these data are recorded on a Personal Computer and are studied in order to evaluate their behavior at different oscillatory frequencies.
During the study, at each frequency heart rate, blood pressure and gas parameters are monitored in order to verify the stability of the newborns condition.

5.1.3 Population

Newborns are recruited based on the following inclusion/exclusion criteria.

Inclusion criteria:

- Pre-term neonates (Gestational age < 37 weeks)
- Babies who need HFO ventilation for any prematurity-related respiratory disease.

Exclusion criteria:

- Pneumothorax
- Congenital heart diseases
- Congenital malformations relevant to lung function
- Absence of consent from the parents.

Ten neonates have been admitted to the study to date (from 16/04/2014 to 20/11/2014):

Table 8 Patients clinical characteristics.

Patient ID	*Gender*	*Gestational Age (week+days)*	*Age at the Study*	*Body Weight (Kg)*	*Pulmonary Disease*
1	M	30+1	9h	1.43	Pulmonary Hypoplasia
1Bis	M	30+1	6 days	1.425	Early BPD signs on chest X-ray
2	M	27+6	6 days	0.86	RDS
2Bis	M	27+6	27 days	1.394	Pulmonary Hemorrhage
3	F	25+2	5 days	0.721	Pneumonia
4	F	25+4	15h	0.625	RDS
5	M	26+3	2 days	0.686	RDS
6	M	25+2	3 days	0.755	RDS
7	M	38	3 days	3.17	RDS
8	F	33+5	1 day	2.24	Pneumonia
9	F	26+6	14h	0.97	RDS
10	M	26+3	1 day	0.79	RDS

Patients 1 and 2 were studied twice (1Bis and 2Bis) since the features of their lung diseases changed significantly over time. In particular, Patient 1 had a small lung volume (pulmonary hypoplasia) and when he was studied for the second time (Patient 1Bis) he seemed to have an early evolution towards BPD. In Patient 2, instead, a massive pulmonary haemorrhage intervened the day before the second acquisition.

For these reasons they may be considered as 4 cases since they represent different mechanical features. Therefore, the total number of cases is 12.

Patient 6 flow data and patient 2 OEP camera's data are missed because of technical problems.

Demographical features of the studied population are summed up in Table 9.

Table 9 Population demographic features.

Patients Features	
Number of cases	12
Gender:	
Male	66.7%
Female	33.3%
Gestational Age (mean value/standard deviation)	28 wks + 4 wks
Age at the study (median value/range)	5 ± 7 days
Body Weight (median value/range)	1.26 Kg ± 0.76 Kg
Disease:	
Isolated RDS	59%
Pulmonary Hypoplasia	8%
Pulmonary Hemorrhage	8%
Pneumonia in Sepsis	17%
Early BPD	8%

Baseline parameters are presented in Table 10: they include the optimal CDP (chosen during the inflation-deflation trial), the baseline ventilation frequency (choose according to the infant weight), ETT diameter and other clinical parameters that can describe the newborn pulmonary condition.

Table 10 Physiological and ventilation basal parameters.

Pt ID	***CDP*** ***(cmH_2O)***	***f*** ***(Hz)***	***ΔP*** ***(cmH_2O)***	***ETT*** ***(mm)***	***$PtcO_2/FiO_2$*** ***(cmH_2O)***	***$PtcCO_2$*** ***(cmH_2O)***	***V_T/Kg*** ***(ml/kg)***	***DCO_2/Kg*** ***(ml/s*kg)***
1	20	15	28	2.5	174	40	1.68	42.25
1Bis	13	10	40	2.5	100	43	3.09	95.34
2	12	10	32	2.5	150	39	2.67	71.53
2Bis	12	12	31	3.5	107	33	2.80	93.93
3	10	10	19	2.5	147	35	3.33	110.80
4	10	12	25	2	252	32	1.76	37.17
5	8	15	27	2.5	343	38	2.33	81.60
6	10	15	38	2.5	444	49	1.90	53.87
7	10.5	10	27	3.5	156	43	2.15	46
8	12	12	35	3.5	185.7	51	1.61	30.99
9	8	12	38	2	319	35	1.20	18.37
10	9.5	12	22	2.5	257	38	1.39	23.27

5.1.4 Statistical Analysis

The statistical analysis is performed by using SigmaStat® (Systat Software, Inc., Chicago, IL, USA).
Firstly, a descriptive analysis of the sample is performed considering gender, gestational age, age at the study, birth weight and disease. Results are shown in terms of mean and CI 95% when data are normally distributed, otherwise they are presented as median and range.
OEP data have been analyzed by using One Way ANOVA for Repeated Measurements using frequency as factor for global variables and Two Way ANOVA for Repeated Measurements using frequency and compartment as factors for compartmental analysis. All Pairwise Multiple Comparison Procedure (Holm-Sidak method) is performed as post hoc test.

If a significant difference of a parameter is found at different frequencies an All Pairwise Multiple Comparison Procedure (Holm-Sidak method) is performed in order to understand which frequency differs from the others.
If data are not normally distributed the ANOVA test on Ranks is performed and Tukey Test is used as post-hoc test.
Differences were considered significant for $p<0.05$.
The Pearson Comparison Method and his correlation index has been used between two statistical variables to evaluate correlation and the Bland-Altman test, instead, has been used to evaluate the linear regression between two variables.

5.2 CLINICAL STUDY RESULTS

The use of the OEP system, combined with FOT, allows acquiring pressure, flow and cameras data simultaneously. Pressure and flow signals have been used for the input impedance computation, while the measurement of marker 3D coordinates allowed two different types of analysis: motion analysis and regional transfer impedance computation.

5.2.1 Frequency dependence of lung impedance

From the pressure and flow signals recorded at the airway opening, the input impedance has been computed for each patient. It has been expressed as real and imaginary part (top panels) and as magnitude and phase (bottom panels):

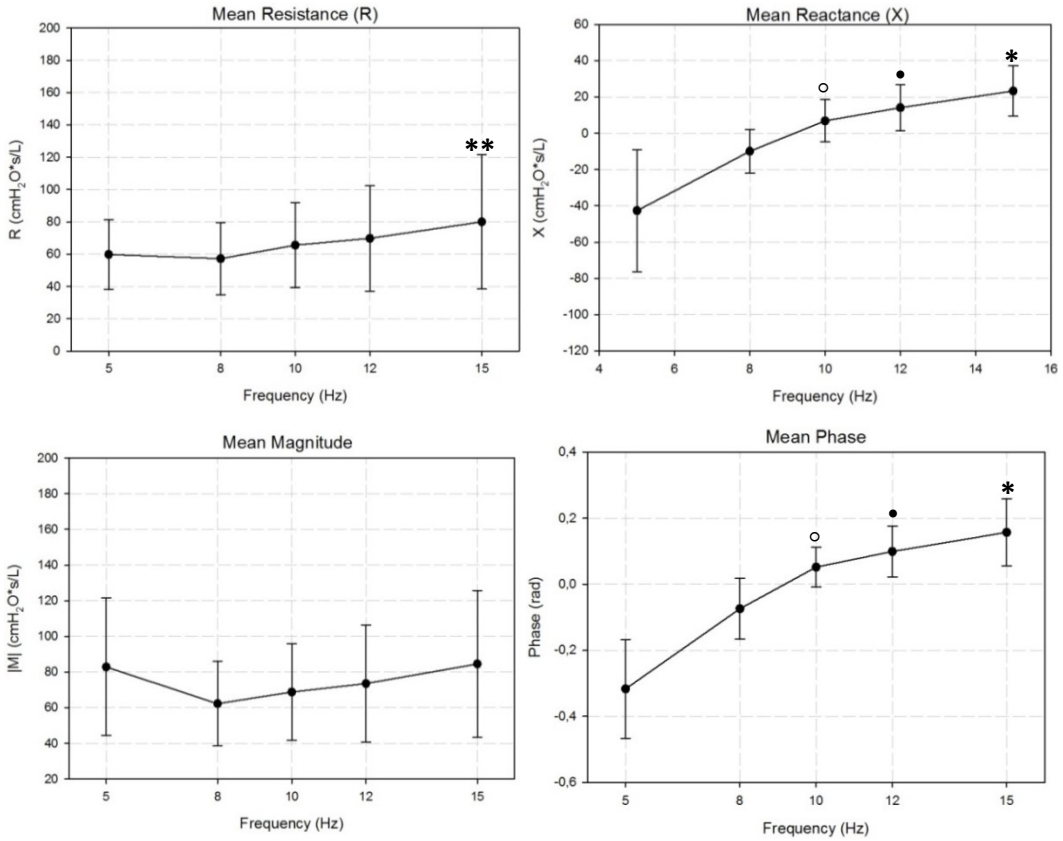

Figure 5.2 Magnitude of the input impedance of 10 patients at 5 different frequencies (5, 8 10, 12 15 Hz). Data are presented as mean value and standard deviation. A statistically significant difference has been observed for 15 Hz (*), 12 Hz (●) and 10 Hz (°): single symbol means P<0.05, double symbol means P<0.001 (*=P<0.05; **=P<0.001).

The resistance value at 5 Hz is 59.7 ± 21.51 and it decreases to 80 ± 41.58 at 15 Hz (mean ± SD cmH_2O *s/L). Conversely the reactance increases from -42.6 ± 33.6 at 5 Hz to about 23.3 ± 13.9 (mean ± SD cmH_2O *s/L) at 15 Hz.
The magnitude mean value at 5 Hz is 82.8 ± 38.58 and decreases till 84.5 ± 41.22 (mean ± SD cmH_2O *s/L) at 15 Hz. The phase, instead, increases from -0.31 ± 0.14 at 5 Hz to about 0.15 ± 0.1 (mean ± SD cmH_2O *s/L) at 15 Hz.

While in real part there is only a statistically significance at 15 Hz in respect to 5 Hz and 8 Hz (P=0.001); in reactance there is a statistically significant difference between 15 Hz and 12 Hz in respect to 5 Hz and 8 Hz; between 10 Hz in respect to 5 Hz. In phase component there is a statistically significant difference between 15 Hz and 12 Hz in respect to 8 Hz and 5 Hz ; between 10 Hz in respect to 5 Hz.
For the magnitude, instead, there's no significant difference (P = 0.097).

The impedance has been corrected through the in vitro measurements to obtain the total resistance of the respiratory system without the ETT contribute. The flow dependent resistance of the endotracheal tube was subtracted from newborns real part of the input impedance for each frequency at the correspondent flow.
The real part of the input impedance represent the resistance of the respiratory system and it remains almost constant at each frequency for all the newborns.
Figure 5.3 shows the impedance imaginary part, that represents the respiratory system reactance (X) for each patient.

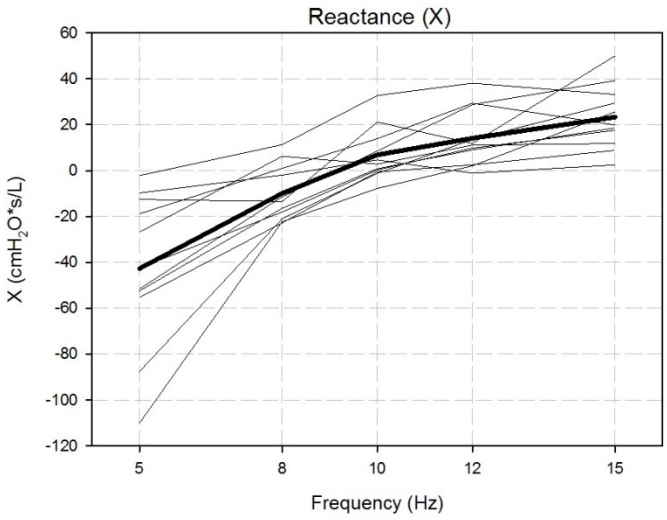

Figure 5.3 Reactance vs. frequency**.** Data are shown for each studied patient.

All the neonates have a similar trend in their reactance: X tends to increase with increasing frequencies. Moreover, we can notice that reactance variation is extremely different among the studied neonates.

The frequency at which reactance becomes zero is the so called resonant frequency (f_0). Table 11 shows the resonant frequency for each neonate obtained with the fitting curve described in chapter 4 and its relative coefficients.

The mean r^2 for the fitting curves is 0.92, with a minimum value of 0.69 for patient 10.

Table 11 Fitting coefficients for each patient and their r-square value.

Patient ID	*a*	*c*	r^2
Pt 1	-624.98	4.89	0.97
Pt 1Bis	-148.48	2.59	0.85
Pt 2	-278.48	2.54	0.99
Pt 2Bis	-151.32	1.81	0.83
Pt 3	-324.69	2.37	0.96
Pt 4	-529.23	4.72	0.98
Pt 5	-368.66	4.50	0.99
Pt 7	-53.13	0.48	0.69
Pt 8	-325.63	2.92	0.99
Pt 9	-79.62	3.15	0.8
Pt 10	-328.37	4.35	0.92

Discussion

Clinicians are used to set frequency referring to patient weight; in particular, they use 15 Hz frequency when the baby weights less than 1500g, conversely they ventilate neonates with about 10 Hz oscillatory frequency. Preterm babies with lower weight are associated with smaller pulmonary volume, and thus a stiffer lung. The theoretical study of reference[3] demonstrates that compliant lungs filtered the high frequencies, therefore they should be ventilated with lower frequencies; conversely stiff lungs could be ventilated with higher frequencies, since they are not affected by the low pass tissue filtering.

Different compliant lungs have different frequency mechanical response, therefore the resonant frequency is inversely proportional to the lung compliance.

The resonant frequencies of the newborns acquired during this study have been compared with their weight in order to verify if there is a linear correlation between two variables and there are no significant results.

Resonant frequencies are highly variable and not predictable by body weight and this is probably due to the dependence of the lung compliance from the disease. Our patient resonant frequencies are reported in table 12, with their respective body weight and disease.

Table 12 Resonant frequency correlation with body weight and lung disease.

Patient ID	*Resonant Frequency (Hz)*	*Body weight(Kg)*	*Pulmonary Disease*
Pt 1	11.3	1.43	Pulmonary Hypoplasia
Pt 1Bis	7.58	1.425	Early BPD signs on chest
Pt 2	10.48	0.86	RDS
Pt 2Bis	9.1	1.394	Pulmonary Hemorrhage
Pt 3	11.7	0.721	Pneumonia
Pt 4	10.5	0.625	RDS
Pt 5	9.05	0.686	RDS
Pt 6	10.5	3.17	RDS
Pt 7	10.56	2.24	Pneumonia
Pt 8	5.2	0.97	RDS
Pt 9	9.36	0.79	RDS
Mean ± sd	9.57 ± 1.86 Hz	1.26 ± 0.76	-

Resonant frequency ($f0$) obtained is not as high as reported in literature: Venegas and Fredberg assert that resonant frequency is very high in neonates affected by RDS, even higher than the frequencies used in clinical practice[3]. Therefore they proposed to ventilate the neonate at the corner frequency (fc).

From a mechanical point of view, resonant frequency represents the optimal frequency since compliance and inertance cancel each other out; in this condition the only obstacle to the pressure wave propagation is respiratory resistance and the ventilation reaches the maximum of efficiency. Corner frequency, instead, represent the point of maximum impedance drop: the elastic and inertial components are of little account; the clinical

advantage of corner frequency is its lower value than resonant frequency; too high frequencies, in fact, cannot guarantee sufficient volumes for the ventilation, so aren't present in a lot of ventilators.

No one before has ever computed resonant or corner frequency in ventilated neonates. Our results disprove the theoretical knowledge: resonant frequency is not higher than 15 Hz. In fact, it has found resonant frequencies between 7 and 12 Hz, with an outlier (Patient 8 with 5.2 Hz); in this situation corner frequencies are not necessary. The $f0$ computed are lower than theoretical ones because they have been calculated on the entire respiratory system, conversely Venegas et al. have computed $f0$ on computer models of the only lung. Moreover, recent studies[51] propose that the neonate's respiratory system has to be considered into, at least, two compartments: the abdomen and the rib cage. Considering these two compartments, in fact, it's possible to suppose that the resonant frequency is influenced by the proper characteristics of both the rib cage and the abdomen. Having the abdomen an elevated inertial component, it is expected to have a very low resonant frequency; on the contrary the lung (as theoretical studies affirmed) and then the rib cage probably have a higher resonant frequency. Considering both these components, the resonant frequency of the entire system has a moderate value, probably nearer to the abdominal $f0$ since abdomen is the more represented compartment. The same reasoning should be also due for different lung zones in a non-homogeneous lung: the more the heterogeneity of the lung, the greater the number of compartments that should be considered and the hardest the choice of the optimal ventilation frequency.

The theoretical model used by Venegas for the frequency behaviour, however, doesn't describe entirely the lung mechanics: from the obtained measurements real part isn't totally constant at all the frequencies, and imaginary part crosses the zero at a reasonable value.

This happens because of the excessive simplification of the model; in fact it doesn't consider nonlinearities, different compartments responses and phase lags created during the oscillatory propagation.

5.2.1 Pressure wave propagation

The pressure amplitude (ΔP) imposed to the newborn by Sensormedics produces vibrations on newborn chest wall with the same frequency of the input wave. Such vibrations are detected by OEP cameras and saved on the OEP workstation and allow characterizing the regional heterogeneities of chest wall mechanical properties and displacements at different oscillatory frequencies (f).

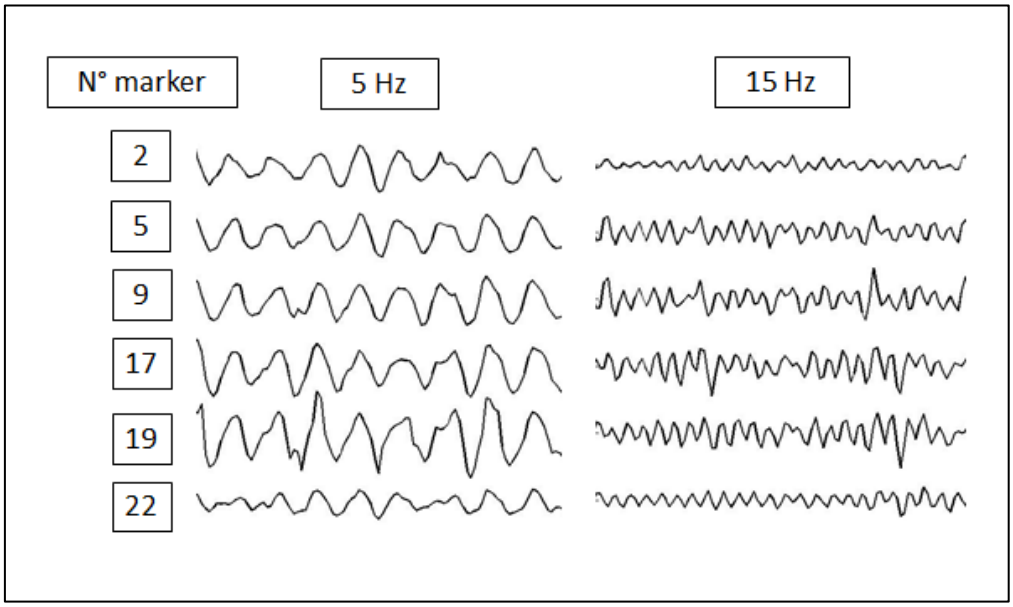

Figure 5.4 Example of marker oscillation signals at different frequencies (5Hz and 15Hz).

Phase shift

The propagation of the forced wave was studied using the phase of the displacement signal of 12 areas (described in paragraph 3.2.2 OEP Data Analysis) and marker N°2 during oscillations.

The phase shift distribution is shown in the following colored maps that represent phase lag in a virtual averaged neonate. Each map represents a different oscillatory frequency and the color depends on the phase lag: the darker the color, the greater the lag. In the maps the lag is represented as the phase shift of the oscillatory wave.

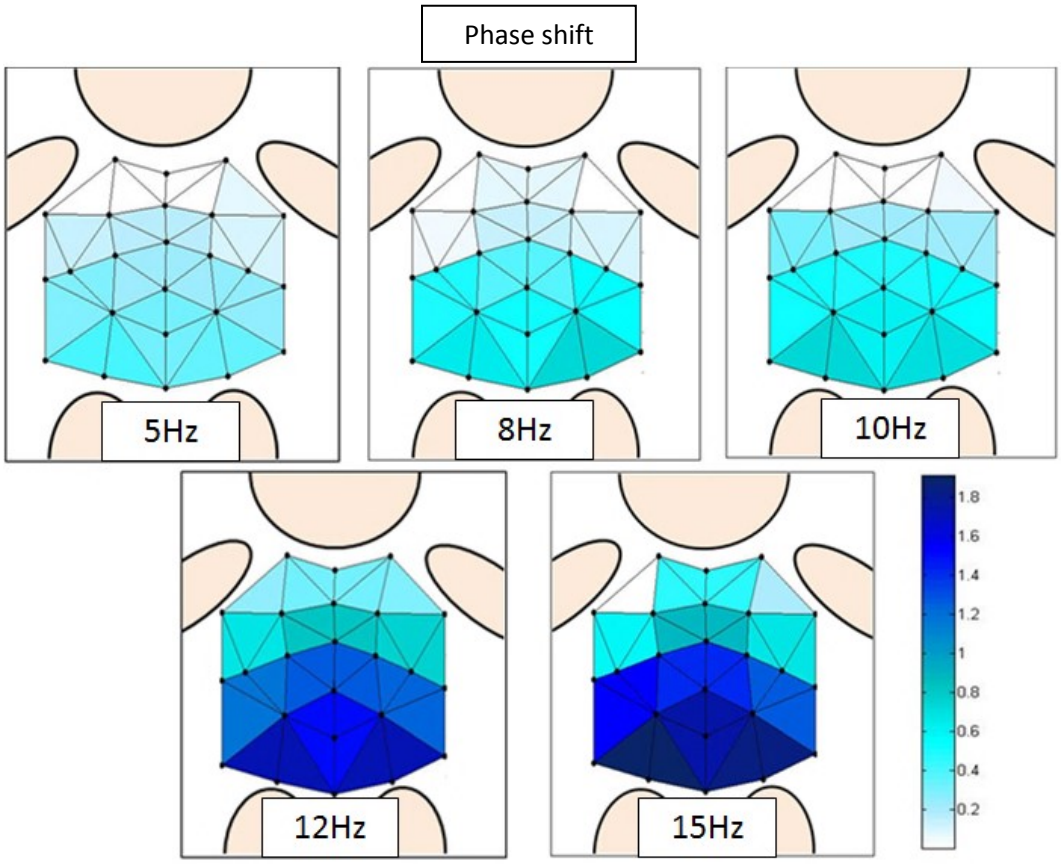

Figure 5.5 Phase shift between areas and marker N°2. Data are averaged for all patients and represented as a colourful map. The lag is represented as phase shift (radians) of the sinusoidal wave.

A progressive increment of the phase shift along the craniocaudal direction was found, both at low and high frequency. The abdomen behaviour is less homogeneous than the rib cage at increasing frequencies, in fact the abdomen areas show a more variable phase lag than the areas that compose the rib cage. This means that abdomen and rib cage cannot be described as one compartment, but they should be represented as more compartments.
In particular abdomen should be divided in lower costal margin, umbilicus area and superior iliac spine due to the different characteristics of these areas.

Since the pressure wave propagation is supposed to occur in cranio-caudal direction prevalently, the lag along the midline is also represented in terms of time (s) (Figure 5.5).
It includes the area from marker N°2 to marker N°22 that synthesizes how the pressure wave given by the ventilator is propagated along the respiratory tree. Moreover the x-axis is shown in distance (mean of all newborns) in order to have a more correct spatial representation of the markers.

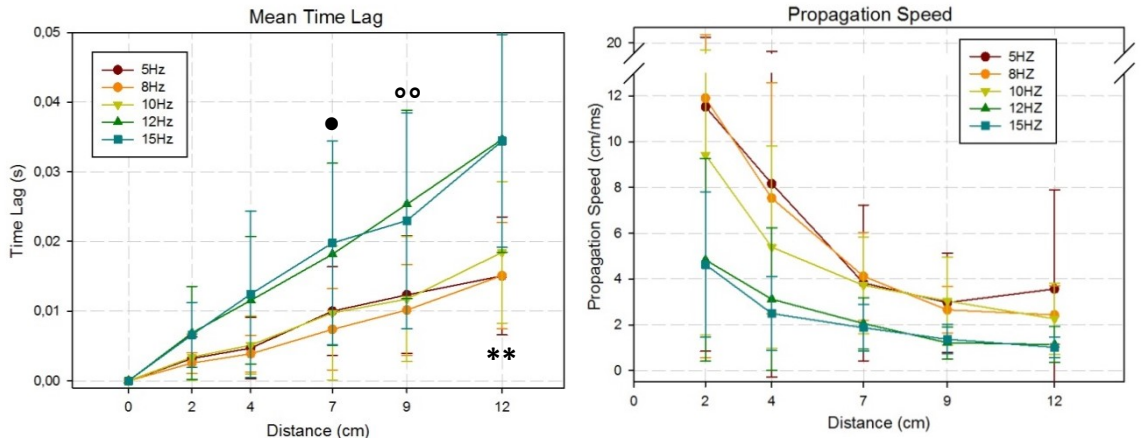

Figure 5.6 Time-lag of midline areas referred to marker N°2 and propagation speed of the pressure wave along the midline. *X*-axis is proposed as mean distance of the midline markers. Data are presented as mean value and standard deviation. A statistically significant difference has been observed for marker N°22 (distance 12cm)(*) , marker N°19 (distance 9 cm)(°) and marker N°17 (distance 7 cm)(•): single symbol means P<0.05, double symbol means P<0.001 (*=P<0.05; **=P<0.001).

From these data it is possible to notice that not only the lag, but also the standard deviation increases with increasing frequency and moving toward the abdomen. The phase shift is particularly high in the abdominal compartment and this effect is more evident increasing frequency. At 15 Hz, the phase lag in the most caudal regions approaches 180° (0.03s in Figure 5.6), indicating opposite movements in different regions.

Since the lag increases with frequencies, the propagation speed decreases with frequencies and with distance from marker N°2.

About frequency-dependence, we could differentiate two time-lag zones: the lower time lag (from 0.0016-0.0029 s to 0.0129-0.0147 s) is obtained at the lower frequencies, 5 and 8, 10 Hz; the greater time-lag (from 0.0048-0.007 s to 0.0373-0.035 s) is obtained at 12 and 15 Hz.

As regards the marker position, the lag increases towards the abdomen at every oscillatory frequency: the mean lag at marker N°5 is 0.0038±0.002 s and increases till 0.025 ± 0.011s at marker N°22.

Data are presented as mean value and standard deviation. Marker N°17 has a statistically significant delay at 15 Hz in respect to 5 and 8 Hz (P=0.002). Marker N°19 has a statistically significant delay at: 15 Hz in respect to 5Hz (P=0.001) and 8Hz (P=0.002); 12 Hz in respect to 5 Hz (P<0.001) and 8 Hz (P=0.002). Marker N°22 has a statistically

significant delay at: 15 Hz in respect to 5 Hz and 8 Hz (P<0.001); 12 Hz in respect to 5 Hz, 8 Hz (P<0.001) and 10 Hz (P=0.006).

The oscillatory displacement at each marker along the midline has also been computed: Figure 5.7 shows the displacement of marker N°2, 5, 9 17, 19, the central markers in the model used for this study.

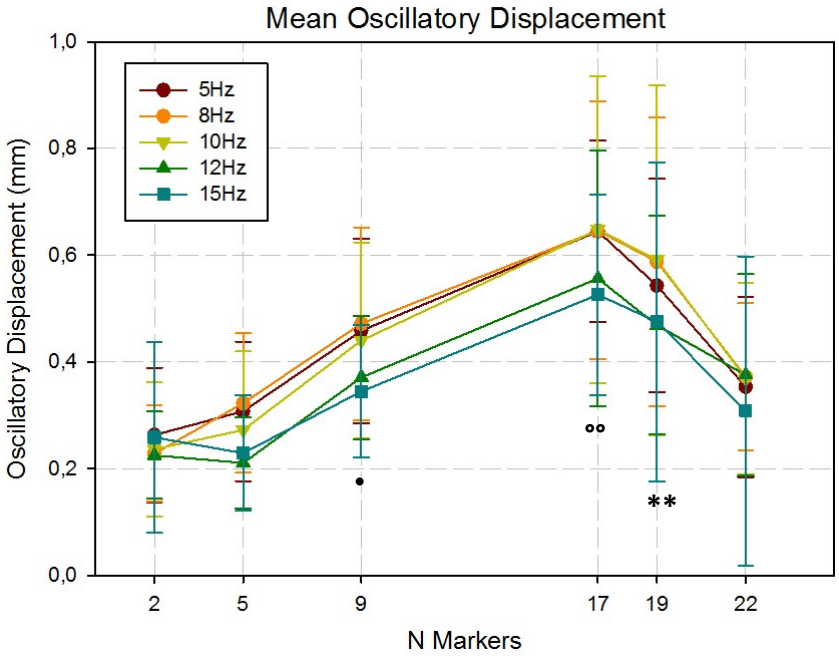

Figure 5.7 Mean oscillatory displacements of the markers along the midline. The graph shows the oscillations of the thoraco-abdominal wall at each frequency. Data are presented in terms of mean and standard deviation. A statistically significant difference has been observed for marker N°19 (*) , marker N°17 (°) and marker N°9 (•): single symbol means P<0.05, double symbol means P<0.001 (*=P<0.05; **=P<0.001).

Markers oscillatory displacement increases along the midline till the upper abdomen (from 0.2 to 0.7 mm) at the marker N°17 and, then, decreases till 0.35 at marker N°22. The abdomen oscillatory amplitude seems to be greater than rib cage vibration and this is in accordance with the greater elasticity of the abdominal compartment.

Moreover oscillatory displacements tend to be statistically different between lower frequencies (5 Hz, 8 Hz and 10 Hz) and higher frequencies (12 Hz and 15 Hz).

Marker N°9 has a significantly higher oscillatory movement in respect to marker N°2 (P=0.003). Marker N°17 has a significantly higher oscillatory movement in respect to marker N° 2, 5, 22 (P<0.001) and marker N°9 (P=0.001). Marker N°19 has a significantly

higher oscillatory movement in respect to marker N°2 and N°5 (P<0.001). The reduction of oscillatory displacement in the lower abdomen is probably due to the quasi-static behaviour of marker N°22, which is a closure marker of the iliac spine. Moreover oscillatory displacement tends to be similar at each frequency.

Volume contribution

Chest wall volumes depend on the regional mechanical characteristics of the lungs and the chest wall. On the basis of previously defined geometrical models that describe the whole chest wall and its compartments, dedicated software was used to calculate the absolute volumes and their changes during respiration. In particular tracks of each marker have been analysed and computed in order to obtain compartmental volume information.

The following graphs report an example of oscillation signals, which represent the total and compartmental volume changes at different frequencies (5Hz and 15Hz).

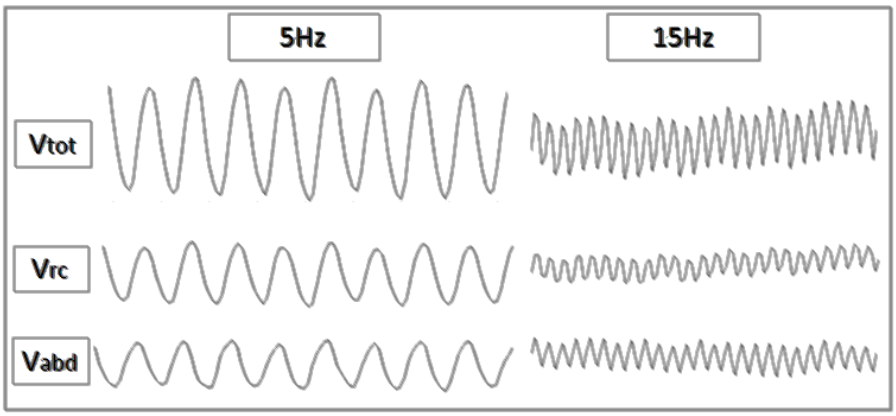

Figure 5.8 Example of total and compartmental volume changes at different ventilatory frequencies.

Figure 5.8 shows an example of total and compartmental volume changes at 5 Hz and 15 Hz which are the maxima and minima frequencies used in the clinical study. The total volume oscillation amplitude shows a reduction at increasing frequency, and this is due to the reduction of both contribution (rib cage and abdominal compartment).

From OEP data tidal volumes pro-Kg have been also calculated and their distribution in the thoraco-abdominal compartments has been provided thanks to the OEP features (Figure 5.9).

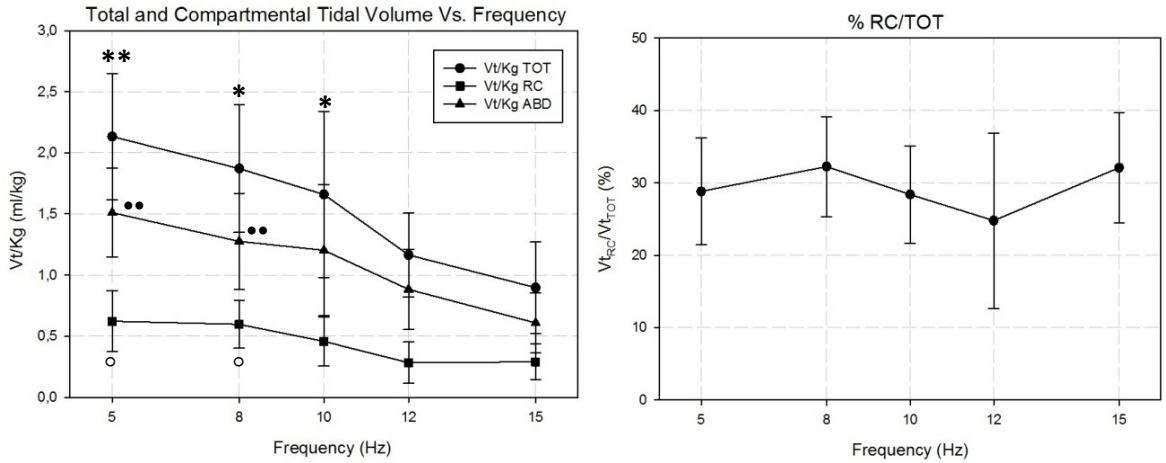

Figure 5.9 V_T distribution in thoraco-abdominal compartments. *Panel a)* shows the frequency dependence of total V_T (V_T TOT -●), rib cage V_T (V_T RC -■) and abdominal V_T (V_T ABD -▲). *Panel b)* represents the percentage contribution of the rib-cage to the total V_T. A statistically significant difference has been observed for Vt TOT at 5 and 8 Hz and at 10 Hz (*), for Vt ABD (•) and for Vt RC (°). Single symbol means P<0.05, double symbol means P<0.001 (*=P<0.05; **=P<0.001).

Figure 5.9 shows a decrease in total and compartmental V_T at increasing frequencies. Total V_T reduces of about 1.5 ml/kg at from 5 to 15 Hz frequency; increasing frequencies V_T principally reduces in the abdominal compartment, while rib cage volume reduction from 5 to 15 Hz is less than 0.4 ml/kg: the percentage contribution of the rib cage, in fact, remains almost constant between ~ 25% and 30%.

There is a statistically significant difference in V_T TOT: between 5 Hz and 15, 12 and 10 Hz (P=0.006); between 8 Hz and 15 and 12 Hz (P=0.001); between 10 Hz and 12 (P=0.011) and 15 Hz (P<0.001). A statistical significant difference is also demonstrated in V_T RC: between 5 Hz and 15 Hz and between 8 Hz and 15 Hz.

V_T ABD, instead, has a statistical significant difference between 5 Hz in respect to 8 Hz (P=0.012); between 5 Hz in respect to 10 Hz (P=0.01); between 5 Hz in respect to 12 Hz and 15 Hz (P<0.001); between 5 Hz in respect to 8 Hz (P=0.012); between 8 Hz and 10 Hz in respect to 12 Hz and 15 Hz; between 12 Hz in respect to 15 Hz (P=0.04).

For the VT % there is not a statistically significant difference (P = 0.113).

Table 13 Total and compartmental volume at each studied frequency (mean ± standard deviation).

Volume [ml/kg]	*5 Hz*	*8 Hz*	*10 Hz*	*12 Hz*	*15 Hz*
Vt TOT	2.13 ± 0.52	1.87 ± 0.52	1,66 ± 0.68	1.16 ± 0.34	0.89 ± 0.37
Vt RC	0.62 ± 0.25	0.59 ± 0.19	0,46 ± 0.20	0.28 ± 0.17	0.29 ± 0.15
Vt ABD	1.51 ± 0.36	1.27 ± 0.39	1,20 ± 0.54	0.88 ± 0.33	0.61 ± 0.24

Discussion

Thoraco-abdominal vibrations are one of the most used parameters to assess HFOV in clinical practice. A clinician evaluates vibrations qualitatively looking at the chest wall and paying attention to the synchrony of the thoraco-abdominal oscillations.

Since the neonate is ventilated at high frequencies, the expectation is to find some compartmental differences in mechanical response.

In this study compartmental oscillations in terms of lag and amplitude have been quantified and the lag has been analysed as both phase shift (rad) and time lag (s). The lag increases at increasing frequencies and in cranio-caudal direction.

The oscillatory displacement, instead, is more relevant at the level of the abdomen than of the rib cage where bony structures oppose to the movement.

This is also confirmed by the compartmental lung volume changes: abdomen volume changes are always greater than rib cage volume changes; however, as frequency is increased and tidal volume is reduced, the reduction in abdomen volume changes is greater than at the level of the rib cage.

Such differences are probably due to the different mechanical features of these two compartments. In particular, tissues with more inertance, as the abdomen, at high frequencies don't have time enough to reach the steady-state, while at low frequencies tissues have time enough to be distended by the pressure wave.

This seems to be even more true since, at increasing frequencies, the standard deviation of the time-lag increases: different neonates have different mechanical features, therefore at higher frequencies each neonate behaves in a manner strictly dependent on his tissues mechanical features (compliance and inertance).

A compartmental response of the respiratory mechanics has already been found by Dellacà et al. in healthy adults studied by OEP.[52]

Up to the present, neonatal respiratory system has always been considered as a single compartment, nevertheless our study confirms that the presence of a frequency-dependent lag and a non-homogeneous behaviour of the thoraco-abdominal wall is present not only in adults but also in newborns. Therefore, the multi-compartmental approach for the study of the newborns' respiratory system mechanics has to be considered.

A reduction in tidal volume and an increase in pressure amplitude (ΔP) can be seen moving from 5 Hz to 15 Hz of frequency. It is quite consistent (on a physics point of view) with the ventilator-setting changes applied in this study: at increasing frequency a reduction in VT is required in order to maintain DCO_2 constant; moreover, an increase in pressure amplitude (ΔP) with increasing frequency is required to obtain a proper flow. Furthermore, such ΔP increasing causes similar values of the oscillatory displacement recorded by OEP at the level of the thoraco-abdominal wall at different ventilatory frequencies, hiding the dumping phenomenon.

Moreover, the different contribution of compartments to the total volume represents different approaches to the evaluation of gas delivery: if in conventional ventilation the gas delivery is totally due to the convective fluid motion, in HFOV it is also due to other non-convective principles. The displacement that did not result in VT may not have been wasted (as happens in conventional breathing) because in HFOV also non-convective fluid motion promotes the gas exchange. The rib cage contribute to non-convective gas exchange increases with increasing frequencies; its contribute to convective gas delivery, instead, is almost constant (25-30%) regardless ventilatory frequency.

5.2.3 Total and regional transfer impedance

The main objective of the present study is to combine the FOT method with OEP to study the frequency dependent behaviour of mechanical properties of the total respiratory system, the lung, and the chest wall (inclusive of its individual compartments) for frequencies surrounding breathing. Data were acquired by forcing pressure at the mouth and measuring the flow both at the mouth and at the chest wall surface (as the time derivative of the total and compartmental volumes).

The use of the OEP system allows to acquire analogical data and cameras' data simultaneously: in this way pressure and total volume (with its time derivative respective) can be used to estimate the transfer impedance of the respiratory system.

The total transfer impedance is shown in its real and imaginary part, as the mean and standard deviation of all the newborns acquired in the present study.

The real and imaginary part are shown in Figure 5.10:

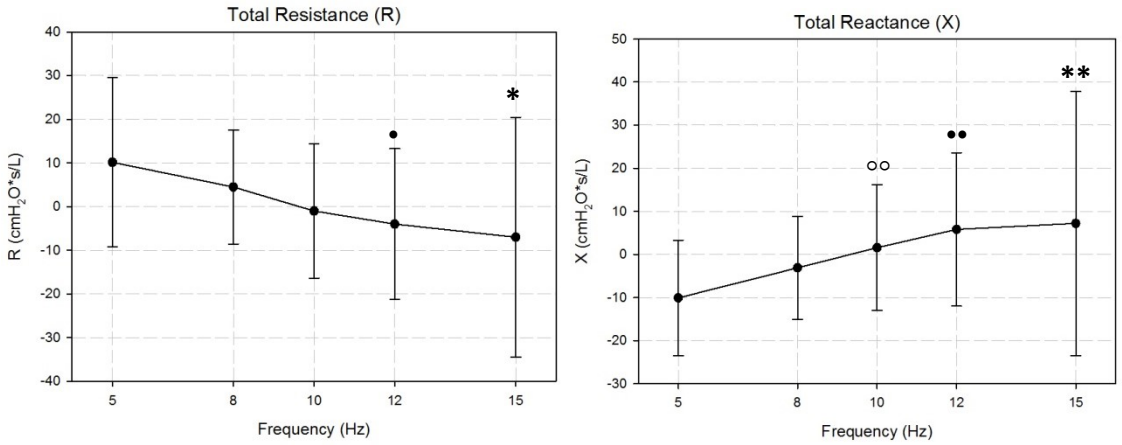

Figure 5.10 Real part (on the left panel) and imaginary part (on the right panel) of the transfer impedance. A statistically significant difference has been observed for resistance at 15 Hz (*) and at 12 Hz (•) and for reactance at 15 Hz (*), 12 Hz(•) and 10 Hz (°). Single symbol means P<0.05, double symbol means P<0.001 (*=P<0.05; **=P<0.001).

The resistance mean value at 5 Hz is 10.1 ± 6.4 (mean ± SD cmH_2O*s/L) and decreases till -7.02 ± 9.6 (mean ± SD cmH_2O *s/L) at 15 Hz. Conversely the reactance increases from -10 ± 7.4 (mean ± SD cmH_2O *s/L) at 5 Hz to about 7.1 ± 10.3 (mean ± SD cmH_2O *s/L) at 15Hz.

There is a statistically significant difference in both resistance and reactance: in resistance between 15 Hz in respect to 5 Hz and 8 Hz and between 12 Hz versus 5 Hz; in reactance between 15 Hz in respect to 5 Hz ($P<0.001$) and 8 Hz ($P=0.003$); between 12 Hz versus 5 Hz ($P<0.001$) and 8 Hz ($P=0.005$); between 10 Hz versus 5 Hz ($P<0.001$).
Since the respiratory system cannot be considered as a single compartment, these results are not useful for the mechanical response analysis because they are referred to the total volume. In fact, X and R behaviours have no significant changes in frequency and the standard deviation is too large to make any assumption.

The solution for this problem is to consider rib cage volume and abdomen volume in separated elaborations with the same oscillating pressure signal imposed at the mouth. The OEP system in combination with the infant model (24 markers) allows to reconstruct the thoraco-abdominal surface as an approximation of 34 triangles, which is the maximum possible subdivision with this model.
The transfer impedance of each single triangle has been computed and the following graphs report its real and imaginary part.

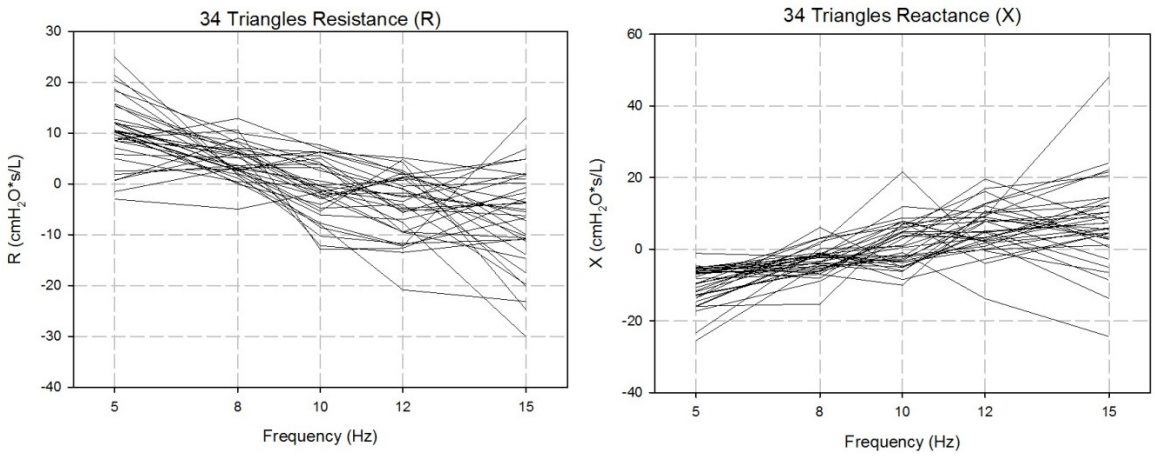

Figure 5.11 Real and imaginary part of the transfer impedance of 34 triangles (maximum subdivision of the thoraco-abdominal surface allowed by the infant model used for this study).

Figure 5.11 shows a trend for both components of the transfer impedance, but the dispersion is augmented by the high noise. In fact the 34 triangles regional subdivision involves a reduction of the size of the considered areas and the displacements are affected by low signal-to-noise ratio.

To increase the signal-to-noise ratio, 9 regions of the chest wall have been considered made by one or more triangles, and the volume of these elements was obtained simply from the sum of the volumes associated with all the triangles included in the considered region. The transfer functions between the local flow and pressure were estimated to describe the spatial distribution of respiratory system transfer impedance. The additional information is represented by a spatial position of the regional transfer impedance values on the thoraco abdominal surface of the newborns.

A virtual grid has been superimposed on the maps to give the idea of the dimension of the considered areas and the spatial location of each triangle. The maximum and minimum mean value are reported on the right side colorbar (red and blue color respectively) and in particular the zero crossing is represented by the green color for the reactance and yellow color for the resistance.

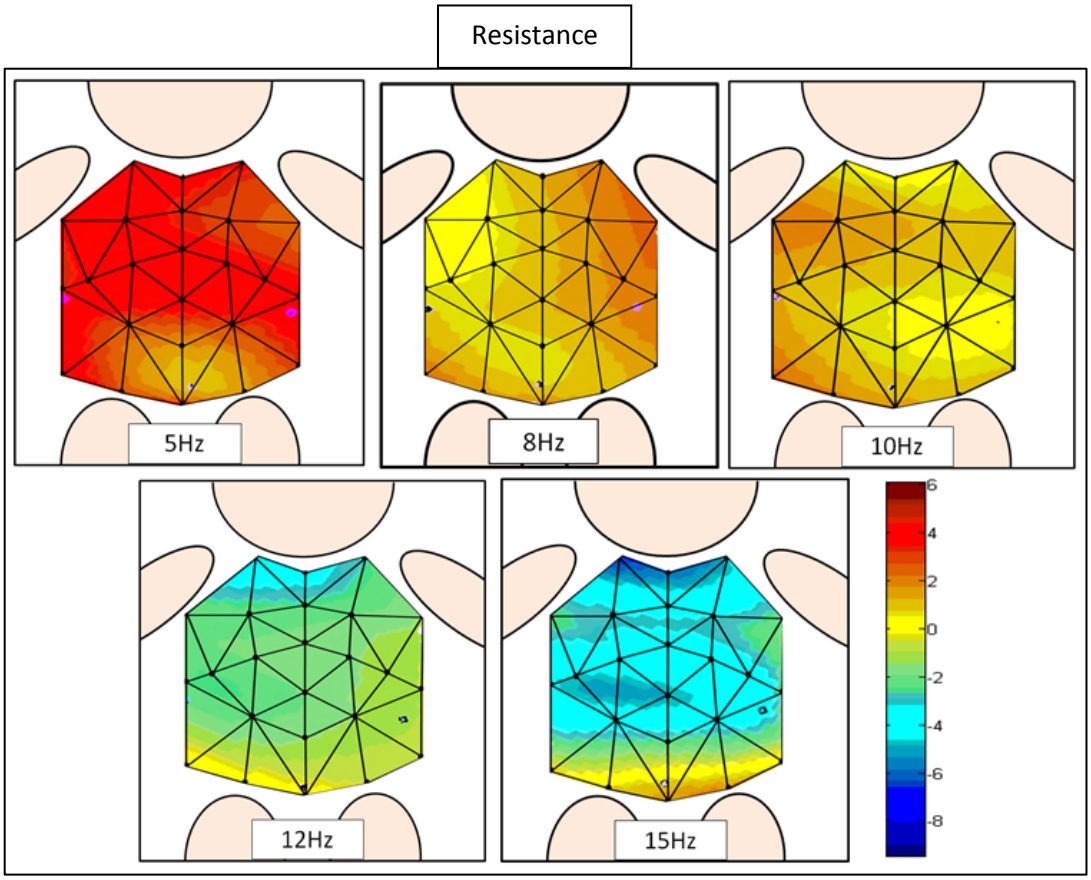

Figure 5.12 Representation of the regional transfer impedance (9 zones) spatial distribution: real part. Values are presented in cmH_2O *s/L

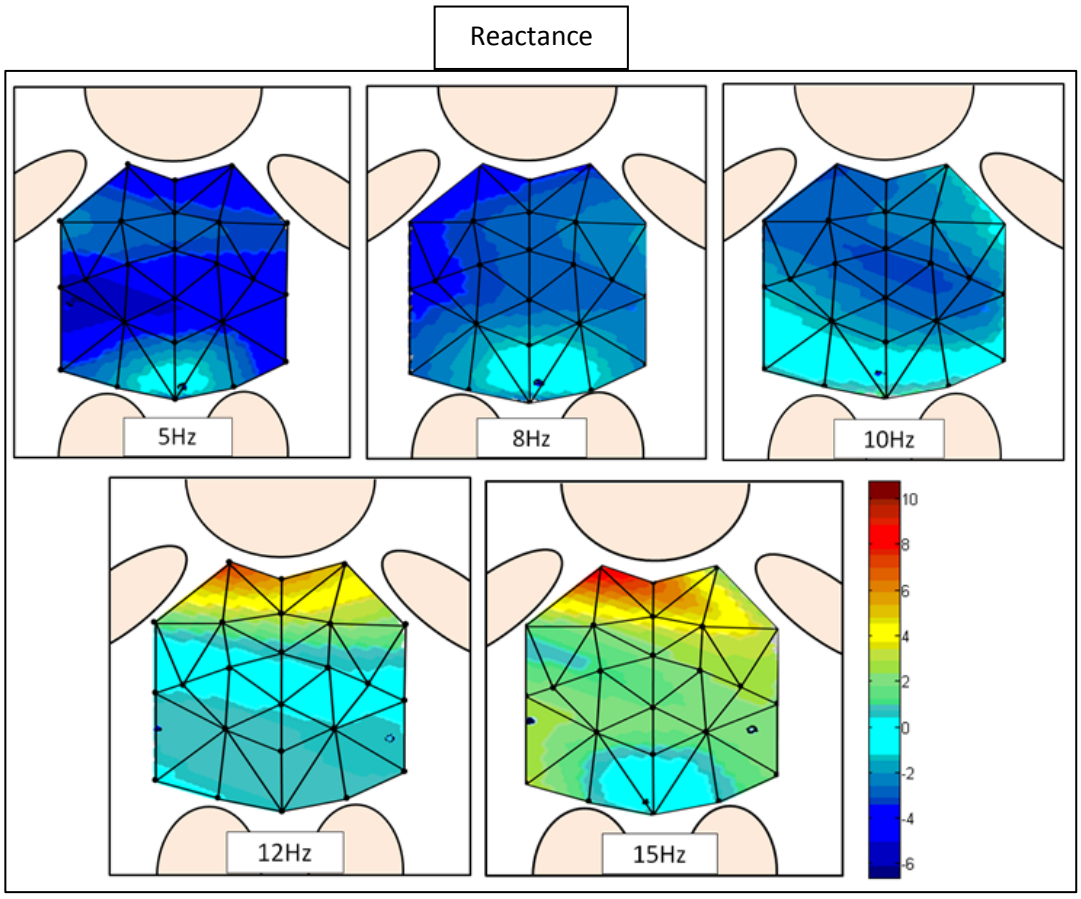

Figure 5.13 Representation of the regional transfer impedance (9 zones) spatial distribution: imaginary part. Values are presented in cmH_2O *s/L.

Figure 5.12 and Figure 5.13 show the colormaps of the 9 zones regional transfer impedances divided in its component, real and imaginary part. In respect to the 34 triangles regional transfer impedances, the signal-to-noise-ratio has been increased and the spurious peaks have been removed. The inhomogeneity of the compartments increase with frequency and at the maximum frequency different zones have different mechanical behaviours due to their different composition and stiffness: *i.e.* abdominal compartment is affected by high inertance at high frequencies.

Even if there are inhomogeneities between different zones, there are two evident components of the chest wall: zones belonging to rib cage have similar trend in real and imaginary parts and have different frequency behaviours in respect to abdominal zones.

For this reason the most suitable division for the infants chest wall is two or three compartments, because this areas provide a useful mechanical description and frequency response. Figure 5.14 shows the real and imaginary part of the compartmental transfer impedance.

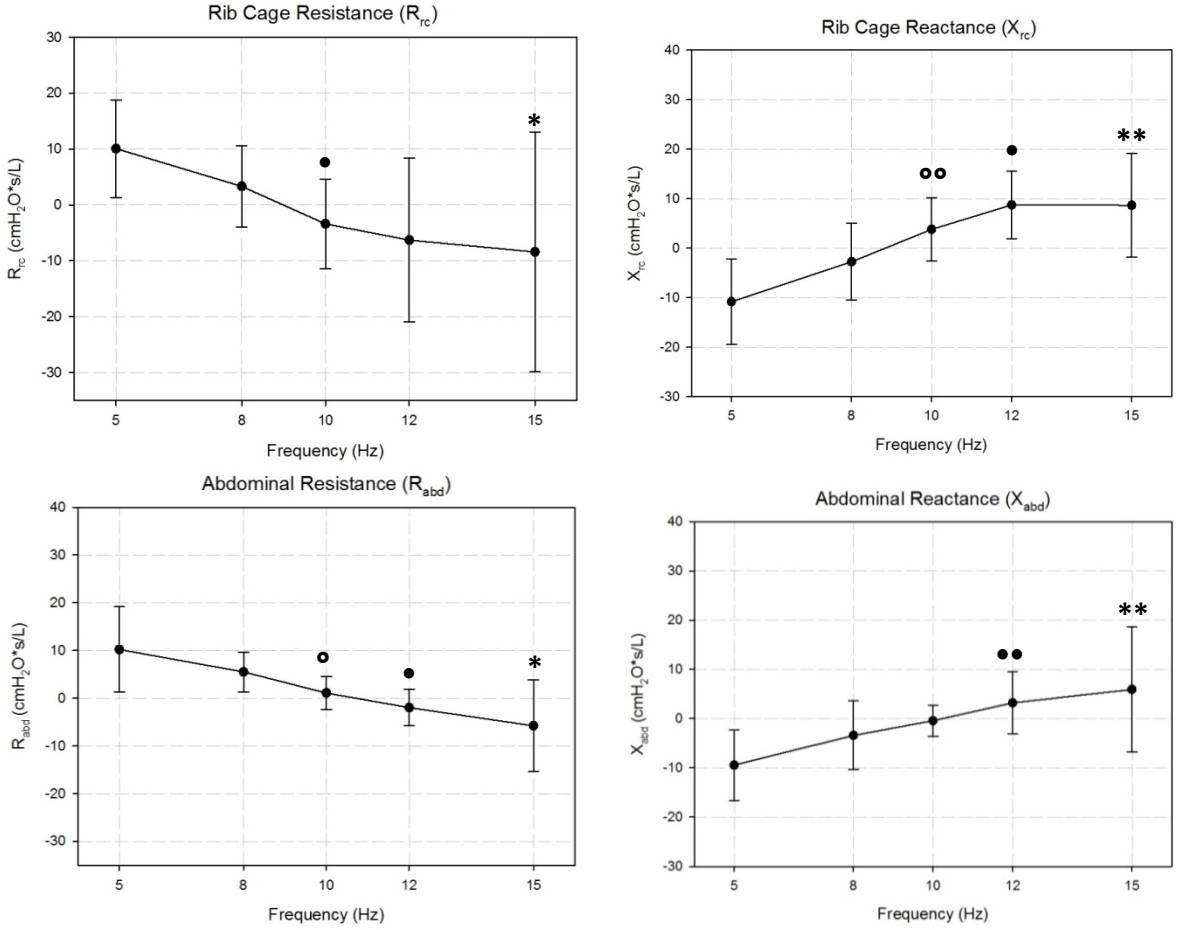

Figure 5.14 Real and imaginary part of compartmental transfer impedance. A) Resistance and B) Reactance of rib cage; C) Resistance and D) Reactance of abdominal compartment. A statistically significant difference has been observed for rib cage resistance at 15 Hz (*) and at 10 Hz (•) and for rib cage reactance at 15 Hz (*), 12 Hz (•) and 10 Hz (°); for abdominal resistance 15 Hz (*), 12 Hz (•) and 10 Hz (°) and for abdominal reactance at 15 Hz (*) and 12 Hz (•). Single symbol means P<0.05, double symbol means P<0.001 (*=P<0.05; **=P<0.001).

The rib cage resistance mean value at 5 Hz is 10 ± 8.75 (mean ± SD cmH_2O *s/L) and decreases till -8.4 ± 21.4 (mean ± SD cmH_2O *s/L) at 15 Hz. Conversely the reactance increases from -10.8 ± 8.5 (mean ± SD cmH_2O *s/L) at 5 Hz to 8.6 ± 10.4 (mean ± SD cmH_2O *s/L) at 15 Hz.

The abdomen resistance mean value at 5 Hz is 10.2 ± 8.93 (mean ± SD cmH_2O *s/L) and decreases till -5.77 ± 9.6 (mean ± SD cmH_2O *s/L) at 15 Hz. Conversely the reactance increases from -9.44 ± 7.16 (mean ± SD cmH_2O *s/L) at 5 Hz to 5.9 ± 12.65 (mean ± SD cmH_2O *s/L) at 15Hz.

There is a statistically significant difference in both resistance and reactance of abdominal and rib cage compartments.

In rib cage resistance between 15 Hz and 10 Hz in respect to 5 Hz ($P<0.05$); while in abdominal resistance between 15 Hz versus 5 Hz, 8 Hz ($P=0.01$) and 10 Hz ($P=0.009$); between 12 Hz in respect to 5 Hz ($P=0.01$) and 8 Hz ($P=0.005$) ; between 10 Hz in respect to 5 Hz ($P=0.001$).

In rib cage reactance between 15 Hz versus 8 Hz ($P=0.003$) and 5 Hz ($P<0.001$); 12 Hz versus 8 Hz ($P=0.002$) and 5 Hz ($P<0.001$); 10 Hz versus 5 Hz ($P<0.001$). therefore in abdominal reactance there is a statistically significance between 15 Hz and 12 Hz in respect to 5 Hz ($P<0.001$).

Panel A) and C) of Figure 5.14 show the real part of the rib cage and abdominal transfer impedance: both of them decrease at increasing frequency, crossing the zero line at about 9 Hz for the rib cage and about 11 Hz for the abdomen. This situation has already been described by Lutchen[55] as $R0$; in fact his study demonstrates that real part of adults transfer impedance starts from positive values, crosses the zero line at about 35 Hz and then becomes negative[55]. Since this study includes only newborns, the R0 values we found are reasonably different from adults values.

The reactance (panel B and D of Figure 5.14), instead, shows $f0$ value of 8.5 Hz and 10 Hz for rib cage and abdomen respectively, according to the different mechanical features of these two compartments.

Discussion

With the use of both FOT and OEP it has been possible to describe the whole mechanics: while Z_{in} considers the whole respiratory system, Z_{tr} (highly sensitive to heterogeneous lung constriction) is minimally distorted by shunting of flow into alveolar gas and upper airway walls.

Z_{tr} provides specific information about tissues and airways; it is potentially clinically valuable and it is less influenced by upper airways shunting, nevertheless there are very few reports of Z_{tr} measurements in both health and disease. This is mainly due to the difficulty in acquiring reliable measurements in the modified body plethysmograph. The

OEP combined with FOT during HFOV allows computing the regional transfer impedances of different chest wall compartments in a non-invasively way.

The total transfer impedance showed a very large standard deviation, due to different mechanical response of different chest wall zones. This situation has led to increase the subdivision of the chest wall compartments up to the maximum allowed by the used model, but the results have been overwhelmed by high noise. Markers flickering leads to spurious peaks and the transfer impedance computation was not reliable, so the number of zones should be chosen on signal-to-noise ratio compromise.

Therefore it's possible to see that these differences are masked in total Z_{tr}, maybe because of the much lower modulus of the pulmonary rib cage Z_{tr} that, being in parallel with the abdomen, strongly dominates the resulting total chest wall mechanical behavior.

A recent study on human adults[4] provides information about total and compartmental respiratory transfer impedance over a large range of frequencies (from 4Hz to 12Hz). The results confirmed that real parts of rib cage and abdomen cross the zero line at different frequencies and also the reactance has a different resonant frequency: at high frequencies different mechanical properties are more evident, particularly inertial ones.

A reasonable explanation of negative real parts is that at high frequencies volume changes are affected by asynchronies, that are mainly due to the flow pathways propagation. At high frequencies wavelengths were comparable to the dimensions of the abdomen, resulting in opposite movements in the different abdominal regions.

Furthermore, as it happens for the input impedance, also for the transfer one it isn't possible to describe the respiratory system behaviour just simulating it with an electrical model. In fact, for example, the decreasing of the resistance can't be reproduced with an electrical model which does not consider phase lag or flows in opposition during the mechanical ventilation (that, instead, really happen).

6. Conclusions

HFOV is a valid invasive-ventilation technique in newborns with respiratory failure; it permits, with appropriate settings, to achieve low tidal volume ventilation while avoiding barotrauma to proximal alveolar units.

The high frequencies and flows used by this ventilation modality disclose the complexity and non-linearities of the respiratory system. Changes in the relative importance of compliance, resistance and inertance, which depends on the flow pattern, oscillatory frequency and lung condition, determine different responses to the therapy: *i.e.* magnitude of flow and pressure transmitted to the distal lung.

Nowadays the optimization of oscillatory frequency (f) in HFOV is still an open issue.

Excised lungs expand asynchronously and non-uniformly during high frequency ventilation (15 Hz), suggesting marked interregional airflow and elastic wave propagation in the parenchyma.[55] Since to date no tools are available for the assessment of optimal ventilation frequency at bedside, in current clinical practice f is set based on body weight. Moreover at high frequencies the lung does not behave as a single compartment.

Moreover, in healthy adults there are significant local variations in chest wall mechanical properties above 4 Hz, resulting in inhomogeneous propagation of pressure oscillations applied at the mouth.[51]

The objective of this thesis was characterizing the global and regional mechanical properties of the respiratory system as well as chest wall displacements at different oscillatory frequencies (f) in newborns receiving HFOV.
To characterize the mechanical response of the respiratory system to HFOV, in this work we used two non-invasive systems: Optoelectronic Plethysmography (OEP) and Forced Oscillation Technique (FOT). Global mechanics is measured by FOT without discontinuing mechanical ventilation and measuring pressure and flow at the mouth using a monitoring device that is commonly used in the clinical setting, without requiring any dedicated device. The OEP system allows, through the use of subsets of the markers placed on the thorax, the measurement of separate compartments, such as the rib cage, abdomen, or smaller components.[4]
These characteristics can be combined to obtain regional information about the mechanical properties and oscillatory pressure wave propagation, such as compartmental transfer impedance computation and regional impedance maps.

In this study we first developed an experimental set-up for the analysis of the global and regional respiratory system mechanics in infants receiving HFOV. Specific algorithms have been developed for the computation of impedance, for the compensation for the low-pass filtering effect of the measurement system, and for the flow dependence of the endotracheal tube disclosed by the high amplitude ventilation waveform. This set-up has been validated in vitro against standard FOT and proved to be accurate over a wide range of mechanical characteristics.

Global and regional chest wall vibrations, lung volume changes and transfer impedance have been measured using an OEP system combined with dedicated geometrical models of the infant chest wall developed purposely for the present application.

Changes in X_{rs} have been observed without requiring interruption or changes in the ventilator waveforms, increasing the feasibility of this approach in clinical settings.
For the first time, with this study, it has also been possible to measure f_0 on preterm babies undergoing HFOV, showing a far lower range (between 7.5 and 12 Hz) than the one calculated in theoretical models[2]. Consequently f_0 are included in the range of frequencies delivered by commonly used ventilators, so resonant frequency can be set in clinical practice as optimal frequency. In fact HFOV decreases risk of barotrauma by reducing pressure swings in the airways during artificial ventilation and resonance frequency is the frequency at which oscillatory ventilation is most efficient owing to the elimination of compliance through the mechanics of oscillation: the combination of these two factors maybe determine an optimal ventilation.

However OEP shows that considering the chest wall as a unique compartment implies excessive simplification; in fact, in infants receiving HFOV, the chest wall oscillates asynchronously and non-uniformly. This behavior is more evident with increasing oscillatory frequencies, with the abdominal compartment being, in average, more sensitive to changes in f.
This phenomenon implies more sophisticated models than a single lumped resistance-inertance-elastance to describe the mouth pressure and abdominal volume relationship.

From our results, especially as it is shown in transfer impedance maps, we can conclude that increasing the frequency, the abdominal and rib cage inhomogeneities increase as a result of very different mechanical properties.
Evaluating the oscillatory displacements and the lag values along the midline, it has been demonstrated that there's a very high contribution of the abdomen area for its highest compliance (it is the farthest from any rigid structure) and its very high inertance.
For all these reasons, regional alterations in chest wall mechanical properties cannot be identified from the total Z_{tr} but only from local measurements, and OEP technique offers the possibility of studying it. Mechanical properties of the two compartments should be investigated in order to characterize the optimal frequency that allows to obtain maximum efficiency in terms of ventilation and minimum inhomogeneities avoiding to stretch tissue (that is the consequence of gas flow and tissue movement opposition in nearby areas).

Future developments of the present work include increasing the sample size, including patients with different diseases and dimensions in order to have a broader spectrum of mechanical characteristics to compare.
Moreover, in order to understand if ventilating the neonate at the resonant or any other frequency could be beneficial, it should be useful to consider gas exchange and other clinical indicators.
This could be optimal for a future integration of clinical data and mechanical properties computed with OEP-FOT to achieve an optimal ventilation for the baby.

Finally, if studies confirm the usefulness of the assessment of respiratory mechanics or the calculation of the resonant frequency in clinical practice, an improvement in setup devices will be necessary to have instantaneous regional X, R and f_0 values. Then, there will be grounds to draw clinical controlled trials to compare treatment based on quantitative measures with standard treatment, evaluating short term (biochemical) and long term lung damages as outcome. It is possible that resonance frequency can be incorporated as part of the management strategy to provide more efficient HFOV.

7. References

1. Blencowe, H. *et al.* National, regional, and worldwide estimates of preterm birth rates in the year 2010 with time trends since 1990 for selected countries: a systematic analysis and implications. *Lancet* **379,** 2162–72 (2012).

2. Froese, A. B. & Kinsella, J. P. High-frequency oscillatory ventilation: Lessons from the neonatal/pediatric experience. *Crit. Care Med.* **33,** S115–S121 (2005).

3. Venegas, Fredberg. New Therapies for Neonatal respiratory failure. Cap.11-Oscillatory mechanics, the pressure cost of high-frequency ventilation.

4. Aliverti, a., Dellacà, R. L. & Pedotti, a. Transfer Impedance of the Respiratory System by Forced Oscillation Technique and Optoelectronic Plethysmography. *Ann. Biomed. Eng.* **29,** 71–82 (2001).

5. Aliverti, A. *et al.* Compartmental Analysis of Breathing in the Supine and Prone Positions by Optoelectronic Plethysmography. *Ann. Biomed. Eng.* **29,** 60–70 (2001).

6. Cavity, N. & Passageways, S. C. Parts of the Respiratory System The Nose or Nasal Cavity. 1–15 (2014).

7. Miserocchi. Testo-atlante di fisiologia umana - fisiologia e fisiopatologia respiratoria.

8. Frappell, P. B. & MacFarlane, P. M. Development of mechanics and pulmonary reflexes. *Respir. Physiol. Neurobiol.* **149,** 143–54 (2005).

9. Bryan AC, W. M. in *American Physiological Society* 1986 (1986).

10. Nelson textbook of pediatrics.

11. Smith, J. H. Infant Respiratory Distress Syndrome (IRDS).

12. Swarnam, K., Soraisham, A. S. & Sivanandan, S. Advances in the management of meconium aspiration syndrome. *Int. J. Pediatr.* **2012,** 359571 (2012).

13. Jain, L. & Eaton, D. C. Physiology of fetal lung fluid clearance and the effect of labor. *Semin. Perinatol.* **30,** 34–43 (2006).

14. Donn, S. M. & Sinha, S. K. Invasive and Noninvasive Neonatal Mechanical Ventilation. 426–441 (2003).

15. Benitz, W. Mechanical Ventilation. 127–135

16. Brown, M. K. & DiBlasi, R. M. Mechanical ventilation of the premature neonate. *Respir. Care* **56,** 1298–311; discussion 1311–3 (2011).

17. Clark, R. H. *et al.* Lung injury in neonates: causes, strategies for prevention, and long-term consequences. *J. Pediatr.* **139,** 478–86 (2001).

18. Gattinoni, L. & Protti, A. Ventilation in the prone position: for some but not for all? *CMAJ* **178,** 1174–6 (2008).

19. Guy, W., Hollingsworth, H. M., Talavera, F. & Mosenifar, Z. Barotrauma and Mechanical Ventilation. *MedScape* (2013).

20. Boynton, B. R. & Carlo, W. A. in *New Therapies for Neonatal Respiratory Failure* (eds. Boynton, B. R., Carlo, W. A. & Jobe, A. H.) 202–217 (1994).

21. Pillow, J. J. High-frequency oscillatory ventilation: Mechanisms of gas exchange and lung mechanics. *Crit. Care Med.* **33,** S135–S141 (2005).

22. Lachmann, B. Intensive Care Medicine Editorial Open up the lung and keep the lung open. 319–321 (1992).

23. De Jaegere, A., van Veenendaal, M. B., Michiels, A. & van Kaam, A. H. Lung recruitment using oxygenation during open lung high-frequency ventilation in preterm infants. *Am. J. Respir. Crit. Care Med.* **174,** 639–45 (2006).

24. Luecke, T. *et al.* Setting mean airway pressure during high-frequency oscillatory ventilation according to the static pressure--volume curve in surfactant-deficient lung injury: a computed tomography study. *Anesthesiology* **99,** 1313–22 (2003).

25. Van Genderingen, H. R. *et al.* Oxygenation index, an indicator of optimal distending pressure during high-frequency oscillatory ventilation? *Intensive Care Med.* **28,** 1151–6 (2002).

26. Van Genderingen, H. R., van Vught, A. J., Duval, E. L. I. M., Markhorst, D. G. & Jansen, J. R. C. Attenuation of pressure swings along the endotracheal tube is indicative of optimal distending pressure during high-frequency oscillatory ventilation in a model of acute lung injury. *Pediatr. Pulmonol.* **33,** 429–36 (2002).

27. Wolf, G. K., Grychtol, B., Frerichs, I., Zurakowski, D. & Arnold, J. H. Regional lung volume changes during high-frequency oscillatory ventilation. *Pediatr. Crit. Care Med.* **11,** 610–5 (2010).

28. Weber, K. *et al.* Detecting lung overdistention in newborns treated with high-frequency osicllatory ventilation. *J. Appl. Physiol.* **89,** 364–372 (2000).

29. Meyer, J., Cox, P. N., McKerlie, C. & Bienzle, D. Protective strategies of high-frequency oscillatory ventilation in a rabbit model. *Pediatr. Res.* **60,** 401–6 (2006).

30. Pillow, J. J. Dependence of Intrapulmonary Pressure Amplitudes on Respiratory Mechanics during High-Frequency Oscillatory Ventilation in Preterm Lambs. *Pediatr. Res.* **52,** 538–544 (2002).

31. New Therapies for Neonatal respiratory failure. Cap.13-High-frequency oscillatory ventilation and High-frequency flow interruption.

32. Amini, R. & Kaczka, D. W. Impact of ventilation frequency and parenchymal stiffness on flow and pressure distribution in a canine lung model. *Ann. Biomed. Eng.* **41,** 2699–711 (2013).

33. Slutsky. CO2 elimination by High frequency oscillation in dogs. 1982.

34. Regional lung mechanics and gas transport in lungs with inhomogeneous compliance. 20

35. Bauer, K. & Brücker, C. The role of ventilation frequency in airway reopening. *J. Biomech.* **42,** 1108–13 (2009).

36. Venegas, J. G., Hales, C. A. & Strieder, D. J. A general dimensionless equation of gas transport by high-frequency ventilation. *J. Appl. Physiol.* **60,** 1025–1030 (1986).

37. Frantz, I. D. & Close, R. H. Alveolar pressure swings during high frequency ventilation in rabbits. *Pediatr. Res.* **19,** 162–6 (1985).

38. Pillow, J. J., Neil, H., Wilkinson, M. H. & Ramsden, C. A. Effect of I/E ratio on mean alveolar pressure during high-frequency oscillatory ventilation. *J. Appl. Physiol.* **87,** 407–14 (1999).

39. Rrt, D. S. H., Katz, A. L., Craig, D. M., Rrt, J. D. D. & Faarc, I. M. C. Carbon Dioxide Elimination and Gas Displacement Vary With Piston Position During High-Frequency Oscillatory Ventilation. 361–366 (2005).

40. Pillow, J. J., Wilkinson, M. H., Neil, H. L. & Ramsden, C. A. In Vitro Performance Characteristics of High-Frequency Oscillatory Ventilators. **8000,**

41. Dellacà, R. L. in *Mechanics of Breathing. Patophysiology, diagnosis and treatment* (eds. Aliverti, A., Brusasco, V., Macklem, P. & Pedotti, A.) 157–169 (Springer-Verlag, 2002).

42. Dellacà, R. L. *et al.* Assessment of dynamic mechanical properties of the respiratory system during high-frequency oscillatory ventilation*. *Crit. Care Med.* **41,** 2502–11 (2013).

43. DuBois, A. B., Brody, A. W., Lewis, D. H. & Burgess, B. F. Oscillation Mechnics of Lungs and Chest in Man. *J. Appl. Physiol.* **8,** 587–594 (1956).

44. Oostveen, E. *et al.* The forced oscillation technique in clinical practice: methodology, recommendations and future developments. *Eur. Respir. J.* **22,** 1026–1041 (2003).

45. Vieira, D. S. R., Myrrha, M. A. C., Pessoa, I. M. B. S., Lage, S. M. & Britto, R. R. Optoelectronic plethysmography : a review of the literature. **16,** (2012).

46. Dellaca, R. L. *et al.* Measurement of Total and Compartmental Lung Volume Changes in Newborns by Optoelectronic Plethysmography. **67,** 1–6 (2010).

47. Bts oep system.Operator's manual.

48. sensormedics. 3100A High frequency oscillatory ventilator Operator's manual.

49. Manual, O. NEONATAL RESPIRATION MONITORING Florian. 1–40

50. Sandberg, K. L., Brynjarsson, H. & Hjalmarson, O. Transcutaneous blood gas monitoring during neonatal intensive care. *Acta Paediatr.* **100,** 676–9 (2011).

51. Dellaca', R. L. *et al.* Measurement of total and compartmental lung volume changes in newborns by optoelectronic plethysmography. *Pediatr. Res.* **67,** 11–6 (2010).

52. Dellacà, R. L., Aliverti, a., Lutchen, K. R. & Pedotti, a. Spatial Distribution of Human Respiratory System Transfer Impedance. *Ann. Biomed. Eng.* **31,** 121–131 (2003).

53. Gaio, E. & Melo, C. A Pattern to Evaluate Airway Resistive Phenomenon Using Rohrer ' s Equation. 2006–2007 (2014). doi:10.1152/advan.00082.2006

54. Rotta, A. T. & Steinhorn, D. M. Conventional mechanical ventilation in pediatrics. *J Pediatr (Rio J)* **83,** S100–8 (2007).

55. Lutchen, K. R., Sullivan, A., Arbogast, F. T., Celli, B. R. & Jackson, A. C. Use of Transfer Impedance Measurements for Clinical Assessment of Lung Mechanics.

56. Lehr. Photographic measurement of pleural surface motion during lung oscillation. **59,** 1985 (1985).

8. Appendix

A. Inflation-Deflation trial

Continuous Distending Pressure (CDP) recruits alveolar units and maintains lung volume. It must be set at the lower value necessary to maintain alveoli opened; during HFOV the correct CDP value can be obtained through alveolar recruitment maneuver.

Alveolar recruitment maneuver is based on the nonlinear behaviour of the lung during inflation and deflation, which configures the hysteresis phenomenon.

There are several strategies to define the optimal CDP. The most used is the one based on oxygen saturation: during recruitment the lung is over-distended by increasing CDP (till the opening point); then it is deflated till the alveolar collapse (closing point). The optimal CDP is just above the collapse value on the deflation limb. This is the "inflation-deflation trial" or "incremental-decremental trial",used for the preliminary phase of the clinical study.

A.1 Clinical optimization of the oscillatory parameters.

The clinical protocol currently in use in S.Gerardo's Hospital Neonatal Intensive Care Unit (NICU) is followed in this phase.

A recruitment maneuver is performed in order to identify the Optimal Continuous Distending Pressure (CDP) by using the "incremental decremental CDP trial" based on SpO2 proposed by DeJaegere.[23]

The starting settings are the following:

- CDP: 6-8 cmH_2O
- FiO_2: adjusted to obtain a correct oxygenation (form 0.21 to 0.5)
- P/P pressure: at minimum to obtain normocarbia
- Oscillatory frequency: 10-15 Hz.

A stepwise recruitment maneuver is performed following this procedure:

5. CDP is increased stepwise: 2 cmH_2O every 3 minutes. At each step an increase in oxygenation (SpO_2 and $PtcO_2$) occurs; SpO_2 must be kept between 86% and 94% by adjusting FiO_2. The lung inflation is carried on till we observe a worsening in

oxygen saturation or FiO_2 becomes less than 30%. It identifies the apex of the lung hysteresis curve: the so called CDP Opening.

6. CDP is decreased stepwise with steps of 2 cmH_2O every 3 minutes. The lung deflation is carried on till we reach the CDP Closing: the CDP value at which a worsening in SpO_2 is registered (because of the alveolar closing), that is a drop in SpO_2 equal or more than 5% of the SpO_2 measured at CDP Opening or an absolute SpO_2 value inferior to 86%.
7. The CDP is set at CDP Opening for 2-3 minutes in order to re-open the lung.
8. The CDP is set at CDP Optimal, that is 2 cmH_2O above the CDP Closing on the deflation limb.

P/P pressure is kept constant during the whole maneuver.

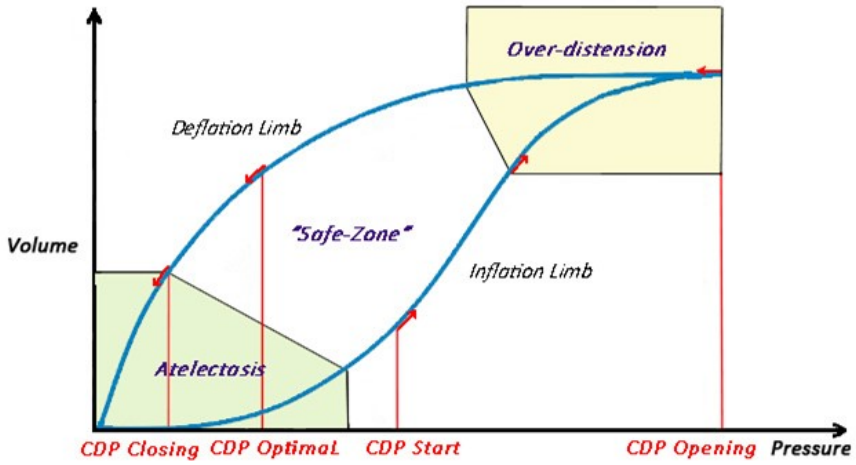

Figure 8.1 Incremental-Decremental CDP trial. (Modified from A.T. Rotta et al.[54])

At each step clinical measures are recorded (see further text). At CDP Opening, CDP Closing and CDP Optimal the thoraco-abdominal movements are also acquired by OEP System and air pressure and flow waves by Florian.

A.2 Pressure wave propagation during Inflation-Deflation trial

The inflation deflation trial was studied on a single subject (Patient N°8): a clinical optimization of continuous distending pressure (CDP) is performed in order to place the lung in the best possible condition for the current knowledge.
The steps were:

- The starting point was a CDP value of 8 cmH_2O, an FiO_2 value equal to 1 and peak to peak pressure of 37 cmH_2O;
- then CDP has been increased stepwise of 2 cmH_2O every 3 minutes; At each step an increase in oxygenation (SpO_2 and $PtcO_2$) occurs;
- We continue the lung inflation till we observe a worsening in saturation and the FiO_2 become less than 30% and the saturation decreased (less than 90%); at this point the CDP value was 14 cmH_2O and this was the so called CDP opening;
- CDP has been decreased stepwise with steps of 2 cmH_2O every 3 minutes. We continue to deflate the lung till we reach the CDP Closing (8 cmH_2O);
- We set the CDP at CDP Opening (14 cmH_2O) for 2-3 minutes in order to re-open the lung;
- We set the CDP at CDP Optimal, that is 4 cmH_2O above the CDP Closing on the deflation limb.

The pressure amplitude (ΔP) imposed to the newborn by Sensormedics produces vibrations on his chest wall with the same frequency of the input wave. Such vibrations are detected by OEP cameras and saved on the OEP workstation.
During offline elaboration the lags between 12 areas and the area 5 were calculated in all the steps of the inflation deflation trial and they are represented in coloured maps.
In this maps the lag is represented as phase shift of the oscillatory wave. Each map represents a different CDP in inflation and deflation phase and the colour depends on the phase lag: the darker the color, the greater the lag.

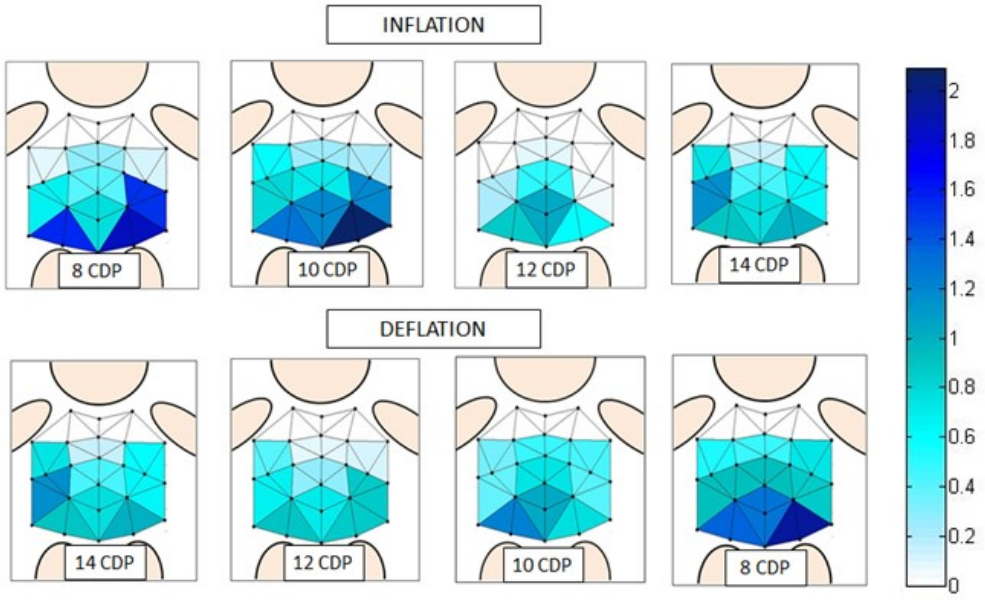

Figure 8.2 Phase lag [rad] between 12 areas and the area 5 during the inflation and deflation phase.

The inflation phase shows a decrease in the phase lag [rad] as the CDP has been increased, as explained in figure 8.2. This is probably due to the opening of the lung (alveoli recruitment) that increases the homogeneity of the rib cage and abdominal compartments. During the deflation phase, instead, the phase lag increases, according to the lung closing and the increasing inhomogeneity of the two compartments.

Also the magnitude of the transfer function between pressure and flow during alveolar recruitment was computed.

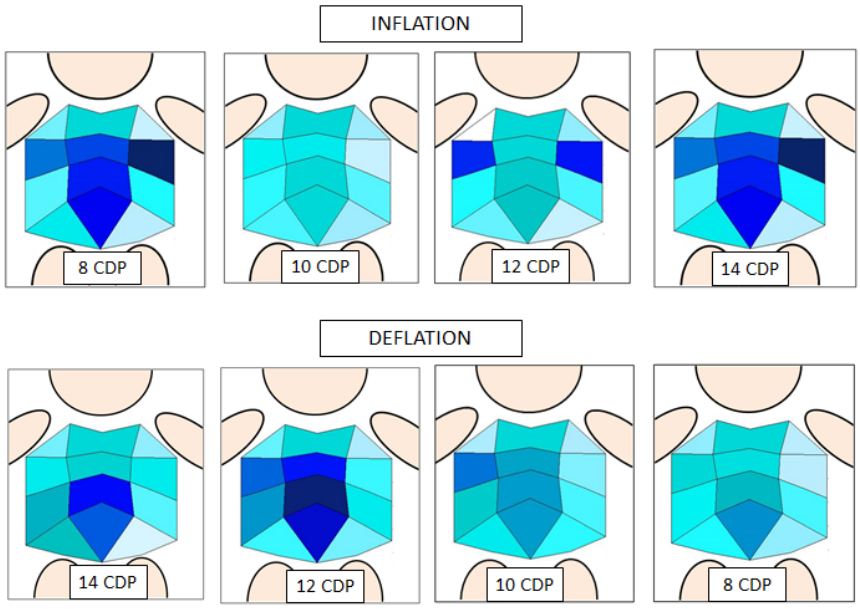

Figure 8.3 Magnitude map of the incremental-decremental trial. Value are expressed in cmH_2O*s/L.

B. Plexiglas cover validation

During first clinical studies it was realized that very preterm babies have a rapid loss of temperature if not kept in an adequate environment and the infa warmer incubator takes a long time to reach the setting temperature.
Neonatal incubator couldn't be used because of reflexing\refraction phenomenon that interfere with camera's acquisitions.
For this reason custom-made cover has been produced to make the cot environment more similar to an incubator. It has been decided to make it with Plexiglas® for its resistance, transparency and its acceptable weight.

B.1 Plexiglas® cover project

The choice of Plexiglas® as most suitable material was determined by the clinical requirements, in particular transparency was essential in order to monitor the baby's condition during the acquisition. Moreover the cover should have squared angles and flat surface in order to avoid optical distortion phenomena that couldn't be compensated.
The first step of the Plexiglas® cover project was take measurements of an open coat and design a geometric shape whose base could stay inside the neonatal cot and whose high doesn't interfere with clinical instrumental settings, such as warmer lamp or light. Moreover, the cover should be higher that the calibration triad, because the calibration procedure must be performed inside the cover in order to compensate eventually linear distortion and verify the maximum error.

Another important factor that was taking into account, was the temperature loss: the cover has been projected with a hole that allows the insertion of the ventilator's tube and other clinical connection, and to avoid too high losses of temperature, this hole was built with rounded shape corners.

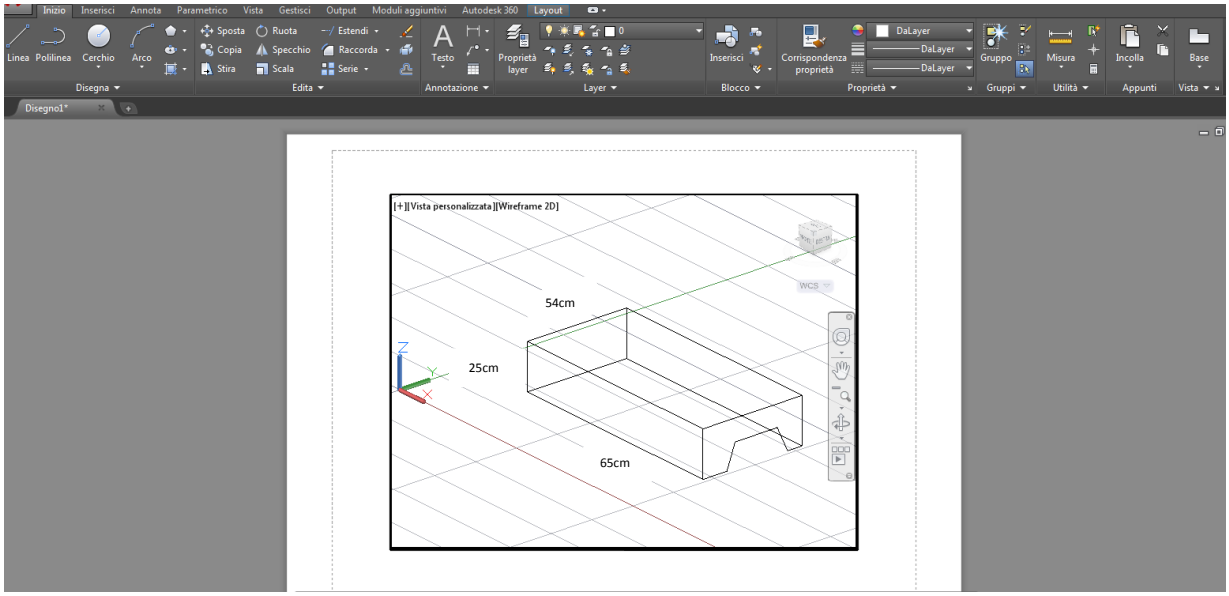

Figure 8.4 Autocad project of the Plexiglas cover

To validate the possibility of using the Plexiglas® cover during the clinical study, it has been tested applying forced oscillations to a rigid plastic conic glass (300 ml) covered by a stretched rubber membrane (Figure 8.5).

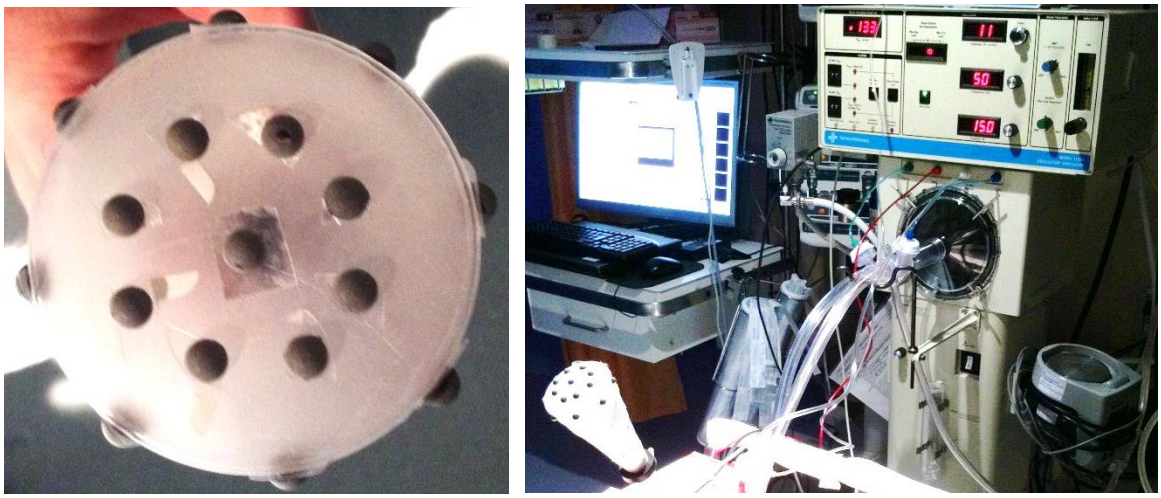

Figure 8.5 Set up for the plexiglass cover validation. A) marker configuration on the plastic glass, B) plastic glass connected to the ventilatior during the test without the cover.

The bottom of the glass was connected to the pressure generator and the membrane was glued to the lip of the plastic glass to prevent an air leak.

Seventeen hemispherical markers were placed on the membrane with an that is showed in Figure 8.5: one marker was placed in the centre of the membrane; the other markers were placed on two concentric circumferences, each composed of eight markers.
The external circle was placed on the contact line between the glass and the membrane, while the internal circle was placed between the border and the centre of the rubber sheet.
The OEP acquisition system cameras were calibrated to optimally frame the movement of the membrane during forced oscillations; input flow and pressure were measured by the Florian monitor.

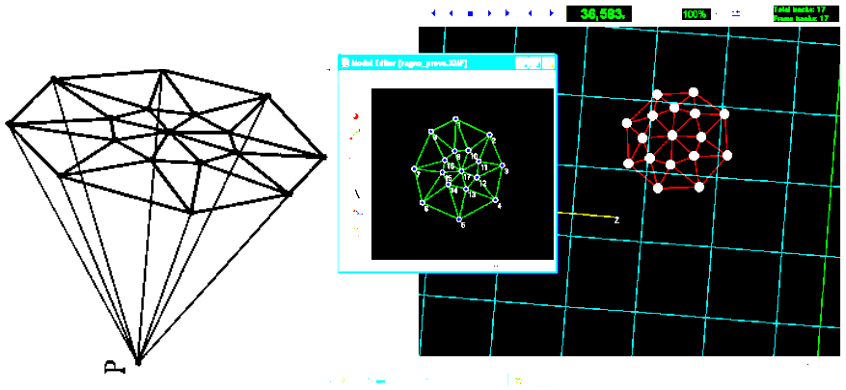

Figure 8.6 A) model of the configuration of the marker on the plastic glass and B) tracking.

The set up with the Plexiglas® cover has been compared with the clinical setup without cove during the acquisition of the membrane connected to the ventilator (SensorMedics® 3100A). All the calibration procedure is tested inside the custom-made Plexiglas® cover in order to measure the mean and the standard deviation of the error of the cameras and compare them to the once obtained without the cover. Using this setting we tested 5, 8, 10, 12, 15 Hz of oscillatory frequency with a pressure peak of 18 cmH_2O; other ventilator parameters were not manually changed. For each step 30'' pressure and flow waves are acquired. Cameras' data and analogical data are saved on the OEP workstation. It has been possible to measure the error between the volume of the test lung calculated with the Plexiglas® cover and volume without it.

B.2 Calibration

Two calibration procedures are used to determine the 3D coordinates. The first corrects optical distortions and consists of the acquisition of a set of markers placed on a metallic piece (triad) in three different axes: X, Y, and Z. The second procedure determines the geometric parameters of the collinearity equations used to calculate the 3D coordinates based on the real coordinates of a set of control points with known location. The second part involves taking the y-axis of the triad (the wand) and moving it within the space that the subject will be placed. The cameras must be detecting the wand as it moves throughout the space for calibration to be complete.

The calibration has been performed inside the Plexiglas® cover and it has been compared with the one without the cover in terms of mean and standard deviation of the calibration procedure error.

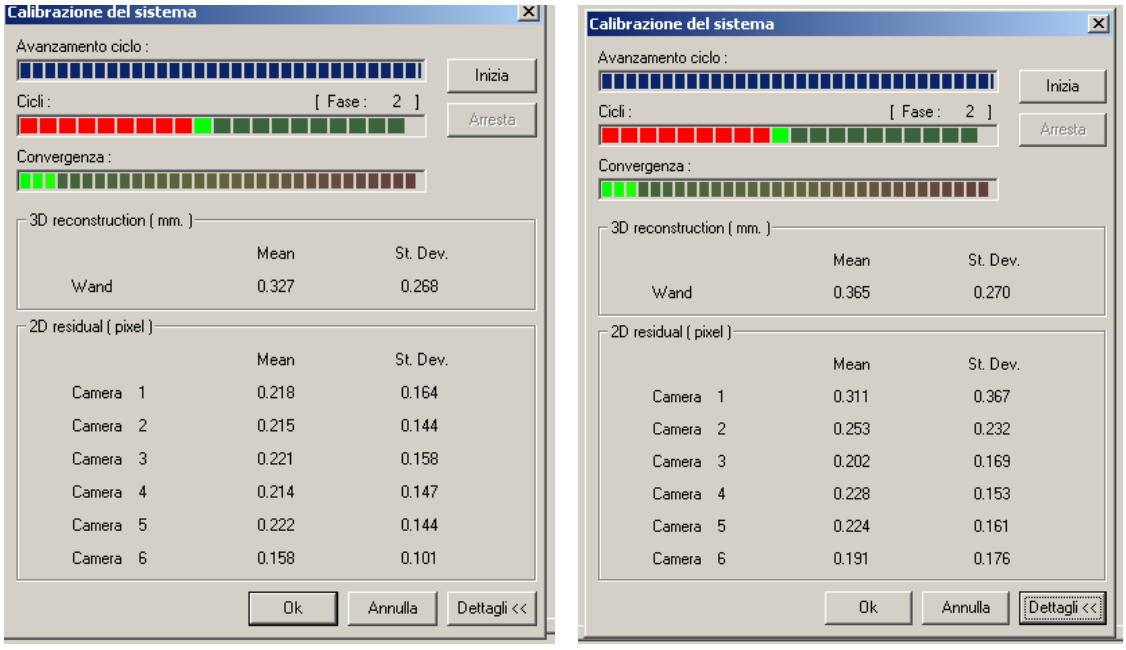

Figure 8.7 Mean and standard deviation errors of the calibration procedure without the plexiglass cover (A) and with the plexiglass cover (B). In case B the calibration procedure is performed inside the cover.

Mean and standard deviation are comparable with both calibration procedure: this means that to calibrate inside the Plexiglas® cover allows to compensate for eventually linear distortion.

B.3 Volume comparison

Thanks to the OEP acquisition system it has been possible to record the movements of the marker on the membrane and from this measurement the volume of the plastic glass model has been computed. A new SmartCapture model was created to track the data and the volume was obtained through the *'vemgbis.exe'* function adapted to the glass model. The main result is that the percentage error between measure with and without the Plexiglas® cover are less than 5% of the total volume.

Table 14 Error results

Error	*Standard deviation*
3.37%	±3.46%
0.084 mL	±0.09 mL

In terms of volume [ml] it corresponds to less than 0.1 mL, that is an acceptable result for this test.

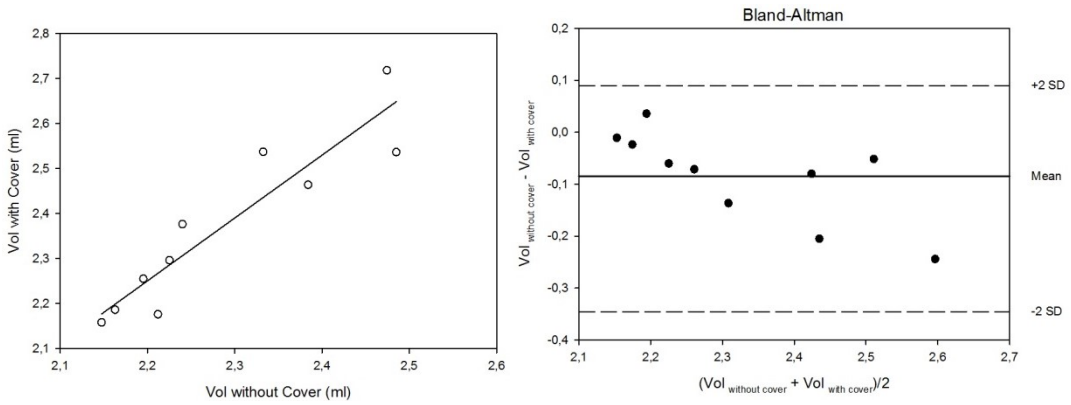

Figure 8.8 A) Linear regression of tidal volume comparison with and without plexiglass cover and B) Bland Altman analysis (the lines represent mean and mean ± 2*standard deviation).

The linear regression shows a coefficient value (m) of 1.39, an intercept (q) of -0.8 and a r^2 coefficient of 0.92 that demonstrates the reliability of the test. The Bland Altman analysis shows that all points are in the range of mean ± 2*standard deviation, that means that the 2 methods (with and without cover) may be used interchangeably.

C. Regional Transfer impedance

In the present study the transfer impedance of the respiratory system was computed by forcing pressure at the mouth and measuring the flow as the time derivative of the chest wall volume by OEP. In this way, the regional transfer impedances of the different thoracic and abdominal compartments can be estimated too. In this chapter are presented the regional transfer impedance of 9 zones already presented in chapter 5 as coloured maps maps: 4 zones for the rib cage and 5 zones for the abdomen. They include symmetrical and anatomical division that reflects the properties of the underlying tissues and are presented in terms of single areas line and mean of different zones.

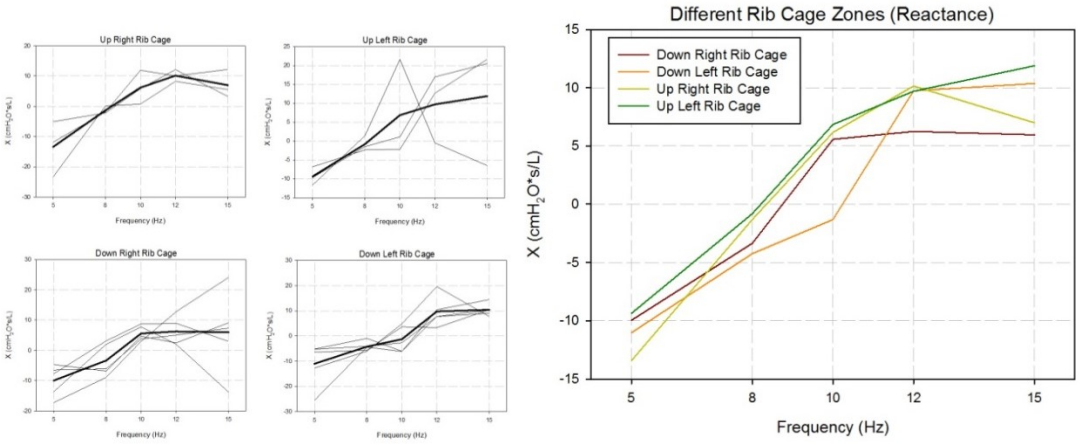

Figure 8.9 Regional transfer impedance: reactance of the rib cage presented in terms of single lines of the areas (A) and mean of different zones (B).

Mean values are from -13 - -9.3 cmH2O*s/L at 5Hz to 5.9-11.8 cmH2O*s/L at 15Hz.

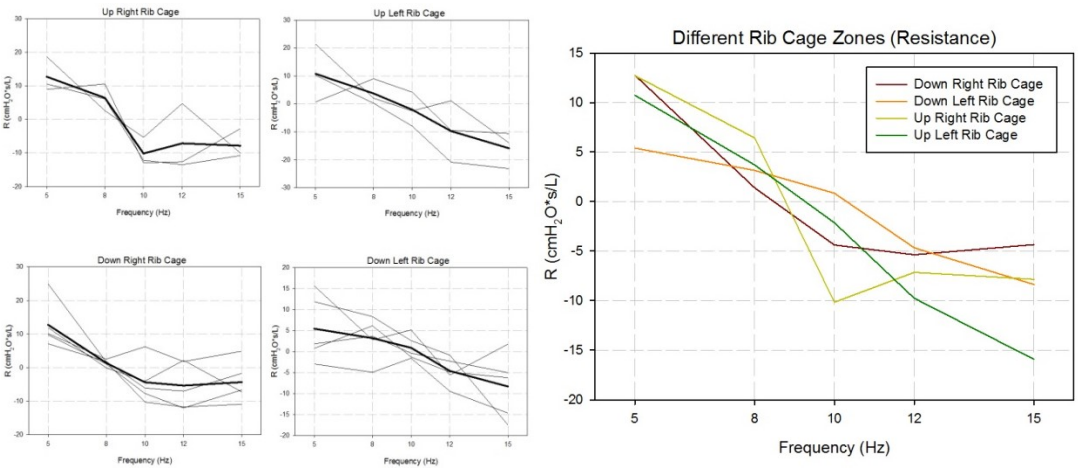

Figure 8.10 Regional transfer impedance: resistance of the rib cage presented in terms of single lines of the areas (A) and mean of different zones (B).

Mean values are from -5.39- -12.75 cmH2O*s/L at 5Hz to -15.9- -4.3 cmH2O*s/L at 15Hz.

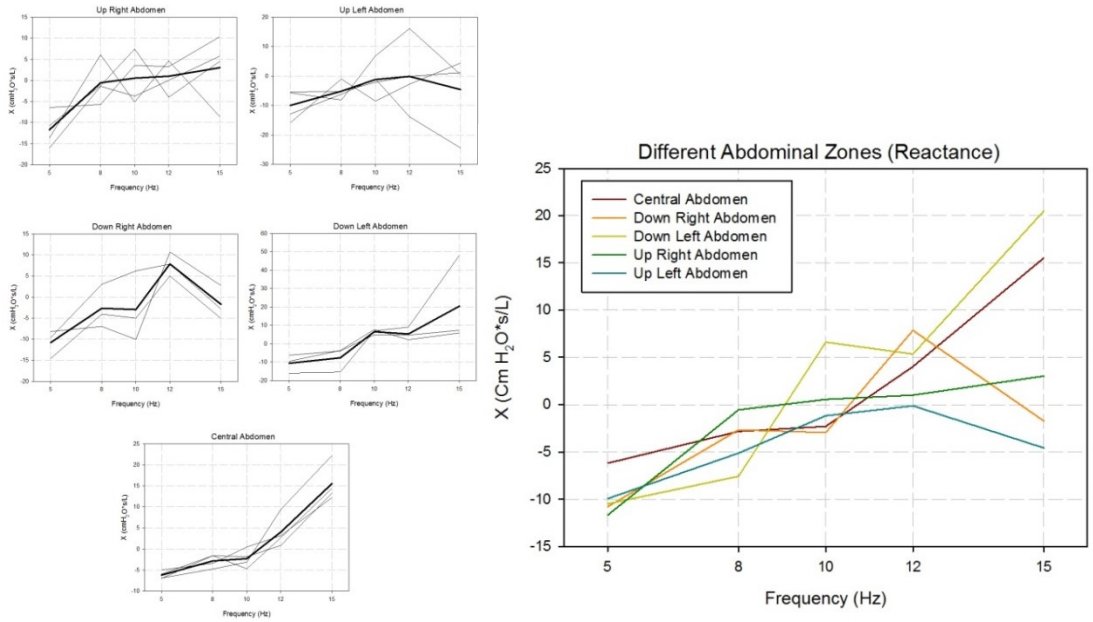

Figure 8.11 Regional transfer impedance: reactance of the abdomen presented in terms of single lines of the areas (A) and mean of different zones (B).

Mean values are from -11.6 - -6.2 cmH2O*s/L at 5Hz to -4.5-20.4 cmH2O*s/L at 15Hz.

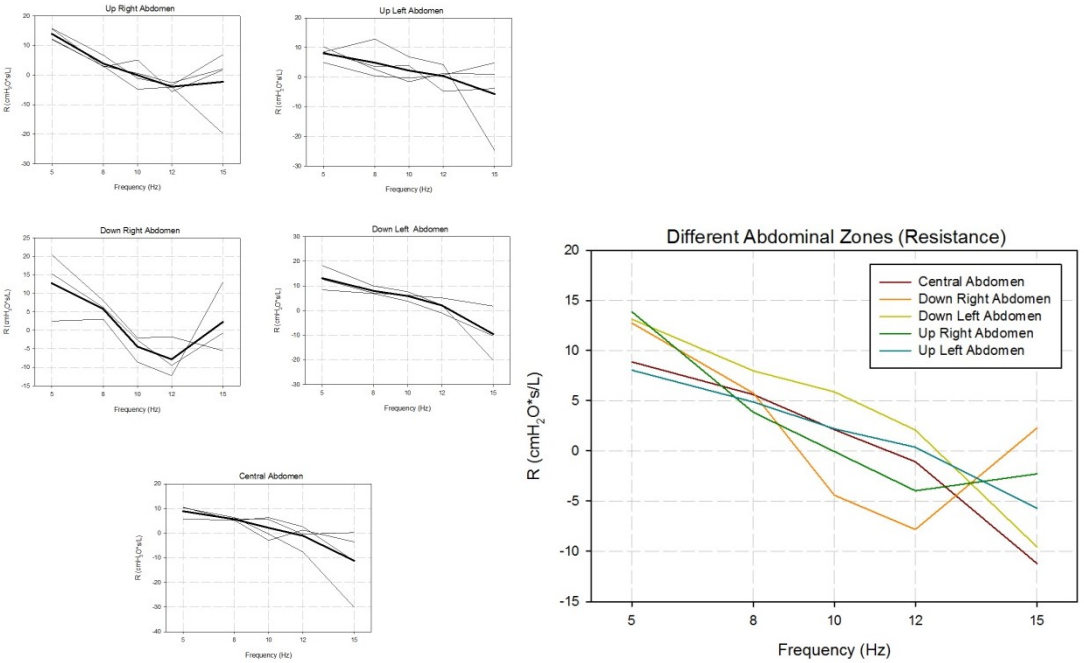

Figure 8.12 Regional transfer impedance: resistance of the abdomen presented in terms of single lines of the areas (A) and mean of different zones (B).

Mean values are from 8-13.87 cmH2O*s/L at 5Hz to -11.1-2.27 cmH2O*s/L at 15Hz.

D. Implemented codes

```
%% Input impedance

% for each frequency
[startTime,frequency,labels,Data,ChMap]=tdfReadDataGenPurpose('pat
ient.tdf');

press = Data(2,:)*100;
flow = Data(1,:)*10/60;

[P,F]=spectrum(flow,press,480,240,[],240);
[val_max pos_max]= max(P(:,2));
freq_vent= F(pos_max);              % ventilation frequency
coerenza= P(pos_max,5);             % max coherence
fdt=P(pos_max,4);                   % Re + Im

Real_part=real(fdt);
Imaginary_part=imag(fdt);
```

```
%% Transfer impedance

% for each frequency
[frequency,D,R,T,labels,links,tracks]=tdfReadData3D
('patient.tdf');
for i=1:3:72
    marker(i)=tracks(:,i:i+3);         % marker(x,y,z)
end

% centers of mass(x,y,z)
x1=mean([marker1(1,1),marker2(1,1),marker3(1,1)]);
y1=mean([marker1(1,2),marker2(1,2),marker3(1,2)]);
z1=mean([marker1(1,3),marker2(1,3),marker3(1,3)]);

fs=240;
Wn= 1/(fs/2);                     % high pass filter: fc=1Hz
n=4;
[b,a] = butter(n,Wn,'high');

for i=1:24
    marker(i)=sqrt(((marker1(:,1)-x1).^2)+((marker1(:,2)-
    y1).^2)+((marker1(:,3)-z1).^2));
     marker(i)=filtfilt(b,a,marker(1));
end

marker(:,1)=(mean([marker1,marker2,marker7,marker4,marker5],2)).*a
rea(1);
```

```
marker(:,2)=(mean([marker2,marker3,marker5,marker6,marker8],2)).*a
rea(2);
marker(:,3)=(mean([marker4,marker5,marker7,marker9,marker10,marker
11,marker12],2)).*area(3);
marker(:,4)=(mean([marker5,marker6,marker8,marker9,marker13,marker
14,marker15],2)).  *area(4);
marker(:,5)=(mean([marker9,marker13,marker14,marker15,marker17,mar
ker18,marker24],2)).*area(5);
marker(:,6)=(mean([marker9,marker10,marker11,marker12,marker17,mar
ker16,marker20],2)).*area(6);
marker(:,7)=(mean([marker17,marker19,marker22],2)).*area(7);
marker(:,8)=(mean([marker16,marker20,marker21,marker12],2)).*area(
8);
marker(:,9)=(mean([marker18,marker23,marker24,marker15],2)).*area(
9);
marker=marker.*1000000;

[startTime,frequency,labels,Data,ChMap]=tdfReadDataGenPurpose('pat
ient.tdf');
press=Data(2,:)*100;
press=filtfilt(b,a,press);
t=[1:1:size(markers,2)];
x=linspace(min(t),max(t),size(press,2));

for i=1:9

[P,F]=spectrum(markers_camp_5(i,8600:9700),press(8600:9700),480,24
0,[],240);
    [val_max pos_max]= max(P(:,2));
    coerenza(i,1)= P(pos_max,5);
    fdt(i,1)=P(pos_max,4);
end
%pressure correction and derivate of transipedance
fdt_press=(fdt_press05+fdt_press1)./2;
fdt_corr=correzione_fdt(dp,fdt_press);
for i=1:9
    fdt(i,:)=fdt(i,:)./(freq*j*2*pi);
    fdt_new(i,:)=fdt(i,:).*fdt_corr;
end



% Phase shift: 12 areas vs marker2

[frequency,D,R,T,labels,links,tracks]=tdfReadData3D
('patient.tdf');
for i=1:24
    marker(i,:)= tracks(1,1:3);
end

area(1)=(1/2)*norm(cross(marker(4,:)-marker(1,:), marker(4,:)-
marker(2,:)));
area(2)=…
```

```
% 12 areas
area_tetra(1)=area(7);
area_tetra(2)=area(6)+area(5)+area(8);
area_tetra(3)=area(19)+area(20)+area(25);
area_tetra(4)=area(24)+area(23);
area_tetra(5)=area(1)+area(2)+area(15)+area(9);
area_tetra(6)=area(4)+area(3)+area(14)+area(13);
area_tetra(7)=area(17)+area(18)+area(26)+area(27);
area_tetra(8)=area(21)+area(22)+area(33)+area(34);
area_tetra(9)=area(10);
area_tetra(10)=area(11)+area(12)+area(16);
area_tetra(11)=area(28)+area(29)+area(30);
area_tetra(12)=area(31)+area(32);

% normalization
dat5=importdata('patient.sec');
for i=1:34
    tetra5(:,i)=dat5(:,i)/area(i);
end

[frequency,D,R,T,labels,links,tracks] = tdfReadData3D
('patient.tdf');
marker2=tracks(:,4:6);

%filtering
fs=frequency;
Wn= 3/(fs/2);
n=4;
[b,a] = butter(n,Wn,'high');
marker2(:,2) = filtfilt(b,a,marker2(:,2));

for i=1:12
     tetra_norm5(:,i)=filtfilt(b,a,tetra_norm5(:,i));
end

for i=1:12
     [P,F]=spectrum(marker2(:,2),tetra_norm5(:,i),120,60,[ ],60);
     [val_max pos_max]= max(P(:,1));
     freq5(i)= F(pos_max);
     coerenza5(i)= P(pos_max,5);
     fdt5(i)=P(pos_max,4);
     ritardo_tetra_5(i)= phase(fdt5(i));
end
```

%% Volume contribution

```
% for each frequency
dat5=importdata('patient.dat');
t5=dat5(:,1);            % time
vrc_5=dat5(:,2);         % rib cage volume
```

```
vabd_5=dat5(:,3);        % abdominal volume
vtot_5=dat5(:,4);        % total volume

fs=60;
Wn= 3/(fs/2);
n=4;
[b,a] = butter(n,Wn,'high');
vrc_5 = filtfilt(b,a,vrc_5);
vabd_5 = filtfilt(b,a,vabd_5);
vtot_5 = filtfilt(b,a,vtot_5);

% when all mxn for each frequency have be computed with Zview is
possible to use this code for vt_tot, vt_abd and vt_rc:

vol=importdata('Vtot.mat');
vol5=vol(:,1);
vol8=vol(:,2);
vol10=vol(:,3);
vol12=vol(:,4);
vol15=vol(:,5);

dat5=importdata('Vabd_patient_5Hz.mxn');
vt5=abs(diff(vol5(dat5(:,2))));
vt_rc5=mean(vt5);

…
vt_tot=[vt_rc5 vt_rc8 vt_rc10 vt_rc12 vt_rc15];
```

```
%% Pressure correction
function [fdt] = correzione_fdt(dp,fdt_press)
      p=[10,18,25,33,40];
      for i=1:5
              fdt_corr=fdt_press(:,i);
            [rp,m,q] = regression(p,fdt_corr');
            fdt(i)=m.*dp(i)+q;
      end
end
```

```
%% Flow compensation
function [R_corr] = correz_R(flussi,m,q)
      for i=1:5
            R_corr(i)=m(1).*flussi(i)+q(1);
      end
end
```